



UNIVERSIDADE ESTADUAL DE CAMPINAS  
Instituto de Física Gleb Wataghin

GUSTAVO LINHARES TEIXEIRA

NONPERTURBATIVE STRUCTURE OF THE TRANSVERSELY  
PROJECTED QUARK-GLUON VERTEX

Estrutura não-perturbativa do vértice  
quark-glúon projetado transversalmente

CAMPINAS

2024

GUSTAVO LINHARES TEIXEIRA

NONPERTURBATIVE STRUCTURE OF THE TRANSVERSELY  
PROJECTED QUARK-GLUON VERTEX

Estrutura não-perturbativa do vértice quark-glúon  
projetado transversalmente

*Dissertation presented to the Gleb Wataghin Institute  
of Physics of the University of Campinas in partial  
fulfillment of the requirements for the degree of Mas-  
ter in Physics, in the area of Physics.*

*Dissertação apresentada ao Instituto de Física Gleb  
Wataghin da Universidade Estadual de Campinas  
como parte dos requisitos exigidos para a obtenção  
do título de Mestre em Física, na área de Física.*

ORIENTADORA: PROFA. DRA. ARLENE CRISTINA AGUILAR

ESTE EXEMPLAR CORRESPONDE À VERSÃO FINAL  
DA DISSERTAÇÃO DEFENDIDA PELO ALUNO GUS-  
TAVO LINHARES TEIXEIRA, E ORIENTADA PELA  
PROFA. DRA. ARLENE CRISTINA AGUILAR

---

CAMPINAS

2024

Ficha catalográfica  
Universidade Estadual de Campinas (UNICAMP)  
Biblioteca do Instituto de Física Gleb Wataghin  
Lucimeire de Oliveira Silva da Rocha - CRB 8-9174

T235n Teixeira, Gustavo Linhares, 1999-  
Nonperturbative structure of the transversely projected quark-gluon vertex  
/ Gustavo Linhares Teixeira. – Campinas, SP : [s.n.], 2024.

Orientador(es): Arlene Cristina Aguilar.  
Dissertação (mestrado) – Universidade Estadual de Campinas  
(UNICAMP), Instituto de Física Gleb Wataghin.

1. QCD não perturbativa. 2. Equações de Schwinger-Dyson. 3. Vértice  
quark-glúon. I. Aguilar, Arlene Cristina, 1977-. II. Universidade Estadual de  
Campinas (UNICAMP). Instituto de Física Gleb Wataghin. III. Título.

Informações complementares

**Título em outro idioma:** Estrutura não-perturbativa do vértice quark-glúon projetado  
transversalmente

**Palavras-chave em inglês:**

Non-perturbative QCD

Schwinger-Dyson equations

Quark-gluon vertex

**Área de concentração:** Física

**Titulação:** Mestre em Física

**Banca examinadora:**

Arlene Cristina Aguilar [Orientador]

Adriano Lana Cherchiglia

Bruno Omar El Bennich

**Data de defesa:** 18-10-2024

**Programa de Pós-Graduação:** Física

**Identificação e informações acadêmicas do(a) aluno(a)**

- ORCID do autor: <https://orcid.org/0000-0002-3638-1170>

- Currículo Lattes do autor: <https://lattes.cnpq.br/4380118825050658>



INSTITUTO DE FÍSICA  
GLEB WATAGHIN

MEMBROS DA COMISSÃO EXAMINADORA DA DISSERTAÇÃO DE MESTRADO DO ALUNO GUSTAVO LINHARES TEIXEIRA - RA 253574, APRESENTADA E APROVADA AO INSTITUTO DE FÍSICA GLEB WATAGHIN, DA UNIVERSIDADE ESTADUAL DE CAMPINAS, EM 18/10/2024.

COMISSÃO JULGADORA:

- Profa. Dra. Arlene Cristina Aguilar – Presidente e Orientadora (IFGW/ UNICAMP)
- Prof. Dr. Adriano Lana Cherchiglia (IFGW/ UNICAMP)
- Prof. Dr. Bruno Omar El Bennich (UNIFESP – Campus Diadema)

**OBS.:** Ata da defesa com as respectivas assinaturas dos membros encontra-se no SIGA/Sistema de Fluxo de Dissertação/Tese e na Secretaria do Programa da Unidade.

CAMPINAS

2024

# Acknowledgements

Over the past two years working on this project, I have had the opportunity and privilege to meet people whose contributions have been invaluable, both to the completion of this work and to my education. I would like to express my sincere thanks to them.

First of all, I would like to thank my supervisor, Profa. Dr. Arlene Cristina Aguilar, for her invaluable support, trust, and patience, as well as her careful and attentive guidance. I am deeply grateful for the opportunities she has provided. I would also like to express my appreciation to Professor Dr. Joannis Papavassiliou and Dr. Antônio Maurício, both from the University of Valencia, Spain. Their insightful discussions and comments during meetings were immensely helpful in the execution of this work.

This project would not have been possible without the incredible collaboration of my friend Bianca Maria S. de Oliveira, with whom I have had the privilege of working closely over the past two years. I would also like to extend a special thanks to my friend Leonardo Rodrigues dos Santos. Both are exceptional individuals who welcomed me into the group with open arms, and I am proud to have cultivated an invaluable friendship with them.

Furthermore, I would like to thank the professors at IFGW who have contributed directly or indirectly to my education over the past two years. In particular, I am grateful to the professors who participated in the evaluation panels for qualification and prerequisites: Prof. Dr. Adriano L. Cherchiglia, Prof. Dr. João P. Pitelli, and Prof. Dr. Pedro Holanda. Their comments, questions, and critiques were essential in the preparation of this dissertation.

I would also like to acknowledge the financial support received from the Brazilian Ministry of Science, Technology, and Innovation through the National Council for Scientific and Technological Development (CNPq), under grant number 131385/2022 – 4. My

thanks extend to the IFGW and the State University of Campinas (UNICAMP) for their infrastructure, as well as to the staff for their support. I am particularly grateful to the Feynman cluster team at the John David Rogers Computing Center for their assistance during the numerical calculations phase of this work.

I would also like to thank the many friends I have made along the way, over the last few years, whether here at IFGW or in São Carlos.

Finally, I would like to express my immense gratitude to my parents, Francisco Elso and Flávia Luana, for their constant presence in my life, their support, sacrifices, and the opportunities they have provided to me and my siblings.

# Abstract

The quark-gluon vertex is a fundamental component in Quantum Chromodynamics, playing a crucial role in understanding nonperturbative phenomena such as chiral symmetry breaking and the subsequent dynamical generation of mass for quarks, as well as in the formation of bound states that compose the hadronic spectrum through the Bethe–Salpeter equations and their variants. Given the importance of the nonperturbative description of this Green’s function, in this work, we study the quark-gluon vertex through its Schwinger–Dyson equation. In particular, we focus on the form factors of the transversely projected vertex. First, we consider the equation of motion for this Green’s function derived through the 3PI formalism, where truncation is introduced at the level of the effective action. Then, the decomposition of the vertex into a tensor basis formed by eight elements accompanied by form factors is associated with the corresponding Schwinger-Dyson equation through projections. Thus, the study of the vertex relies on the analysis of each form factor, which is expressed as integral equations solved numerically. In the numerical analysis, two main simplifications are considered. The first decouples the equations, treating only the classical form factor,  $\lambda_1$ , as an integral equation, while the others are calculated as ordinary integrals. In the second simplification, we employ the most recent result for the three-gluon vertex, the so-called planar degeneracy approximation, where the full three-gluon vertex is approximated by its classical form factor expressed in terms of a unique Bose symmetric variable. We solve the problem numerically, using as external inputs data for the gluon and quark propagators and the three-gluon vertex computed by lattice QCD simulations. Finally, the results for the eight form factors are presented in general kinematics, establishing a clear hierarchy among them using dimensionless effective couplings. Comparisons are also made with the results from lattice QCD, which calculates the quark-gluon vertex in the soft-gluon limit.

Keywords: Nonperturbative QCD; Schwinger-Dyson Equations; Quark-gluon vertex.

# Resumo

O vértice quark-glúon é um componente fundamental na Cromodinâmica Quântica, desempenhando um papel crucial no entendimento de fenômenos não-perturbativos, como a quebra de simetria quiral e a subsequente geração dinâmica de massa para os quarks, bem como na formação de estados ligados que compõem o espectro hadrônico através das equações de Bethe–Salpeter e suas variantes. Dada a importância da descrição não-perturbativa desta função de Green, neste trabalho estudamos o vértice quark-glúon por meio de sua equação de Schwinger-Dyson. Em particular, focamos nos fatores de forma do vértice projetado transversalmente. Primeiramente, consideramos a equação de movimento para esta função de Green derivada através do formalismo 3PI, onde o truncamento é introduzido no nível da ação efetiva. Em seguida, a decomposição do vértice em uma base tensorial formada por oito elementos acompanhados por fatores de forma é associada às Equações de Schwinger-Dyson através de projeções. Com isso, o estudo do vértice recai na análise de cada fator de forma, que são expressos como equações integrais resolvidas numericamente. Na análise numérica, são consideradas duas simplificações principais. A primeira desacopla as equações, tratando apenas o fator de forma clássico,  $\lambda_1$ , como uma equação integral, enquanto os demais são calculados como integrais ordinárias. Na segunda simplificação, utilizamos o resultado mais recentes para o vértice de três glúons, a chamada aproximação de degenerescência planar, onde seu fator de forma é descrito por uma função que depende de uma única variável que possui simetria de Bose. Resolvemos o problema numericamente, utilizando como inputs externos dados para os propagadores do glúon e do quark e o vértice de três glúons calculados pelas simulações de QCD na rede. Por fim, os resultados para os oito fatores de forma são apresentados em cinemática geral, estabelecendo-se uma hierarquia clara entre eles por meio dos acoplamentos efetivos adimensionais. Também são feitas comparações com os resultados da rede, que calcula o vértice quark-glúon no limite soft-glúon.

Palavras-chave: QCD não-perturbativa; Equações de Schwinger-Dyson; Vértice quark-glúon.

# List of Acronyms

---

<b>Acronym</b>	<b>Meaning</b>
1PI	one-particle irreducible
2PI	two-particle irreducible
3PI	three-particle irreducible
IR	infrared
MOM	momentum subtraction
$n$ PI	$n$ -particle irreducible
QCD	Quantum Chromodynamics
QED	Quantum Electrodynamics
QFT	Quantum Field Theory
RGI	renormalization-group invariant
SDE	Schwinger-Dyson equation
STI	Slavnov-Taylor identity
UV	ultraviolet

---

# Contents

<b>Introduction</b>	<b>12</b>
<b>1 An Overview of QCD</b>	<b>16</b>
1.1 Lagrangian of QCD . . . . .	18
1.1.1 Chiral symmetry . . . . .	20
1.1.2 Feynman rules . . . . .	21
1.2 Asymptotic Freedom . . . . .	22
<b>2 Functional methods</b>	<b>26</b>
2.1 Functional formalism . . . . .	27
2.2 The SD master equation . . . . .	30
2.2.1 SDEs general feature . . . . .	31
2.3 SDE for the quark propagator . . . . .	33
2.4 Equation for the quark-gluon vertex . . . . .	37
2.4.1 The $n$ PI effective action . . . . .	39
2.4.2 The quark-gluon vertex from 3PI effective action . . . . .	44
<b>3 The quark-gluon vertex</b>	<b>49</b>
3.1 The transversely projected quark-gluon vertex . . . . .	50
3.1.1 General tensorial structure . . . . .	52
3.2 The SDE for the quark-gluon vertex . . . . .	55
3.2.1 Form factors from the SDE . . . . .	57
3.2.2 Renormalized form factors . . . . .	58
<b>4 Numerical analysis of the quark-gluon vertex</b>	<b>60</b>
4.1 Quark-gluon vertex SDE in Euclidean space . . . . .	61
4.2 Numerical inputs . . . . .	63
4.3 General results . . . . .	67

---

4.3.1	Tree-level form factor . . . . .	67
4.3.2	Remaining form factors . . . . .	70
4.3.3	Hierarchy of form factors . . . . .	72
4.3.4	Comparisons with lattice . . . . .	73
4.3.5	Varying the inputs . . . . .	76
4.4	Checking multiplicative renormalizability . . . . .	77
<b>5</b>	<b>Conclusions</b>	<b>80</b>
	<b>Bibliography</b>	<b>83</b>
<b>A</b>	<b>Transformation from Minkowski to Euclidean space</b>	<b>92</b>

# Introduction

In the Standard Model of particle physics, the strong interactions between quarks and gluons are described by a non-Abelian gauge theory based on the  $SU(3)$  color symmetry group, known as Quantum Chromodynamics (QCD)[1, 2]. QCD is a renormalizable quantum field theory (QFT) that exhibits the property of asymptotic freedom in the ultraviolet (UV) region [3, 4], where the coupling—and thus the interactions—become increasingly weak as the energy increases. Consequently, quarks behave as free particles in the high-energy limit, and in this UV region, QCD is treated perturbatively, as the weak coupling allows the effective use of perturbation theory.

Conversely, as energy or momentum decreases, we move from the UV region to the infrared (IR) region, the coupling of the theory becomes increasingly strong and perturbative methods are no longer applicable. However, it is in this low-momentum region that some of the most intriguing phenomena of QCD occur, such as color confinement, which states that quarks and gluons cannot be observed as free (colored) particles, and the dynamical mass generation for quarks and gluons [5–13].

To achieve a comprehensive understanding of the theory, nonperturbative approaches are crucial for investigating the IR region of QCD. The nonperturbative formalisms concentrate on examining the Green's functions of the theory—specifically, the full propagators and vertices. These functions capture all the information about the underlying dynamics, both perturbative and nonperturbative, making them fundamental objects. The Green's functions are not physical observables themselves, as they depend on gauge and renormalization choices. Nonetheless, they can be combined to produce physical observables like cross sections, decay rates, and hadron masses, which are gauge and renormalization invariant [11, 12].

The two leading approaches employed in the nonperturbative study of QCD, both formulated from first principles, are lattice QCD [14, 15] and the Schwinger-Dyson equations (SDEs) [16, 17].

The first method, lattice QCD, involves discretizing spacetime into a lattice, where quarks are represented as nodes and gluons as edges. The interactions between these elements are governed by a discretized version of the QCD Lagrangian [14, 15]. The accuracy of this method depends on parameters such as the lattice spacing  $a$  and the total volume  $V$ ; smaller spacing and larger volume lead to higher accuracy. This method is applicable only in Euclidean space, where lattice QCD employs Monte Carlo simulations, and QFTs are treated similarly to statistical mechanics.

In addition to the dependence on the choice of spacing and volume parameters, the computational power available encounters challenges in handling fermionic fields and managing the wide range of physical scales in QCD, such as the differing mass scales of quarks [18–20]. This makes exploring alternative methods, which demand fewer resources, an interesting option.

Another nonperturbative approach for QCD is the SDE. This is a functional method in QFTs that describes the dynamics of Green’s functions through equations of motion, analogous to the Euler-Lagrange equations in field theory [5–9, 21–23]. Each SDE for an  $n$ -point Green’s function is a nonlinear integral equation that involves at least one  $(n + 1)$ -point function, resulting in an infinite system of coupled equations. Consequently, this nonperturbative approach is inherently complex, and to work with it effectively, a self-consistent truncation scheme must be devised [23–29].

Each method has its own advantages and disadvantages, but the exchange of information between these two approaches is crucial. As we will see in this work, the synergy between them is essential for a solid understanding of the IR behavior of QCD. Our primary nonperturbative tool will be on the SDEs, though we will also engage with lattice QCD at certain points.

In this work, our main focus is one of the most important ingredient in QCD that couple together the gauge and matter sector: the quark-gluon vertex. Specifically we will study the transversely projected quark-gluon vertex, which plays a crucial role in phenomenological studies such as dynamical chiral symmetry breaking [5, 6, 13, 30–35], or the formation of the bound states that comprise the physical spectrum [36–46]. Due to its

theoretical and phenomenological significance, this Green's function has been extensively studied over the years using various approaches, such as perturbative methods [47–50], lattice QCD [51–55], and the continuum [35, 42, 43, 51, 56–65]. In the context of SDEs, a significant challenge in the literature has been the treatment of the three-gluon vertex involved in the equations. Much of the research has focused on studying the quark-gluon vertex, often without a detailed description of the three-gluon vertex. However, our understanding of the three-gluon vertex has substantially advanced in recent years, thanks to the combined efforts of continuum methods and large-volume lattice simulations [66–74].

This thesis is organized into five chapters. In Chapter 1, we present an overview of key aspects of QCD, including the Lagrangian, tree-level Feynman rules, and a discussion on asymptotic freedom. In Chapter 2, we introduce the general framework of functional methods and present the derivation of the standard SDEs method, from 1PI effective action. As an application, we derive the SDE for the quark propagator, which is coupled with the quark-gluon vertex. For our main object of study, the quark-gluon vertex, instead of applying the usual derivation we choose to work with a more sophisticated framework, namely  $n$ PI formalism. Specifically, we derive its SDE for the quark-gluon vertex from 3PI effective action at three-loop order [43, 57, 65, 75–77]. Two key advantages over the standard 1PI derivation are highlighted; first, the usual method typically requires external approximations to break the infinite tower of SDEs. However, in the 3PI formalism, it is not necessary; instead, the truncation is performed directly at the level of the effective action, where calculations are made up to a specified order in the loop expansion. The second advantage concerns the renormalization procedure. In the 3PI effective action, all vertices and propagators are fully dressed. During renormalization, each dressed component is assigned a multiplicative renormalization constant, but these constants ultimately simplify, leaving only a renormalization constant applied to the tree-level contribution. This simplification effectively transforms the renormalization procedure into a subtractive process.

In Chapter 3, we delve into the quark-gluon vertex, exploring its properties and performing its general decomposition into the transverse basis  $\tau_i^\mu(p_2, -p_1)$  [60, 64, 78]. We then link this basis to the SDE for the vertex employing our basis projectors  $\mathcal{P}_i^\mu(q, p_2, -p_1)$ , resulting in integral equations for the form factors  $\lambda_i(q, p_2, -p_1)$  associated with each tensor of the basis [65]. The chapter concludes with the renormalization of these form factors.

At this stage, the central equation we aim to solve—the form factors of the quark-gluon vertex—will be tackled using numerical methods. Consequently, in Chapter 4, we present the numerical results. We begin by transforming our problem from Minkowski space to Euclidean space, which allows us to apply numerical techniques. Next, we define the key inputs for our problem, utilizing fits for the lattice QCD data. Finally, we present the results of our computation for the eight form factors of the quark-gluon vertex in general kinematics. We also compare our results with lattice QCD in soft-gluon limit and we close the chapter showing the property of multiplicity of the renormalization in our results. We conclude the thesis in Chapter 5 with a brief discussion.

---

**Chapter 1**

# An Overview of QCD

The Standard Model of Particle Physics is the theory that brings together three of the four fundamental interactions of nature — electromagnetism, weak force and strong force — within a single framework, while also categorizing the elementary particles that constitute matter. This theory is a non-abelian gauge theory with the symmetry group  $SU(3) \times SU(2) \times U(1)$ . In this scenario, QCD emerges as the  $SU(3)$  gauge theory responsible for describing the strong interactions between quarks and gluons [1, 2].

According to the Standard Model, quarks are elementary particles categorized as fermions with spin  $1/2$ . They come in six flavors: up, down, charm, strange, top, and bottom. Each quark has an electric charge that is a fraction of the electron charge  $e$ :  $+(2/3)e$  for up (u), charm (c), and top (t) quarks, and  $(-1/3)e$  for down (d), strange (s), and bottom (b) quarks [79, 80]. Additionally, quarks possess color charge, the quantum number in QCD analogous to the electric charge in Quantum Electrodynamics (QED), but in three different types: red, green, blue, and their respective anticolors [1, 81]. Hadronic bound states are formed by combinations of three quarks (or three antiquarks) in different colors, as seen in baryons, or by pairs of quarks and antiquarks with color and anticolor combinations, as seen in mesons.

Gluons, the mediators of the strong interaction, are vector bosons (spin 1) whose role in QCD is analogous to that of photons in QED. However, unlike photons, which are neutral with respect to electric charge, gluons carry a color charge [82]. This allows them to interact not only with quarks but also with each other. Formally, this remarkable property arises from the non-Abelian nature of the  $SU(3)$  group, distinguishing QCD as a significantly richer and more complex theory compared to its Abelian counterpart, QED.

---

As a result, QCD exhibits a range of physical properties and phenomena that are unprecedented in other QFTs. A striking example is *asymptotic freedom*, where the value of the QCD coupling constant decreases as energy increases, leading to increasingly weaker interactions. This means that in the UV region, the coupling tends to zero, and quarks behave as free particles. Due to this feature, perturbative methods are effective for studying QCD at high energies, as the coupling constant becomes a suitable parameter for applying perturbation theory.

In contrast, in the low-energy limit, known as the IR region, the theory exhibits the opposite behavior: it becomes strongly coupled. Consequently, perturbative methods lose their validity in this domain. However, it is precisely in this region that several intriguing and theoretically challenging phenomena, such as color confinement, unfold [10]. Color confinement, in essence, means that quarks are only found in bound states with “white” color in nature, never as free particles. When one tries to separate quarks within a hadron, the required energy increases with distance. Eventually, the energy needed to separate the quarks becomes so large that new hadrons are created instead of isolating the quarks. The complete description of color confinement remains an open problem in theoretical physics.

Another interesting phenomena concerns the masses of the hadron spectra. When one naively sums the three current quark masses (the ones which appear in the QCD lagrangian), composing the proton (uud), the total amounts to only about 15 MeV, whereas the proton mass is around 1 GeV. This discrepancy indicates that the total mass is dynamically generated in QCD. This dynamical mass generation, for both quarks and gluons, can only be understood through nonperturbative mechanisms.

In this chapter, we will provide a QCD overview, beginning with its lagrangian and the associated tree-level Feynman rules. We will then compute the QCD  $\beta$  function at the one-loop level to illustrate the emergence of asymptotic freedom. In the subsequent section, we will initiate the exploration of the main nonperturbative methods QCD, which forms the core focus of this work.

## 1.1 Lagrangian of QCD

The description of a QFT is provided through its Lagrangian. The QCD Lagrangian is derived from the combination of the classical Yang-Mills theory [82], which describes the non-Abelian gauge theory and the Dirac lagrangian. After performing the quantization procedure through the Faddeev-Popov approach [83], the lagrangian is given by

$$\mathcal{L}_{\text{QCD}} = \mathcal{L}_{\text{Dirac}} + \mathcal{L}_{\text{YM}} + \mathcal{L}_{\text{GF}} + \mathcal{L}_{\text{Ghost}}, \quad (1.1)$$

where

$$\mathcal{L}_{\text{Dirac}} = \bar{\psi}(i\gamma^\mu D_\mu - m)\psi, \quad (1.2)$$

$$\mathcal{L}_{\text{YM}} = -\frac{1}{4}(F_{\mu\nu}^a)^2, \quad (1.3)$$

$$\mathcal{L}_{\text{GF}} = \frac{1}{2\xi}(\partial^\mu A_\mu^a)^2, \quad (1.4)$$

$$\mathcal{L}_{\text{Ghost}} = \bar{c}^a(-\partial^\mu D_\mu^{ac})c^c, \quad (1.5)$$

$\mathcal{L}_{\text{Dirac}}$  stands for the Dirac lagrangian,  $\mathcal{L}_{\text{YM}}$  for the Yang-Mills lagrangian,  $\mathcal{L}_{\text{GF}}$  for the gauge-fixing term, and  $\mathcal{L}_{\text{Ghost}}$  represents the ghost contribution.

The Dirac lagrangian describes the quarks and antiquarks dynamics, which are represented by the spinors  $\psi$  and  $\bar{\psi}$  (the spinors indices are omitted). It also describes the interaction between quark field  $\psi$  and gluon vector field  $A_\mu^a$  through the covariant derivative  $D_\mu$  in the fundamental representation,

$$D_\mu = \partial_\mu - ig t^a A_\mu^a, \quad (1.6)$$

where  $g$  is the coupling constant, and the  $t^a = \lambda^a/2$  are the Gell-Mann matrices, hermitian traceless generators of the color group  $SU(3)$ , which obey the relations [84],

$$\left[ \frac{\lambda^a}{2}, \frac{\lambda^b}{2} \right] = if^{abc} \frac{\lambda^c}{2}, \quad (1.7)$$

these relations define the algebra of  $SU(3)$ , with  $f^{abc}$  being the antisymmetric structure constant of the group. The non-Abelian feature of QCD arises from the fact that not all structure constants  $f^{abc}$  are equal to zero, indicating that it is a non-commutative theory. Significant implications arise from this, as seen in the lagrangian that describes gluons, which we discuss below.

The pure Yang-Mills lagrangian, Eq. (1.3), describes only gluons through field-strength tensor  $F_{\mu\nu}^a$  [82],

$$F_{\mu\nu}^a = \partial_\mu A_\nu^a - \partial_\nu A_\mu^a + gf^{abc} A_\mu^b A_\nu^c, \quad (1.8)$$

this part of the QCD lagrangian contains the gluon kinematic term, which is a quadratic term in  $A_\mu^a$  in the derivatives, which is responsible for generating the propagation. Due to the non-Abelian feature of the  $SU(3)$  ( $f^{abc} \neq 0$ ), it also includes the self-interactions of the gluons, with cubic and quartic terms in gluon field, which generate the conventional *three-gluon* and *four-gluon vertices*, see Fig. 1.2. Setting  $f^{abc}$  to zero results in an Abelian, QED-like theory, where the gauge boson has no such self-interactions.

The  $\mathcal{L}_{\text{Dirac}}$  and  $\mathcal{L}_{\text{YM}}$  constitute the classical QCD theory, and are separately invariant under local gauge transformations of the  $SU(3)$  group. For an infinitesimal transformation parameterized by local parameters  $\alpha^a(x)$ , the variations in the quark and the gluon field are given by

$$\psi \rightarrow (1 + i\alpha^a t^a) \psi, \quad (1.9)$$

$$A_\mu^a \rightarrow A_\mu^a + \frac{1}{g} \partial_\mu \alpha^a - f^{abc} \alpha^b A_\mu^c. \quad (1.10)$$

Due to the gauge transformation of the field  $A_\mu^a$ , physical process calculated with  $\mathcal{L}_{\text{YM}}$  exhibits a continuous infinity of physically equivalent field configurations [85]. To eliminate the ambiguities, and count each physical configuration only once the gauge-fixing procedure is employed. The complete QCD lagrangian, including the remaining terms from Eq. (1.1), is obtained after performing gauge fixing and quantizing the classical theory. This is achieved using the covariant Faddeev-Popov method [83], which introduces the gauge-fixing lagrangian  $\mathcal{L}_{\text{GF}}$ , where  $\xi$  is the gauge-fixing parameter, and  $\partial^\mu A_\mu^a = 0$  is the gauge-fixing condition. This procedure not only yields the gauge-fixing term but also generates a residual Lagrangian  $\mathcal{L}_{\text{Ghost}}$ , that introduces new scalar fields,  $c^a$  and  $\bar{c}^a$ , interpreted as particles called ghosts and antighosts, respectively. Additionally, it describes the interaction of these ghost fields with the gluons through the covariant derivative in the adjoint representation, given by

$$D_\mu^{ac} = \delta^{ac} \partial_\mu + g f^{abc} A_\mu^b. \quad (1.11)$$

where  $\delta^{ac}$  is the Kronecker delta.

Ghosts exhibit unique characteristics: they are scalar particles that obey Fermi-Dirac statistics. This means they are spin-0 particles (bosons) whose fields obey anticommutation relations (fermions). This contradiction leads to a violation of the *spin-statistics theorem*. However, this is not problematic within the scope of QCD, as these particles are virtual and do not appear in physical processes, only in internal processes. Their main

contribution is to ensure the unitarity of the theory.

### 1.1.1 Chiral symmetry

Besides color symmetry, the QCD Lagrangian exhibits another symmetry particularly associated with the fermionic sector of the theory: the *chiral symmetry*. In fact, this is an approximate symmetry that arises in the theory when light quarks, such as the *up* and *down* quarks, are assumed to have negligible mass. In this framework, the left-handed and right-handed fermionic fields transform independently, rendering the Lagrangian invariant under such chiral transformations.

Let us consider the decomposition of a spinor  $\psi$  that represents quark fields into its right-handed  $\psi_R$  and left-handed  $\psi_L$  chiral components,

$$\psi = \begin{pmatrix} \psi_L \\ \psi_R \end{pmatrix}. \quad (1.12)$$

Each component is obtained through the chiral projectors  $\mathbb{P}_\pm$  applied to the spinor, as follows,

$$\begin{aligned} \psi_R &= \mathbb{P}_+ \psi, & \bar{\psi}_R &= \bar{\psi} \mathbb{P}_-, \\ \psi_L &= \mathbb{P}_- \psi, & \bar{\psi}_L &= \bar{\psi} \mathbb{P}_+. \end{aligned} \quad (1.13)$$

where the chiral projectors are, respectively

$$\mathbb{P}_\pm = \frac{1}{2} (1 \pm \gamma_5). \quad (1.14)$$

The chirality of a spinor can be defined as the eigenvalue of the matrix  $\gamma_5$ . From Eq. (1.13), we see that the right-handed spinor has an eigenvalue of +1, while the left-handed spinor has an eigenvalue of -1. That is,

$$\begin{aligned} \gamma_5 \psi_R &= \psi_R, & \bar{\psi}_R \gamma_5 &= -\bar{\psi}_R, \\ \gamma_5 \psi_L &= -\psi_L, & \bar{\psi}_L \gamma_5 &= \bar{\psi}_L. \end{aligned} \quad (1.15)$$

To observe the manifestation of the chiral symmetry in the theory, let us consider the Dirac Lagrangian, given by Eq. (1.2), in the massless limit, *i.e.*,

$$\mathcal{L}_D = i\bar{\psi}\gamma^\mu D_\mu\psi. \quad (1.16)$$

We can express the above Lagrangian in terms of the chiral components of the quark field, where we use,

$$\bar{\psi}\gamma^\mu\psi = \bar{\psi}_L\gamma^\mu\psi_L + \bar{\psi}_R\gamma^\mu\psi_R, \quad (1.17)$$

to obtain,

$$\mathcal{L}_D = i\bar{\psi}_L\gamma^\mu D_\mu\psi_L + i\bar{\psi}_R\gamma^\mu D_\mu\psi_R \quad (1.18)$$

In this case, it is evident that in this massless limit, the left-handed and right-handed components do not mix, making Eq. (1.16) invariant under a global phase transformation given by

$$\psi \rightarrow e^{i\theta\gamma_5}\psi, \quad (1.19)$$

where  $\theta$  is a real phase constant. Considering Eq. (1.15), the transformations of the chiral components of the quark field are

$$\psi_L \rightarrow e^{-i\theta}\psi_L, \quad \psi_R \rightarrow e^{i\theta}\psi_R. \quad (1.20)$$

Therefore, each component transforms independently. Due to the change in sign, the fields transform with opposite chirality.

On the other hand, if we consider the mass term of the Dirac Lagrangian,  $m\bar{\psi}\psi$ , expressed in terms of the chiral components

$$m\bar{\psi}\psi = m(\bar{\psi}_L\psi_R + \bar{\psi}_R\psi_L), \quad (1.21)$$

we obtain a mix of the chiral components and, therefore, is no longer invariant under the chiral transformation Eq. (1.19). Thus, the introduction of a non-zero mass for the quarks explicitly breaks the chiral symmetry of the Lagrangian.

Notice that Eq. (1.17), and consequently the transformation given by Eq. (1.19), emerges only because the matrix  $\gamma_5$  anticommutes with the Dirac matrix  $\gamma^\mu$ ,  $\{\gamma_5, \gamma^\mu\} = 0$ . Therefore, one can generalize this concept for further quantities  $Q$ , which says that the general condition for preserving chiral symmetry is [57]

$$\{\gamma_5, Q\} = 0. \quad (1.22)$$

## 1.1.2 Feynman rules

From Eq. (1.1), one can directly derive the Feynman rules in momentum space for the fundamental propagators and vertices of the theory at the tree-level. The expressions for the quark  $S_{(0)}^{ab}(p)$ , gluon  $\Delta_{\mu\nu}^{ab(0)}(p)$ , and ghost  $D_{(0)}^{ab}(p)$  propagators are presented in Fig. 1.1. Similarly, the expressions for the four fundamental vertices: quark-gluon, ghost-gluon, three-gluon, and four-gluon are listed in Fig. 1.2, where we extract the coupling constant and the color structure, when this is feasible.

	$S^{ab(0)}(p) = \delta^{ab} S^{(0)}(p)$	$S^{(0)}(p) = \frac{i(\not{p} + m)}{p^2 - m^2 + i\epsilon}$
	$\Delta_{\mu\nu}^{ab(0)}(p) = \delta^{ab} \Delta_{\mu\nu}^{(0)}(p)$	$\Delta_{\mu\nu}^{(0)}(p) = -i \left[ g_{\mu\nu} - (1 - \xi) \frac{p_\mu p_\nu}{p^2} \right] \frac{1}{p^2 + i\epsilon}$
	$D^{ab(0)}(p) = \delta^{ab} D^{(0)}(p)$	$D^{(0)}(p) = \frac{i}{p^2 + i\epsilon}$

Figure 1.1: Feynman rules for the quark, gluon, and ghost propagators at tree-level.

Of course, these Feynman rules are meaningful only at an energy scale where perturbative treatment is applicable, which, for QCD, corresponds to the UV or high-energy regime. This is because they do not incorporate any quantum corrections, and thus they accurately represent the actual propagation and interaction only when the coupling is small and the corrections are insignificant.

## 1.2 Asymptotic Freedom

Asymptotic freedom emerges from the study of the  $\beta$  function. In renormalizable field theories, the coupling constant receives corrections and becomes dependent on the energy scale. This effect is known as the running coupling and it is described by the renormalization group equation or the  $\beta$  function of the theory.

The  $\beta$  function expresses the rate at which the renormalized coupling  $\alpha_s(\mu^2)$  varies with the renormalization scale  $\mu$ . Therefore, the renormalization group equation is given by

$$\beta(\alpha_s) = \mu \frac{d\alpha_s(\mu^2)}{d\mu}. \quad (1.23)$$

One can expand the  $\beta$  function perturbatively, resulting in

$$\beta(\alpha_s) = \mu \frac{d\alpha_s(\mu^2)}{d\mu} = - \left[ \frac{\alpha_s^2}{\pi} \beta_0 + \frac{\alpha_s^3}{\pi^2} \beta_1 + \dots \right]. \quad (1.24)$$

For an SU(N) gauge theory, the  $\beta$  function was first calculated by Gross and Wilczek [3] and Politzer [4] simultaneously in 1973, yielding:

$$\beta_0 = \left[ \frac{11}{6} C_A - \frac{1}{3} n_f \right], \quad \beta_1 = \left[ \frac{17}{12} C_A^2 - \frac{1}{24} n_f (10 C_A + 6 C_F) \right], \quad (1.25)$$

where  $C_A = N$  and  $C_F = \frac{N^2 - 1}{2N}$  are the eigenvalues of the quadratic Casimir operator in the adjoint representation, and  $n_f$  is the number of fermion flavors.

	$igt^a \Gamma_\mu^{(0)}(q, r, p)$	$\Gamma_\mu^{(0)}(q, r, p) = \gamma_\mu$
	$-gf^{mna} \Gamma_{g,\mu}^{(0)}(r, p, q)$	$\Gamma_{g,\mu}^{(0)}(r, p, q) = r_\mu$
	$gf^{amn} \Gamma_{\mu\alpha\beta}^{(0)}(q, r, p)$	$\Gamma_{\mu\alpha\beta}^{(0)}(q, r, p) = g_{\alpha\beta}(r-p)_\mu + g_{\mu\beta}(p-q)_\alpha + g_{\mu\alpha}(q-r)_\beta$
	$-ig^2 \Gamma_{\mu\nu\rho\sigma}^{mnrs(0)}(q, r, p, t)$	$\Gamma_{\mu\nu\rho\sigma}^{mnrs(0)} = f^{mse} f^{ern} (g_{\mu\rho} g_{\nu\sigma} - g_{\mu\nu} g_{\rho\sigma}) + f^{mne} f^{esr} (g_{\mu\sigma} g_{\nu\rho} - g_{\mu\rho} g_{\nu\sigma}) + f^{mre} f^{esn} (g_{\mu\sigma} g_{\nu\rho} - g_{\mu\nu} g_{\rho\sigma})$

Figure 1.2: Feynman rules for the quark-gluon, ghost-gluon, three-gluon and four-gluon interaction vertices at tree-level; we assume all momenta entering.

In the one-loop approximation, we consider only the leading term in the expansion of the  $\beta$  function. With this approximation we can solve the differential equation given in Eq. (1.24), allowing us to express the coupling as

$$\alpha_s(Q^2) = \frac{2\pi}{\beta_0 \ln(Q^2/\Lambda_{QCD}^2)}, \quad (1.26)$$

where the renormalization scale of the theory is given by,

$$\Lambda_{QCD} = \mu \exp \left[ \frac{\pi}{\alpha_s(\mu^2) \beta_0} \right]. \quad (1.27)$$

In the limit of  $Q^2 \rightarrow \Lambda_{QCD}^2$ , the denominator of Eq.(1.26) approaches a pole, causing the coupling to diverge. This pole, known as the Landau Pole, marks the momentum scale at which the perturbative approach to the theory becomes invalid. However, it is important to note that the expression for the running coupling in Eq.(1.26) loses its validity well before this pole is reached, as it is derived perturbatively. Specifically, it is based on a one-loop calculation and is therefore reliable only as long as higher-order contributions can be neglected, which is true only for small values of  $\alpha_s$ .

Moreover, the sign of  $\beta_0$  indicates the direction in which the Landau pole occurs, thereby determining the regime where the perturbative method is valid. Therefore, it is important to examine the implications of the sign change in Eq.(1.25) for the behavior described by Eq.(1.26). If  $\beta_0$  is negative, QCD has weak coupling in the IR region, with the coupling increasing in the UV. Conversely, a positive  $\beta_0$  ensures strong coupling in the IR, with the theory becoming weak coupling in the UV. Notice that in the asymptotic limit of  $Q^2 \rightarrow \infty$ ,  $\alpha_s(Q^2) \rightarrow 0$ , *i.e.*, the strong force in the nature behaves as free theory in this limit. This behavior is known as *asymptotic freedom* [3, 4].

For QCD, where the gauge group correspond to color SU(3), *i.e.*, with  $C_A = 3$  in the Eq. (1.25), one can conclude that, for known number of quark flavors, generally up until  $n_f \leq 16$  we have the asymptotic freedom, the coupling decreases when the momentum increases. Such a feature results in the quark behaving almost as free particles at short distances, or high energy limit, as experimentally checked in the deep inelastic scattering. Additionally, asymptotic freedom allows us to apply perturbative methods and treat the coupling constant as a good expansion parameter in the UV region.

Regarding the QCD scale,  $\Lambda_{QCD}$  is generally estimated to lie within the 200–400 MeV range. This implies that reaching the nonperturbative regime in QCD does not require delving too far into the IR; it occurs at energy scales typical in particle physics. This regime is particularly fascinating because it gives rise to phenomena like color confinement and dynamical mass generation, which cannot be addressed by the standard perturbative approaches in QFT. One of the primary methods for studying this nonperturbative regime is the SDEs, which will be explored in detail in the next chapter, as they are central to the work presented here.

Lastly, Fig. 1.3 provides a detailed overview of the QCD coupling  $\alpha_s(Q^2)$  as a function of the energy scale  $Q^2$ , based on data from the Particle Data Group [86]. It is important to emphasize that  $\alpha_s(Q^2)$  is not a physical observable by itself; instead, its value is inferred indirectly from experimental measurements

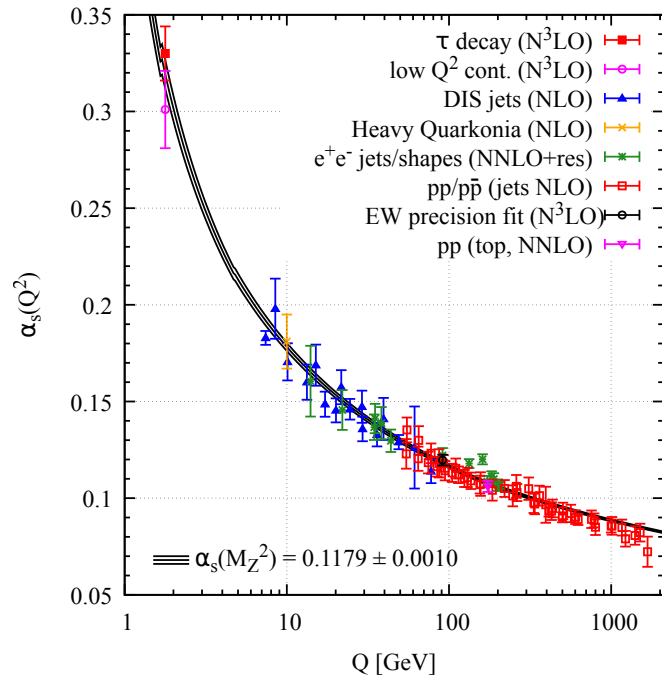


Figure 1.3: Summary of measurements of  $\alpha_s(Q^2)$  as a function of the energy scale  $Q$  obtained from [86]. The corresponding degree of perturbation theory used in the extraction of  $\alpha_s$  is indicated in brackets (NLO: next-to-leading order; NNLO: next-to-next-to-leading order; res. NNLO: NNLO matched to a resummed calculation; N<sup>3</sup>LO: next-to-NNLO).

---

# Chapter 2

## Functional methods

In this chapter, we introduce one of the first principle approaches to treat the non-perturbative regime of QCD: the SDEs. These equations are derived in the context of the path integral formulation of QFT and can be understood as analogous to the Euler-Lagrange equations of a classical field theory, in the sense that they describe the dynamics of Green's functions, such as propagators, vertices, and higher  $n$ -point functions. In their integral form, the SDE constitute an infinite system of coupled non-linear integral equations, making it necessary a truncation scheme to treat them feasibly.

This chapter is outlined as follows: First, we introduce the functional formalism, which allows us to define Green's functions using path integrals and obtain them by calculating functional derivatives from the generating functional. Within this framework, we derive the SD master equation, equivalent to the equation of motion for Green's functions. As an application of the master equation, we derive the SDE for the quark propagator. Finally, we discuss the method that allows us to obtain a truncated SDE for the quark-gluon vertex: The  $n$ PI formalism. We conclude the chapter by presenting the equation for the quark-gluon vertex, obtained from the 3PI effective action, which is central to this thesis.

## 2.1 Functional formalism

The functional formalism is a powerful approach introduced in 1948 by Richard Feynman [87, 88], utilizing path integrals for the formulation of QFT instead of the traditional method of canonical quantization, which uses field operator formulation. It is particularly useful for dealing with gauge theories and performing nonperturbative calculations. Since the path integral approach is the most straightforward method for deriving the SDEs, we will briefly review the main aspects of this formalism in this section, for more details see [21, 89].

A QFT is fundamentally characterized by its correlation functions, also known as Green's functions. An  $n$ -point Green's function is defined as the vacuum expectation value of the time-ordered product of  $n$  fields  $\varphi_i(x)$ :  $\langle 0|T\{\varphi_i(x_1)\cdots\varphi_j(x_n)\}|0\rangle$ . In the functional approach, these functions can be calculated using the path integral [85],

$$\langle 0|T\{\varphi_i(x_1)\cdots\varphi_j(x_n)\}|0\rangle = \frac{\int \mathcal{D}\varphi \varphi_i(x_1)\cdots\varphi_j(x_n)e^{i\mathcal{S}[\varphi]}}{\int \mathcal{D}\varphi e^{i\mathcal{S}[\varphi]}}. \quad (2.1)$$

where the vacuum state is denoted by  $|0\rangle$ ,  $T$  is the time-ordered operator, and  $\varphi$  denotes the collective of the fields  $\varphi_i(x)$ , which may be different types of fields or degree of freedom of one field evaluated at the spacetime point  $x$ . The integration measure extends over all of these fields, *i.e.*,

$$\mathcal{D}\varphi = \prod_i \mathcal{D}\varphi_i, \quad (2.2)$$

In addition, the quantity  $\mathcal{S}$  is the usual classical action

$$\mathcal{S} = \int d^4x \mathcal{L}(x). \quad (2.3)$$

We may write the Eq. (2.1) more compactly by introducing the central quantity of the functional method, the *generating functional*  $Z[J]$ ,

$$Z[J] = \int \mathcal{D}\varphi \exp \left\{ i\mathcal{S}[\varphi] + i \int d^4x J_i(x)\varphi_i(x) \right\}, \quad (2.4)$$

here, the  $J_i(x)$  is the external source associated with the field  $\varphi_i$ , and the  $J$  is defined as the collection of sources  $J_i(x)$ ,

$$J = \int d^4x J_i(x)\varphi_i(x). \quad (2.5)$$

The  $n$ -point Green's functions are attained by taking functional derivatives of the generating functional with respect to the external sources, and subsequently setting them

to zero,

$$\langle 0|T\{\varphi_i(x_1)\cdots\varphi_j(x_n)\}|0\rangle = \frac{1}{Z[0]} \frac{\delta}{i\delta J_i(x_1)} \cdots \frac{\delta}{i\delta J_j(x_n)} Z[J] \Big|_{J=0}. \quad (2.6)$$

Another concept that we must define is the *connected Green's function*. The above definition produces two types of correlation functions, the connected and disconnected diagrams as shown in Fig. 2.1. The connected contribution contains the necessary information, while the disconnected diagrams do not contribute to the S-matrix. Therefore, to compute only the connected part, we define the *connected functional generator*,  $W[J] = -i \ln Z[J]$  [90],

$$\langle 0|T\{\varphi_i(x_1)\cdots\varphi_j(x_n)\}|0\rangle_{\text{conn.}} = \frac{1}{i^{n-1}} \frac{\delta}{\delta J_i(x_1)} \cdots \frac{\delta}{\delta J_j(x_n)} W[J] \Big|_{J=0}. \quad (2.7)$$

The propagator for the field  $\varphi_i$  is the two-point Green's function that we can readily

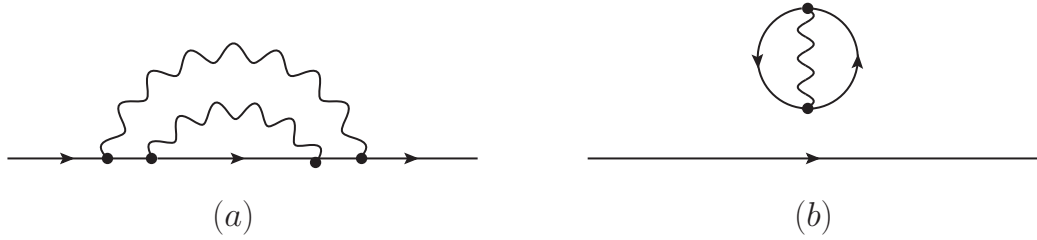


Figure 2.1: Examples of diagrams: connected (a) and disconnected (b).

write down,

$$D_i(x-y) = -i \frac{\delta^2 W[J]}{\delta J_i(x) \delta J_i(y)} \Big|_{J=0}. \quad (2.8)$$

Connected Green's functions can be further divided into two classes of diagrams: *proper* and *improper*, see Fig. 2.2. Improper diagrams are those that can be divided into disconnected parts by removing one internal line, whereas proper diagrams can not be split in this way. The proper diagrams are also called *one-particle-irreducible* (1PI),

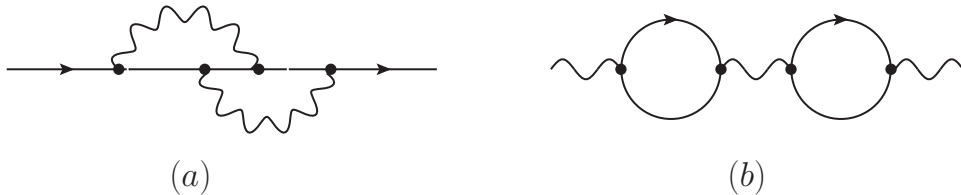


Figure 2.2: Examples of proper (a) and improper diagrams (b).

The 1PI contributions are very useful when we write down the SDEs, since we can generate full diagrams summing them in a simple way [22, 23]. To access only the 1PI

diagrams, the effective action  $\Gamma[\phi]$  is employed, which is defined through the Legendre transform of the connected generating functional, in the following way

$$\Gamma[\phi] = W[J] - \int d^4x J_i(x)\phi_i(x). \quad (2.9)$$

The 1PI correlation functions are calculated in the same way as connected ones, by performing functional differentiation of the effective action, *i.e.*,

$$\langle 0|T\{\varphi_i(x_1)\cdots\varphi_j(x_n)\}|0\rangle_{1PI} = i\frac{\delta}{\delta\phi_i(x_1)}\cdots\frac{\delta}{\delta\phi_j(x_n)}\Gamma[\phi]\Big|_{\phi=0}, \quad (2.10)$$

where the  $\phi_i$  is the vacuum expectation value (*vev*) of the field  $\varphi_i$  in the presence of the source  $J$ , or simply *classical field*,  $\varphi_i^{\text{cl}}$

$$\phi_i \equiv \varphi_i^{\text{cl}} \equiv \frac{\delta W[J]}{\delta J_i(x)} = \frac{1}{Z[J]} \frac{\delta Z[J]}{i\delta J_i(x)} = \langle 0|\varphi_i|0\rangle_J. \quad (2.11)$$

When the sources are turned off, this *vev* is usually zero, except for spontaneously broken symmetry theories. The relation between the sources and the effective action is

$$J_i(x) = -\frac{\delta\Gamma[\phi]}{\delta\phi_i(x)}. \quad (2.12)$$

Using the above definitions, in particular Eqs. (2.11) and (2.12), we derive a few functional relations that will be useful later. First we notice that,

$$\begin{aligned} \delta_{ij}\delta(x-y) &= \frac{\delta\phi_i(x)}{\delta\phi_j(y)} = \int d^4z \frac{\delta J_k(z)}{\delta\phi_j(y)} \frac{\delta\phi_i(x)}{\delta J_k(z)} \\ &= \int d^4z \left( \frac{\delta^2\Gamma[\phi]}{\delta\phi_j(y)\delta\phi_k(z)} \right) \left( \frac{\delta^2W[J]}{\delta J_k(z)\delta J_i(x)} \right), \end{aligned} \quad (2.13)$$

the 1PI two-point function can be connected to the propagator of Eq. (2.8),

$$\frac{\delta^2\Gamma[\phi]}{\delta\phi_i(x)\delta\phi_i(y)} = \left( \frac{\delta^2W[J]}{\delta J_i(x)\delta J_i(y)} \right)^{-1} = iD_i^{-1}(x-y), \quad (2.14)$$

where the rightmost equality is understood to be valid only when the sources and classical fields are set to zero in the derivatives on the left. Therefore, the Eq.(2.13) can be expressed as

$$\delta_{ij}\delta(x-y) = \int d^4z \left( \frac{\delta^2\Gamma[\phi]}{\delta\phi_j(y)\delta\phi_k(z)} \right) \left( \frac{\delta^2\Gamma[\phi]}{\delta\phi_k(z)\delta\phi_i(x)} \right)^{-1}. \quad (2.15)$$

To compute high order 1PI functions one may need to deal with derivatives of propagators. This relation can be obtained by differentiating Eq. (2.15) with respect of the classical field  $\phi$ , after which we attain

$$\begin{aligned} \frac{\delta}{\delta\phi_i(x)} \left( \frac{\delta^2\Gamma[\phi]}{\delta\phi_j(y)\delta\phi_k(z)} \right)^{-1} &= - \int_{[w]} \left( \frac{\delta^2\Gamma[\phi]}{\delta\phi_j(y)\delta\phi_m(w_2)} \right)^{-1} \times \\ &\times \frac{\delta^3\Gamma[\phi]}{\delta\phi_m(w_2)\phi_i(x)\delta\phi_n(w_1)} \left( \frac{\delta^2\Gamma[\phi]}{\delta\phi_n(w_1)\delta\phi_k(z)} \right)^{-1}, \end{aligned} \quad (2.16)$$

where we introduced the shorthand notation

$$\int_{[w]} \equiv \int d^4 w_1 d^4 w_2 . \quad (2.17)$$

## 2.2 The SD master equation

With the formalism established, we can now derive the SD master equation [22, 91]. We begin by considering a change of variables in the functional generator, Eq. (2.4), where the fields  $\varphi_i$  undergo an infinitesimal variation,

$$\varphi_i(x) \rightarrow \varphi'_i(x) = \varphi_i(x) + \varepsilon f_i(x) , \quad (2.18)$$

with  $\varepsilon$  being an infinitesimal parameter, and  $f_i(x)$  an arbitrary function. The integration measure remains unchanged,  $\mathcal{D}\varphi' = \mathcal{D}\varphi$ , because none of the  $f_i$  depends on the fields, resulting in a Jacobian of transformation equal to zero. Hence, the generating functional of Eq. (2.4) is expressed as

$$Z[J] = \int \mathcal{D}\varphi \exp \left\{ i\mathcal{S}[\varphi] + i \delta\mathcal{S}[\varphi] + i \int d^4 x J_i(x) [\varphi_i(x) + \varepsilon f_i(x)] \right\} , \quad (2.19)$$

where the variation of the action is

$$\delta\mathcal{S}[\varphi] = \int d^4 x \frac{\delta\mathcal{S}[\varphi]}{\delta\varphi_i(x)} \delta\varphi_i(x) = \varepsilon \int d^4 x \frac{\delta\mathcal{S}[\varphi]}{\delta\varphi_i(x)} f_i(x) . \quad (2.20)$$

Now we expand the right-hand side to the first order in  $\varepsilon$ ,

$$Z[J] = \int \mathcal{D}\varphi \exp \left\{ i\mathcal{S}[\varphi] + i \int d^4 x J_i(x) \varphi_i(x) \right\} \left[ 1 + i\varepsilon \int d^4 x f_i(x) \left( \frac{\delta\mathcal{S}[\varphi]}{\delta\varphi_i(x)} + J_i(x) \right) \right] . \quad (2.21)$$

Notice that the first term produces just  $Z[J]$  itself, and the remainder term, the coefficient of  $\varepsilon$  must be zero. With differentiation under the integral sign, we attain

$$\begin{aligned} 0 &= \int \mathcal{D}\varphi \left[ \int d^4 x f_i(x) \left( \frac{\delta\mathcal{S}[\varphi]}{\delta\varphi_i(x)} + J_i(x) \right) \right] \exp \left\{ i\mathcal{S}[\varphi] + i \int d^4 x J_i(x) \varphi_i(x) \right\} \\ &= \left[ \int d^4 x f_i(x) \left( \frac{\delta\mathcal{S}[\varphi]}{\delta\varphi_i(x)} \left[ \frac{\delta}{i\delta J_j} \right] + J_i(x) \right) \right] Z[J] . \end{aligned} \quad (2.22)$$

The derivative of the action on the second line is to be evaluated in terms of  $\phi$  field operators, followed by the substitution of each  $\phi_j$  by the functional derivative with respect to  $iJ_j$ .

Since  $f_i$  is an arbitrary function, the integrand must vanish, *i.e.*,

$$\left( \frac{\delta\mathcal{S}}{\delta\varphi_i(x)} \left[ \frac{\delta}{i\delta J_j} \right] + J_i(x) \right) Z[J] = 0 . \quad (2.23)$$

The above expression is the SD master equation for disconnected Green's functions. How-

ever, it is more advantageous to work exclusively with 1PI functions, or at most with connected functions. Therefore, we should eliminate references to  $Z[J]$  at this stage. This can be achieved by recalling that  $W[J] = -i \ln Z[J]$ .

$$e^{iW[J]} \left( \frac{\delta \mathcal{S}}{\delta \varphi_i(x)} \left[ \frac{\delta}{i\delta J_j} \right] \right) e^{-iW[J]} = -J_i(x). \quad (2.24)$$

Applying to it the Baker-Campbell-Hausdorff formula,

$$e^A B e^{-A} = B + [A, B] + \frac{1}{2!}[A, [A, B]] + \frac{1}{3!}[A, [A, [A, B]]] + \dots, \quad (2.25)$$

where  $A$  and  $B$  are operators, we obtain the master equation for connected Green's functions [22],

$$\frac{\delta \mathcal{S}}{\delta \varphi_i(x)} \left[ \frac{\delta}{i\delta J_j} - \frac{\delta W[J]}{\delta J_j} \right] \cdot 1 = -J_i(x). \quad (2.26)$$

The “ $\cdot 1$ ” notation implies that the functional differentiation operator on the left acts on all quantities on the right up to unity [22]. This notation clarifies that Eq. (2.26) does not represent an equality between operators but rather an number equation.

Finally, in order to attain the SD master equation for 1PI functions we may use the definition of the field, Eq. (2.12), and the chain rule,

$$\begin{aligned} \frac{\delta}{i\delta J_i(x)} &= \int d^4y \frac{\delta \phi_j(y)}{i\delta J_i(x)} \frac{\delta}{\delta \phi_j(y)} = i \int d^4y \frac{\delta^2 W[J]}{\delta J_i(x) \delta J_j(y)} \frac{\delta}{\delta \phi_j(y)} \\ &= i \int d^4y \left( \frac{\delta^2 \Gamma[\phi]}{\delta \phi_i(x) \delta \phi_j(y)} \right)^{-1} \frac{\delta}{\delta \phi_j(y)}, \end{aligned} \quad (2.27)$$

which produces [22],

$$\frac{\delta \mathcal{S}}{\delta \varphi_i(x)} \left[ \phi_j(y) + i \int d^4z \left( \frac{\delta^2 \Gamma[\phi]}{\delta \phi_j(y) \delta \phi_k(z)} \right)^{-1} \frac{\delta}{\delta \phi_k(z)} \right] \cdot 1 = \frac{\delta \Gamma[\phi]}{\delta \phi_i(x)}. \quad (2.28)$$

Observe that the derivation of the SD master equation is similar to that of the Euler-Lagrange equation. We make an infinitesimal change in the classical field and find that the variation of the action is zero ( $\delta \mathcal{S} / \delta \varphi = 0$ ). Consequently, SDEs can be thought as generalization of the Euler-Lagrange equations in a QFT, dictating the dynamical behavior of the quantum fields.

### 2.2.1 SDEs general feature

Historically, the SDEs were first derived in the works of J. S. Schwinger [17] and F. J. Dyson [16]. Their building blocks are the complete Green's functions, which contains all possible corrections in the theory, including both perturbative and nonperturbative contributions. These complete Green's functions are usually depicted by filled circles in

the respective diagrams, as illustrated in Fig. 2.3.

Its main characteristic—and major obstacle—is that the SDEs forms an infinite set of coupled nonlinear integral equations, known as the “infinite tower” of SDEs. For example, in QED, the SDEs for the electron and photon propagators, as well as the electron-photon vertex, are respectively given by [92]

$$\begin{aligned} S^{-1}(p) &= S_{(0)}^{-1}(p) - \int_k \gamma_\mu S(k) \mathbb{I}^\mu(p-k, k, p) D_{\mu\nu}(p-k), \\ [D^{\mu\nu}(q)]^{-1} &= [D_{(0)}^{\mu\nu}(p)]^{-1} - \int_k \gamma^\mu S(p+k) \mathbb{I}^\nu(q, k+p, k) S(k), \\ \mathbb{I}_\mu(q, p_2, p_1) &= \gamma_\mu - \int_k \mathbb{I}_\mu(q, p_2+k, p_1-k) S(p_1-k) S(p_2+k) \mathcal{K}. \end{aligned} \quad (2.29)$$

Although the SDEs may seem quite complicated to handle analytically, we can associate them with diagrams that help us visualize schematically how they work, Fig. 2.3 shows the diagrammatic representation of the tree SDEs written explicitly in Eq. (2.29).

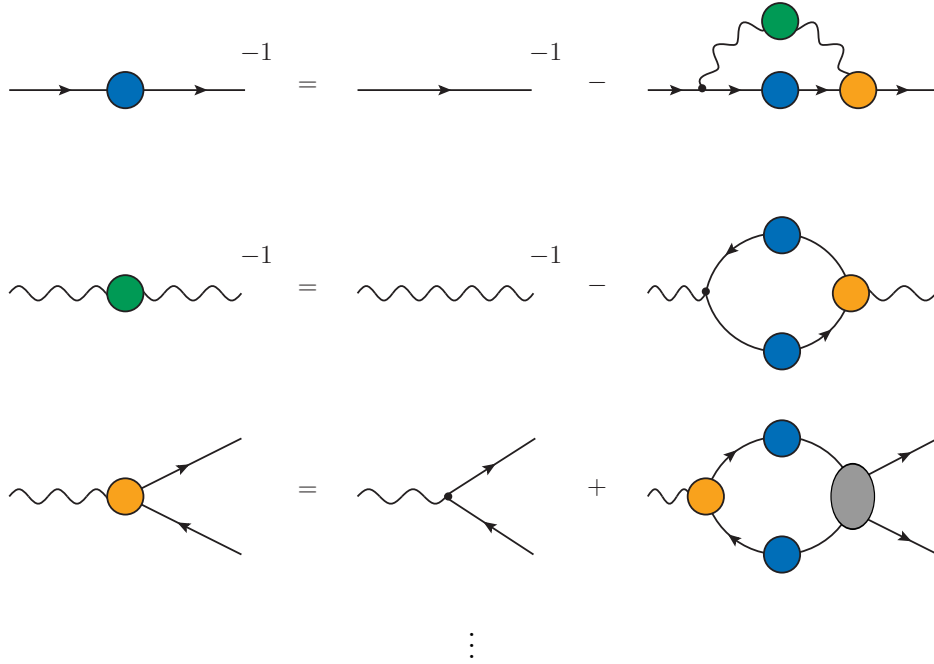


Figure 2.3: SDEs for QED: The gap equation for the inverse of the full electron propagator  $S^{-1}(p)$  (blue circle), the inverse full photon propagator  $D_{\mu\nu}$  (green circle) and electron-photon vertex  $\mathbb{I}_\mu$  (orange circle) [92].

Notice that the SDE for the electron and photon propagators are coupled to each other and to the vertex, which in turn is coupled to a 4-point function scattering kernel,  $\mathcal{K}$ , represented by the gray ellipsis. If we were to write the equation for the 4-point kernel, higher n-point function would be coupled to it and so on, forming a system with

infinite coupled equations. Additionally, there are usually loops involved, resulting in an integration where the Green's function in question appears on both sides, therefore usually we have to deal with integral equations.

In principle, solving this infinite system completely would provide full knowledge of the theory; however, achieving such comprehensive knowledge is infeasible. Consequently, truncations are employed, using approximations to reduce the infinite system to a manageable set of closed equations.

In essence, SDEs are a continuous method that captures the entire IR and UV range of momenta of a theory. They form an infinite system of coupled nonlinear integral equations, and the feasibility of their solution requires a self-consistent truncation scheme. This scheme provides approximations to obtain a finite set of equations that can be effectively treated.

## 2.3 SDE for the quark propagator

Having established the mathematical foundations in the preceding sections, we are now prepared to derive the relevant SDEs. Before addressing the SDE for the quark-gluon vertex, we will begin with the SDE for the quark propagator.

With the SD master equation for 1PI Green's functions, Eq. (2.28), in mind, we start by computing the functional derivative of the QCD action with respect to the antiquark field  $\bar{\psi}(y)$ . The action is given by  $\mathcal{S}_{QCD} = \int d^4x \mathcal{L}_{QCD}$ ,

$$\frac{\delta \mathcal{S}_{QCD}}{\delta \bar{\psi}(y)} = (i\gamma^\mu \partial_\mu^y - m + gt^a \gamma^\mu A_\mu^a) \psi(y). \quad (2.30)$$

For quarks, the relevant term for performing this derivative is related to the Dirac Lagrangian given by Eq. (1.2)

$$\mathcal{L}_{\text{Dirac}} = \bar{\psi}(i\gamma^\mu \partial_\mu - m + gt^a \gamma^\mu A_\mu^a)\psi. \quad (2.31)$$

Then, we insert it into the master Eq. (2.28), resulting in

$$(i\gamma^\mu \partial_\mu^y - m) \psi^{\text{cl}}(y) + gt^a \gamma^\mu \left\{ \left[ A_{\mu,a}^{\text{cl}}(y) + i \int d^4z \left( \frac{\delta^2 \Gamma}{\delta A_{\mu,a}^{\text{cl}}(y) \delta \phi_k^{\text{cl}}(z)} \right)^{-1} \frac{\delta}{\delta \phi_k^{\text{cl}}(z)} \right] \psi^{\text{cl}}(y) \right\} = \frac{\delta \Gamma}{\delta \bar{\psi}^{\text{cl}}(y)}, \quad (2.32)$$

here, we have already taken the derivatives with respect to unity on the left-hand side — referring to the notation “•1” in Eq. (2.28). Additionally, we have omitted specifying

the arguments of the effective action for brevity, which will be our convention from now on. The last functional derivative acting on  $\psi^{\text{cl}}(y)$  will simply result in a Dirac delta, simplifying the integral

$$\frac{\delta\Gamma}{\delta\bar{\psi}^{\text{cl}}(y)} = (i\gamma^\mu\partial_\mu - m)\psi^{\text{cl}}(y) + gt^a\gamma^\mu \left[ A_{\mu,a}^{\text{cl}}(y)\psi^{\text{cl}}(y) + i \left( \frac{\delta^2\Gamma}{\delta A_{\mu,a}^{\text{cl}}(y)\delta\psi^{\text{cl}}(y)} \right)^{-1} \right]. \quad (2.33)$$

In the second derivative, we change the order of differentiation. Next, we differentiate the entire expression with respect to the quark field  $\psi^{\text{cl}}(x)$ , and set the classical field to zero, after which we obtain

$$\begin{aligned} \left. \frac{\delta^2\Gamma}{\delta\psi^{\text{cl}}(x)\delta\bar{\psi}^{\text{cl}}(y)} \right|_0 &= (i\gamma^\mu\partial_\mu - m)\delta(x-y) + igt^a\gamma^\mu \left[ \frac{\delta}{\delta\psi^{\text{cl}}(x)} \left( \frac{\delta^2\Gamma}{\delta\psi^{\text{cl}}(y)\delta A_{\mu,a}^{\text{cl}}(y)} \right)^{-1} \right] \Big|_0 \\ &= (i\gamma^\mu\partial_\mu - m)\delta(x-y) - igt^a\gamma^\mu \left[ \int_{[w]} \left( \frac{\delta^2\Gamma}{\delta\psi^{\text{cl}}(y)\delta\phi_m^{\text{cl}}(w_2)} \right)^{-1} \times \right. \\ &\quad \left. \times \frac{\delta^3\Gamma}{\delta\phi_m^{\text{cl}}(w_2)\delta\psi^{\text{cl}}(x)\delta\phi_n^{\text{cl}}(w_1)} \left( \frac{\delta^2\Gamma}{\delta\phi_n^{\text{cl}}(w_1)\delta A_{\mu,a}^{\text{cl}}(y)} \right)^{-1} \right] \Big|_0, \end{aligned} \quad (2.34)$$

where the transition between these lines was facilitated by using a previously derived identity, as shown in Eq. (2.16), and we introduced the “ $|_0$ ” shorthand notation so we do not list every source being set to zero.

Now the quark fields must be paired with the antiquark fields in Green’s functions, collapsing  $\phi_m^{\text{cl}}$  to  $\bar{\psi}^{\text{cl}}$ , due to the first term of the integrand. Similarly,  $\phi_n^{\text{cl}}$  must be  $A_{\nu,n}^{\text{cl}}$  due to the last term of the integrand, as neither a quark nor an antiquark should be paired with a gluon field alone.

At this point, we may identify in Eq. (2.34) a few correlation functions. Taking into account the definition of the 1PI n-point Green’s functions given by Eq. (2.10), we can write the quark propagator as

$$S^{-1}(x-y) = -i \left. \frac{\delta^2\Gamma}{\delta\psi^{\text{cl}}(x)\delta\bar{\psi}^{\text{cl}}(y)} \right|_0, \quad (2.35)$$

which appears on the left-hand side of the equation and as the first term of the integrand on the right-hand side. The other two-point function present in the integral is the gluon propagator, defined as

$$\Delta_{\mu\nu}^{ab}(x-y) = i \left. \left( \frac{\delta^2\Gamma}{\delta A_{\mu,a}^{\text{cl}}(x)\delta A_{\nu,b}^{\text{cl}}(y)} \right)^{-1} \right|_0. \quad (2.36)$$

As for the remaining three-point function, it is nothing but the quark-gluon vertex,

$$\mathbb{\Gamma}_\mu^a(x, y, z) = i \left. \frac{\delta^3 \Gamma}{\delta A_{\mu,a}^{\text{cl}}(x) \delta \psi^{\text{cl}}(y) \delta \bar{\psi}^{\text{cl}}(z)} \right|_0. \quad (2.37)$$

With these definitions, the quark propagator SDE may be recast as

$$S^{-1}(x - y) = -i (i\not{\partial} - m) \delta(x - y) - g^2 C_F \int_{[w]} \gamma^\mu S(w_2 - y) \mathbb{\Gamma}^\nu(w_1, x, w_2) \Delta_{\mu\nu}(w_1 - y), \quad (2.38)$$

where we separate the color part from the gluon propagator and the quark-gluon vertex as  $\Delta_{\mu\nu}^{ab}(x - y) = \delta^{ab} \Delta_{\mu\nu}(x - y)$  and  $\mathbb{\Gamma}^{\mu,a}(x, y, z) = i g t^a \mathbb{\Gamma}^\mu(x, y, z)$ . We use the fact that  $t^a t^m \delta^{am} = C_F$ , the eigenvalue of the Casimir operator in the fundamental representation.

Then, by Fourier transforming, we finally obtain

$$S^{-1}(p) = -i (\not{p} - m) - g^2 C_F \int_k \gamma^\mu S(k) \mathbb{\Gamma}^\nu(q, k, -p) \Delta_{\mu\nu}(q), \quad (2.39)$$

where we introduced the notation for the integral measure

$$\int_k \equiv \int \frac{d^4 k}{(2\pi)^4}, \quad (2.40)$$

where the use of a symmetry-preserving regularization scheme, such as dimensional regularization, is implicitly assumed.

Notice that we keep the same conventions established earlier, that is, for the quark-gluon vertex, all momenta are entering, and the momenta entrances are arranged in the gluon-quark-antiquark order. We represent this SDE diagrammatically in Fig. 2.4, with the white blobs denoting full quark and gluon propagators and the orange blob, the full quark-gluon vertex. The quark propagator is represented by a solid line, whereas the gluon, by a wavy one.

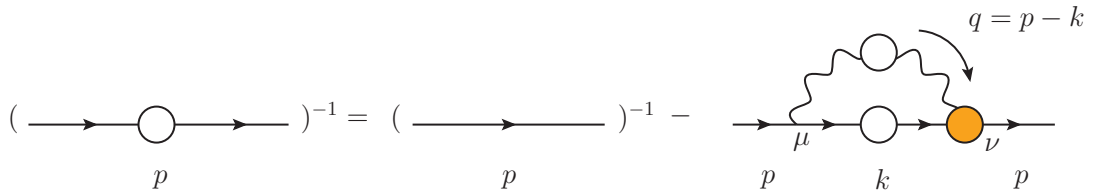


Figure 2.4: Diagrammatic representation of the quark propagator SDE, also known as gap equation. Its analytical expression is given by Eq. (2.39).

At this moment, it is important to acknowledge the complexity of the SDE approach to QFTs. First, note that Eq. (2.39) represents an integral equation for the quark propagator.

This equation not only involves the quark propagator but also incorporates the gluon propagator and the quark-gluon vertex, which, in turn, contain the quark propagator in their respective SDEs. Consequently, writing down the SDEs for all propagators and vertices in the theory results in an infinite system of coupled nonlinear integral equations, as outlined in Section 2.2.1. Due to this complexity, an exact solution for the entire system is generally not feasible. Therefore, the implementation of the truncations schemes where some Green's functions are approximated are often required.

To conclude this section, it is important to highlight one final point regarding the quark propagator equation. The study of chiral symmetry breaking in the continuum often involves some version for the quark propagator equation, as expressed in Eq. (2.39), which is commonly known as the gap equation.

The structure of quark propagator  $S^{-1}(p)$  can generally be decomposed in terms of  $\not{p}$  and  $\mathbb{I}$ . Therefore, one can write it as

$$S^{-1}(p) = A(p^2)\not{p} - B(p^2). \quad (2.41)$$

where  $A(p^2)$  is known as the inverse of the quark wave function, and  $B(p^2)$  is the scalar component (mass function), respectively. It is useful here to define the dynamically generated quark mass  $\mathcal{M}(p^2)$  as the ratio

$$\mathcal{M}(p^2) = \frac{B(p^2)}{A(p^2)}, \quad (2.42)$$

and in this case the full quark propagator is expressed as

$$S^{-1}(p) = A(p^2) [\not{p} - \mathcal{M}(p^2)] \quad (2.43)$$

The dynamical quark mass,  $\mathcal{M}(p^2)$ , provides information about the quark mass, generated due to the IR nonperturbative dynamics of the theory. The dynamical quark mass arises when the chiral symmetry is broken, indicated when we obtain a nonvanishing solution for  $B(p^2) \neq 0$ . Notice that the dynamical equation governing the behavior of the functions  $A(p^2)$  and  $B(p^2)$  can be derived by computing the following traces of the SDE for the quark propagator given by Eq. (2.39).

$$\begin{aligned} p^2 A(p^2) &= \frac{1}{4} \text{Tr} [\not{p} S^{-1}(p)] , \\ B(p^2) &= -\frac{1}{4} \text{Tr} [S^{-1}(p)] . \end{aligned} \quad (2.44)$$

then one can consequently obtain,  $\mathcal{M}(p^2)$ , through the ratio Eq. (2.42).

A key point to be highlighted is that the quark SDE displays a strong dependence

on the nonperturbative behavior of the quark-gluon vertex,  $\Gamma_\mu(q, p_2, -p_1)$ , and the quark mass generation phenomena depends on details of the quark-gluon vertex. Therefore, in the next section, we will focus on the SDE for the quark-gluon vertex.

## 2.4 Equation for the quark-gluon vertex

As mentioned earlier, one of the characteristics of SDEs is that they form a systems of coupled integral equations between correlation functions. As we have seen, the quark SDE not only depends on the quark propagator but is also coupled to the gluon propagator and the quark-gluon vertex. The same holds for the equation governing the quark-gluon vertex, which is diagrammatically represented in Fig. 2.5 with all its contributing diagrams [23].

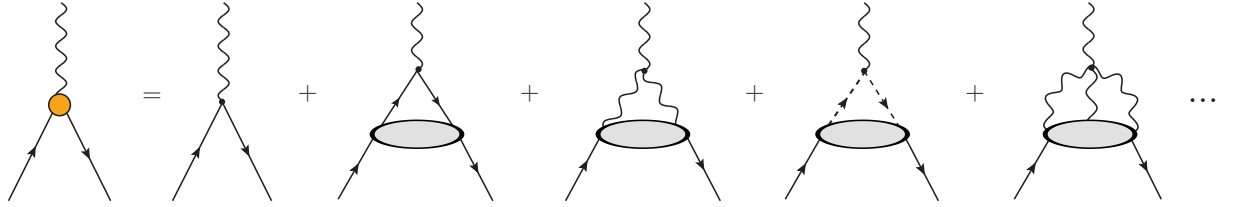


Figure 2.5: The diagrammatic representation of the quark-gluon SDE in terms of scattering kernels (gray blobs), all propagators are considered dressed.

Note that this equation is significantly more complex than the quark SDE equation since it includes not only two-point functions, such as the complete quark, gluon, and ghost propagators, but also four- and five-point Green's functions. These functions are the scattering kernels represented by the gray ellipsis in the Fig. 2.5.

It is possible to obtain the SDE for the quark-gluon vertex from the master equation for 1PI Green's functions by differentiating Eq. (2.33) with respect to the antiquark, quark and gluon fields and turning off the external sources. This third-order derivative of the effective action defines the quark-gluon vertex.

$$\Gamma_\mu^a(x, y, z) = i \frac{\delta^3 \Gamma}{\delta A_{\mu,a}^{\text{cl}}(x) \delta \psi^{\text{cl}}(y) \delta \bar{\psi}^{\text{cl}}(z)} \Big|_0 = i \frac{\delta^3 \Gamma}{\delta \psi^{\text{cl}}(y) \delta \bar{\psi}^{\text{cl}}(z) \delta A_{\mu,a}^{\text{cl}}(x)} \Big|_0. \quad (2.45)$$

Depending on the order of derivation—whether with respect to the gluon or quark leg—we can obtain the SDEs as represented in Fig. 2.6 [23, 35, 75], which are equivalent as long as they are not truncated.

At this point, it is necessary to introduce a truncation scheme to handle this equation. A truncated SDE model for the quark-gluon vertex is shown in Fig. 2.7, corresponding

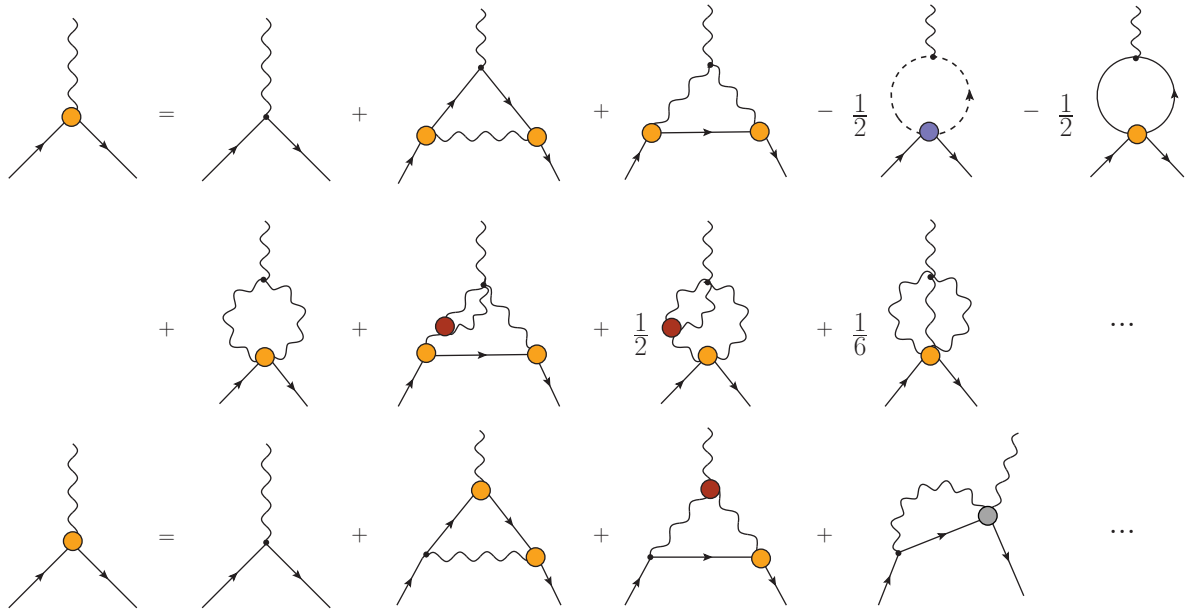


Figure 2.6: The SDE for the quark-gluon vertex, expressed in terms of 1PI Green's functions. The two possible equations derived with respect to the gluon leg (top) and the quark leg (bottom) [23]. The quark-gluon vertex is represented by orange blobs, while the three-gluon vertex is shown in red. Purple and gray blobs represents the scattering kernels of two-quarks-two-ghost and two-quark-two-gluon, respectively. All propagators are considered to be dressed.

to the truncated version of the second equation (with respect to the quark leg) shown in Fig. 2.6. The truncation is performed by neglecting higher-order diagrams and considering only the contributions at the one-loop dressed level. The idea is based on the assumption that higher dressed loops contribute very little, making the loss of information negligible when diagrams functions are omitted. In practice, higher-order diagrams or diagrams containing a specific vertex are simply omitted<sup>1</sup>, or some approximation for the vertex is employed [63].

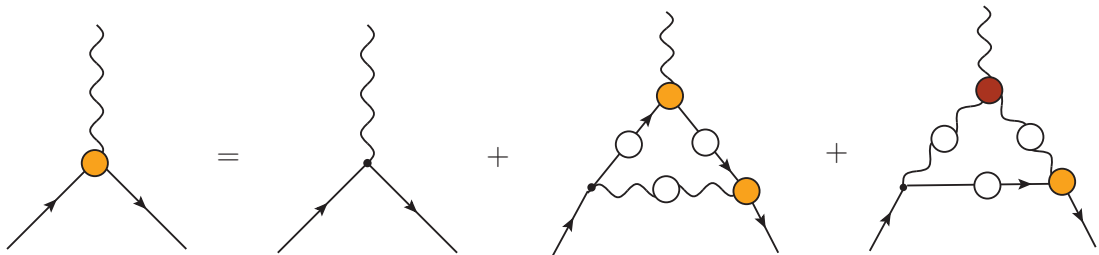


Figure 2.7: SDE for the quark-gluon vertex at one-loop dressed approximation.

<sup>1</sup>In this case, this truncation omits the two-quark-two-gluon kernel, depicted in gray at the bottom of Fig. 2.6.

This truncation scheme is the dominant approach for almost all calculations involving functional methods and has been quite successful. However, its disadvantage is that one cannot initially determine whether a contribution from a given vertex is negligible. Therefore, it relies either on extending the truncation or comparing the results of one's own calculations with those obtained using other methods or – if possible – on a direct comparison with measurements.

The quark-gluon vertex used in this work is based on the 3PI formalism, where additional Legendre transforms are performed on the 1PI effective action, resulting in a 3PI effective action [23, 75, 93]. The truncation of this equation is achieved by expressing the effective action as a loop series and truncating the series at three-loop. In the following, we will discuss this method and present the equation for the vertex.

### 2.4.1 The $n$ PI effective action

All information about a QFT is encoded in the effective action, which is the functional generator for its Green's functions. There are different representations of the effective action, one of which is the  $n$ -particle irreducible ( $n$ PI) effective action. This is a generalization of the 2PI formalism introduced by Cornwall, Jackiw, and Tomboulis [94], where the effective action  $\Gamma[\phi, G]$  is expressed in terms of the *vev*  $\phi$ , Eq. (2.11), and the complete propagator  $G$ . This method is particularly efficient for describing complete two-point functions. However, for describing higher-order Green's functions, such as vertices, the 2PI method becomes inefficient. The idea can be generalized to include these correlation functions by introducing the  $n$ PI effective action,  $\Gamma[\phi, G, V_3, \dots, V_n]$ , where this functional is written in terms of  $\phi$ ,  $G$  and the complete vertices  $V_n$  [75, 93]. From it, the equations of motion for each dressed quantity can be obtained through stationary conditions (functional derivatives) when the external sources vanish, such as

$$\left. \frac{\delta\Gamma[\phi, G, V_3, \dots]}{\delta\phi} \right|_0 = \left. \frac{\delta\Gamma[\phi, G, V_3, \dots]}{\delta G} \right|_0 = \left. \frac{\delta\Gamma[\phi, G, V_3, \dots]}{\delta V_3} \right|_0 = \dots = 0. \quad (2.46)$$

The main difference between SDEs and the  $n$ PI formalism lies in the approach to truncation. In SDEs, the effective action is used to derive an infinite tower of coupled integral equations, and truncation is performed to break this tower and obtain a closed set of equations. In contrast, the  $n$ PI formalism expands the effective action in terms of a series of loops, with truncation introduced by breaking the series at a given loop order [63, 75]. This approach allows for the derivation of a closed set of equations for the

Green's functions using Eq. (2.46). In general, similar to SDEs, these equations result in a nonlinear coupled set of integral equations.

We begin by elaborating on the 2PI effective action and then generalize it to  $n$ PI. First, we define the functional generator in the presence of sources as in Eq (2.4). Now, in addition to the external source  $J$  we introduce a new type of source  $K$  [90, 94],

$$\begin{aligned} Z[J, K] &= \exp(iW[J, K]) \\ &= \int \mathcal{D}\varphi \exp \left\{ i \left( \mathcal{S}[\varphi] + \int_x J_i(x) \varphi_i(x) + \frac{1}{2} \int_{xy} K_{ij}(x, y) \varphi_i(x) \varphi_j(y) \right) \right\}, \end{aligned} \quad (2.47)$$

where the functional  $W[J, K]$  produces connected diagrams. In the presence of these sources, we define the  $vev$  of the fields  $\varphi$  and the connected two-point function  $G$ ,

$$\begin{aligned} \frac{\delta W}{\delta J_i(x)} &= \phi_i(x), \\ \frac{\delta W}{\delta K_{ij}(x, y)} &= \frac{1}{2} [\phi_i(x) \phi_j(y) + iG_{ij}(x, y)]. \end{aligned} \quad (2.48)$$

Let us recall Eq. (2.9), the Legendre transformation that defines the 1PI effective action

$$\Gamma^K[\phi] = W[J, K] - \int_x J_i(x) \phi_i(x), \quad (2.49)$$

in the presence of the source  $K$  the above equation represents the 1PI effective action for a theory governed by a modified classical action

$$\mathcal{S}^K[\varphi] = \mathcal{S}[\varphi] + \frac{1}{2} \int_{xy} K_{ij}(x, y) \varphi_i(x) \varphi_j(y). \quad (2.50)$$

The 1PI effective action can be represented in terms of loop expansions [75, 94], the one-loop term is

$$\Gamma^{(1\text{-loop})}[\phi] = \mathcal{S}[\varphi] + \frac{i}{2} \text{Tr} \ln \left[ G_{(0)}^{-1} \right], \quad (2.51)$$

where  $G_0$  is the bare two-point function. Making modifications due to the source  $K$ ,  $\mathcal{S}[\varphi] \rightarrow \mathcal{S}^K[\varphi]$  and  $G_{(0)}^{-1} \rightarrow G_{(0)}^{-1} - iK$  we are left with

$$\Gamma^{K(1\text{-loop})}[\phi] = \mathcal{S}^K[\varphi] + \frac{i}{2} \text{Tr} \ln \left[ G_{(0)}^{-1} - iK \right]. \quad (2.52)$$

Now, we define the 2PI effective action by performing a Legendre transformation of Eq. (2.49) with respect to the source  $K$  and insert Eq. (2.48),

$$\begin{aligned} \Gamma[\phi, G] &= \Gamma^K[\phi] - \int_{xy} \frac{\delta \Gamma^K[\phi]}{\delta K_{ij}(x, y)} K_{ij}(xy) \\ &= \Gamma^K[\phi] - \frac{1}{2} \int_{x, y} K_{ij}(x, y) \phi_i(x) \phi_j(y) - \frac{1}{2} \text{Tr} KG, \end{aligned} \quad (2.53)$$

where

$$\text{Tr}KG = \int_{x,y} G_{ij}(x,y)K_{ij}(x,y). \quad (2.54)$$

and thus

$$\begin{aligned} \Gamma[\phi, G] &= W[J, K] - \int_x \frac{\delta\Gamma^K[\phi]}{\delta J_i(x)} J_i(x) - \int_{xy} \frac{\delta\Gamma^K[\phi]}{\delta K_{ij}(x,y)} K_{ij}(x,y) \\ &= W[J, K] - \int_x J_i(x)\phi_i(x) - \frac{1}{2} \int_{x,y} K_{ij}(x,y)\phi_i(x)\phi_j(y) - \frac{1}{2}\text{Tr}KG, \end{aligned} \quad (2.55)$$

from this, we derive the following relations, from which we can observe the stationary conditions

$$\begin{aligned} \frac{\delta\Gamma[\phi, G]}{\delta\phi_i(x)} &= -J_i(x) - \int_y K_{ij}(x,y)\phi_j(y), \\ \frac{\delta\Gamma[\phi, G]}{\delta G_{ij}(x,y)} &= -\frac{i}{2}K_{ij}(x,y). \end{aligned} \quad (2.56)$$

In the absence of sources,  $J = 0$  and  $K = 0$ , we obtain the equations of motion for the  $\phi$  and  $G$

$$\left. \frac{\delta\Gamma[\phi, G]}{\delta\phi} \right|_0 = \left. \frac{\delta\Gamma[\phi, G]}{\delta G} \right|_0 = 0. \quad (2.57)$$

Now we express the effective action  $\Gamma[\phi, G]$  at one-loop, plugging the Eq. (2.52) in Eq. (2.53), we find

$$\Gamma[\phi, G] \simeq \mathcal{S}[\varphi] + \frac{i}{2}\text{Tr} \ln \left[ G_{(0)}^{-1} - iK \right] - \frac{1}{2}\text{Tr}KG, \quad (2.58)$$

if we set  $G^{-1} = G_{(0)}^{-1} - iK$ , we can eliminate the dependence on  $K$ ,

$$\Gamma[\phi, G] \simeq \mathcal{S}[\varphi] + \frac{i}{2}\text{Tr} \left[ \ln G^{-1} + (G_{(0)}^{-1} - G^{-1})G \right]. \quad (2.59)$$

The exact expression of the effective action is obtained by adding the remaining terms in the series, which is accomplished through the functional  $\Phi[\phi, G]$ . This functional represents the infinite expansion of loops, starting from two loops onwards.

$$\Gamma[\phi, G] = \mathcal{S}[\varphi] + \frac{i}{2}\text{Tr} \left[ \ln G^{-1} + \left( G_{(0)}^{-1} - G^{-1} \right) G \right] - i\Phi[\phi, G]. \quad (2.60)$$

The explicit form of the functional  $\Phi[\phi, G]$  depends on the specific theory under study. For example, for an action given by

$$\mathcal{S}[\varphi] = \int_x \left[ \frac{1}{2}\varphi(x)iG_{(0)}^{-1}\varphi(x) - \frac{g^2}{4!}V_4^{(0)}\varphi^4(x) \right], \quad (2.61)$$

the expansion up to three-loop  $\mathcal{O}(g^4)$  [75, 90] is

$$\Phi[\phi, G] = \frac{g^2}{2}G^2V_4^{(0)} + \frac{g^4}{24}G^4V_4^{(0)2} + \dots \quad (2.62)$$

$$\Phi[\phi, G] = \text{Diagram 1} + \text{Diagram 2} + \dots$$

Figure 2.8: Diagrammatic representation of the 2PI effective action  $\Phi[\phi, G]$  given in Eq. (2.62).

where  $g$  is the coupling of the quartic interaction  $V_4$  and  $G$  is the propagator. The diagrammatic representation for this expansion is given in Fig. 2.8, where the diagrams are constructed from closed loops containing the full propagators and the bare vertices [75, 90, 93].

The equation for the propagator, in this formalism, is derived from Eq. (2.57), resulting in [90]

$$G^{-1} = G_{(0)}^{-1} - 2i \frac{\delta\Phi[\phi, G]}{\delta G} \Big|_0, \quad (2.63)$$

where the second term represents the self-energy which is diagrammatically represented in the Fig. 2.9.

$$\frac{\delta\Phi[\phi, G]}{\delta G} = \text{Diagram 1} + \text{Diagram 2} + \dots$$

Figure 2.9: Derivative of the 2PI effective action with respect of the propagator, produces the SDE for the  $G$  propagator in the 2PI formalism.

The advantage of working with the 2PI effective action is that the Legendre transformation with respect to the additional source  $K$  makes this functional explicitly dependent on the full propagator [63, 75]. This approach allows for a complete and self-consistent description of the propagators through the stationary conditions in Eq. (2.57). However, for higher-order Green's functions or  $n$ -point vertices, the 2PI effective action becomes less efficient, as it generally contains (bare) *classical vertices*.

The generalization is achieved by introducing external sources, denoted by  $K_3, \dots, K_n$ , which correspond to the  $n$ -point vertices  $V_3, \dots, V_n$ , respectively [75]. Thus, the functional

generator is

$$Z[J, K, K_3, \dots] = \exp(iW[J, K, K_3, \dots]) , \quad (2.64)$$

with the definitions of the *vev* of the field, propagator and the  $n$ -point functions

$$\begin{aligned} \frac{\delta W}{\delta J_i} &= \phi_i , \\ \frac{\delta W}{\delta K_{ij}} &= \frac{1}{2} (\phi_i \phi_j + iG_{ij}) , \\ \frac{\delta W}{\delta K_{3,ijk}} &= \frac{1}{6} (V_{3,ijk} + iG_{ij}\phi_k + iG_{jk}\phi_i + iG_{ki}\phi_j + \phi_i\phi_j\phi_k) , \\ &\vdots \end{aligned} \quad (2.65)$$

and thus we define the  $n$ PI effective action as the Legendre transformation with respect to all sources,

$$\begin{aligned} \Gamma[\phi, G, V_3, \dots] &= W[J, K, K_3, \dots] - \int_x \frac{\delta W}{\delta J_i(x)} J_i(x) - \int_{x,y} \frac{\delta W}{\delta K_{ij}(x,y)} K_{ij}(x,y) \\ &\quad - \int_{x,y,z} \frac{\delta W}{\delta K_{3,ijk}(x,y,z)} K_{3,ijk}(x,y,z) - \dots \end{aligned} \quad (2.66)$$

The resulting effective action  $\Gamma[\phi, G, V_3, \dots]$  depends explicitly on the propagators and complete  $n$ -point vertices. Analogous to Eq. (2.60), it can be written exactly as an infinite loop expansion, now, in terms of the complete vertices.

$$\Gamma[\phi, G, V_3, \dots] = S[\phi] + \frac{i}{2} \text{Tr} \left[ \ln G^{-1} + \left( G_{(0)}^{-1} - G^{-1} \right) G \right] - i\Phi[\phi, G, V_3, \dots] . \quad (2.67)$$

Introducing additional source terms to the functional generator does not change the information we can obtain from the theory; it only alters the method of treatment. All effective actions obtained in this manner are equivalent,

$$\Gamma[\phi] = \Gamma[\phi, G] = \Gamma[\phi, G, V_3] = \Gamma[\phi, G, V_3, V_4] = \dots \quad (2.68)$$

On the other hand, when the truncation of the effective action is performed, as in the loop expansion where we choose which loop to calculate, the equivalence in Eq. (2.68) is no longer true. However, what is established is a hierarchy of equivalence for each order of the expansion [63, 75],

$$\begin{aligned} \Gamma^{(1\text{-loop})}[\phi] &= \Gamma^{(1\text{-loop})}[\phi, G] = \dots \\ \Gamma^{(2\text{-loop})}[\phi] &\neq \Gamma^{(2\text{-loop})}[\phi, G] = \Gamma^{(2\text{-loop})}[\phi, G, V_3] = \dots \\ \Gamma^{(3\text{-loop})}[\phi] &\neq \Gamma^{(3\text{-loop})}[\phi, G] \neq \Gamma^{(3\text{-loop})}[\phi, G, V_3] = \Gamma^{(3\text{-loop})}[\phi, G, V_3, V_4] = \dots \\ &\vdots \end{aligned} \quad (2.69)$$

where  $\Gamma^{(n\text{-loop})}$  is the approximation for the effective action at the  $n$ -loop order, in the

absence of sources. This means that in a two-loop approximation, all  $n$ PI effective actions are equivalent to each other with  $n > 2$ , indicating that the 2PI effective action is sufficient to capture a complete and self-consistent description up to the second order of the expansion. However, for a three-loop approximation, a self-consistent description requires up to the 3PI effective action, and so on.

The vertices of  $n$ -dressed points are treated as functional variables, and the  $n$ PI effective action is constructed so that each of these quantities satisfies its own equations of motion, *i.e.*, Eq. (2.46).

$$\left. \frac{\delta\Gamma[\phi, G, V_3, \dots]}{\delta\phi} \right|_0 = \left. \frac{\delta\Gamma[\phi, G, V_3, \dots]}{\delta G} \right|_0 = \left. \frac{\delta\Gamma[\phi, G, V_3, \dots]}{\delta V_3} \right|_0 = \dots = 0.$$

In summary, the major advantage of the  $n$ PI method is that it provides a systematic expansion where truncation occurs at the action level. This approach allows obtaining a closed set of equations for each complete Green's function. In contrast, SDEs offer an infinite hierarchy of coupled integral equations and require truncation through additional approximations. Next, we apply the  $n$ PI formalism and calculate the equation defining the quark-gluon vertex in 3PI, performing the three-loop expansion.

### 2.4.2 The quark-gluon vertex from 3PI effective action

Using the method discussed in the previous section, the 3PI effective action for a non-Abelian theory is computed in [75] up to the three-loop level of the expansion. Starting from the QCD action  $\mathcal{S}_{QCD}$ , the 3PI effective action is defined in terms of the propagators and vertices of the theory  $\Gamma[\phi, G, V_3]$ , in this notation,

$$\phi = (\psi^{\text{cl}}, A_{\mu,a}^{\text{cl}}, c_a^{\text{cl}}), \quad (2.70)$$

are the *vevs* for the quark, gluon, and ghost fields, which will be omitted here, as at the end of the derivation, the sources are turned off and these classical fields becomes zero,

$$\begin{aligned} G &= (S, \Delta, D), \\ V_3 &= (V_q, V_{3g}, V_{gh}), \end{aligned} \quad (2.71)$$

are the full propagators for the quark, gluon, and ghost, as well as the full triple vertices for quark-gluon, three-gluon, and ghost-gluon interactions, respectively. We utilize the hierarchies from Eq.(2.70) in the three-loop expansion to derive the relation

$$\Gamma[G, V_3] = \Gamma[G, V_3, V_4]. \quad (2.72)$$

Thus, we aim to incorporate the four-gluon vertex into the description, which, as we will see in the three-loop calculation, remains identical to its tree-level. The expansion of the effective action follows the same pattern as Eq.(2.67).

$$\Gamma[G, V_3, V_4] = \mathcal{S}_{QCD} + ic\text{Tr} \left[ \ln G^{-1} + \left( G_{(0)}^{-1} - G^{-1} \right) G \right] - i\Phi[G, V_3, V_4], \quad (2.73)$$

where  $c$  is a constant that is  $1/2$  for bosons and  $-1$  for fermions. We can rewrite it as the sum of the one-loop term and the rest of the series

$$\Gamma[G, V_3, V_4] = \Gamma^{1\text{-loop}}[G, V_3, V_4] - i\Phi[G, V_3, V_4], \quad (2.74)$$

where

$$\begin{aligned} \Gamma^{1\text{-loop}}[G, V_3, V_4] = \mathcal{S}_{QCD} + \frac{i}{2}\text{Tr} \ln \Delta^{-1} + \frac{i}{2}\text{Tr} \Delta_{(0)}^{-1} \Delta - i\text{Tr} \ln S^{-1} - i\text{Tr} S_{(0)}^{-1} S \\ - i\text{Tr} \ln D^{-1} - i\text{Tr} D_{(0)}^{-1} D, \end{aligned} \quad (2.75)$$

and the effective action at two-loop is given by [43, 75]

$$\begin{aligned} \Phi[D, V_3, V_4] = & -\frac{1}{8}g^2\Delta^2V_4^{(0)} + \frac{i}{6}g^2\Delta^3V_{3g}V_{3g}^{(0)} - ig^2\Delta S^2V_qV_q^{(0)} - ig^2\Delta D^2V_{gh}V_{gh}^{(0)} \\ & - \frac{i}{12}g^2\Delta^3V_{3g}^2 + \frac{i}{2}g^2\Delta S^2V_q^2 + \frac{i}{2}g^2\Delta D^2V_{gh}^2 + \frac{i}{24}g^4\Delta^4V_4V_4^{(0)} \\ & + \frac{1}{8}g^4\Delta^5V_{3g}^2V_4^{(0)} - \frac{i}{48}g^4\Delta^4V_4^2 - \frac{i}{24}g^4\Delta^6V_{3g}^4 + \frac{i}{3}g^4\Delta^3S^3V_q^3V_{3g} \\ & + \frac{i}{3}g^4\Delta^3D^3V_{gh}^3V_{3g} + \frac{i}{4}g^4\Delta^2S^4V_q^4 + \frac{i}{4}g^4\Delta^2D^4V_{gh}^4 + \mathcal{O}(g^6). \end{aligned} \quad (2.76)$$

In terms of loop diagrams, this expression can be represented diagrammatically as shown in Fig. 2.10.

In particular, the stationary condition for the quartic vertex in the absence of sources leads to

$$\left. \frac{\delta\Gamma[D, V_3, V_4]}{\delta V_4} \right|_0 = \left. \frac{\delta\Phi[D, V_3, V_4]}{\delta V_4} \right|_0 = 0 \Rightarrow V_4 = V_4^{(0)}. \quad (2.77)$$

This implies that in three-loops, the 4PI effective action describes only complete Green's functions up to 3-points. To include quartic vertices, we would need to truncate the action at the four-loop level.

To obtain the quark-gluon vertex equation, we use the equations of motion that the vertex satisfies in the absence of sources

$$\left. \frac{\delta\Gamma[D, V_3, V_4]}{\delta V_q} \right|_0 = 0. \quad (2.78)$$

Note that not all diagrams contribute to the calculation involving the quark-gluon vertex; only four of them are relevant, which are represented in Figure 2.11

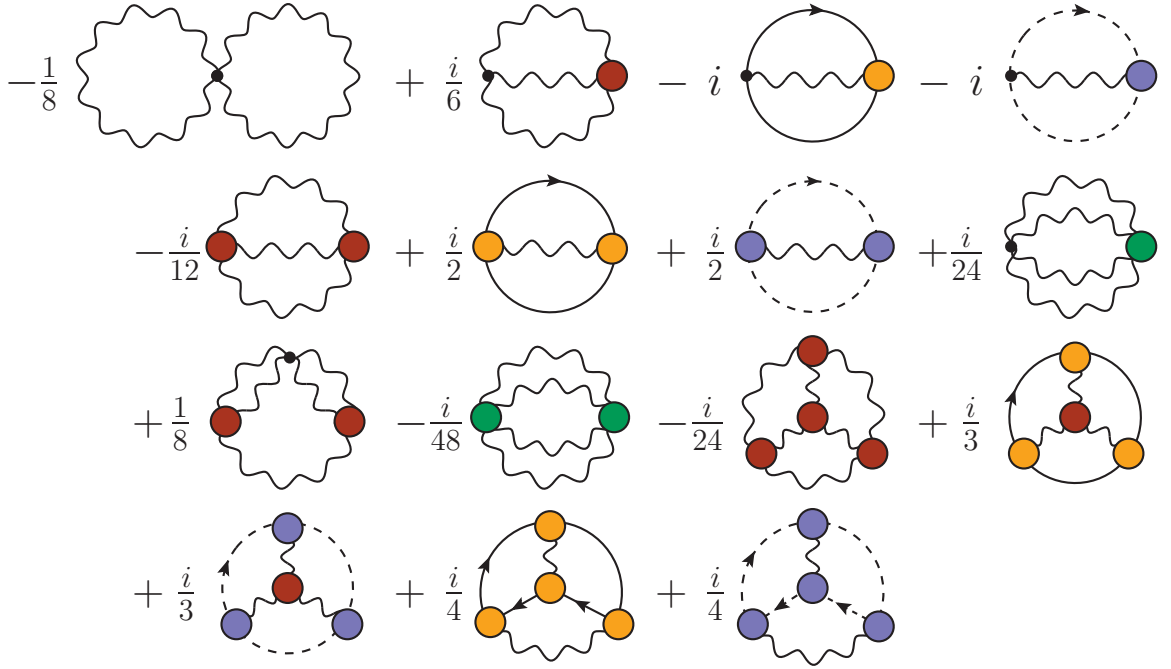


Figure 2.10: Diagrammatic representation of 3PI effective action at three-loop order for QCD given in Eq. (2.76). All propagators are dressed as well the vertices: quark-gluon (orange), ghost-gluon (purple), three-gluon (red), four-gluon (green) [43, 75].

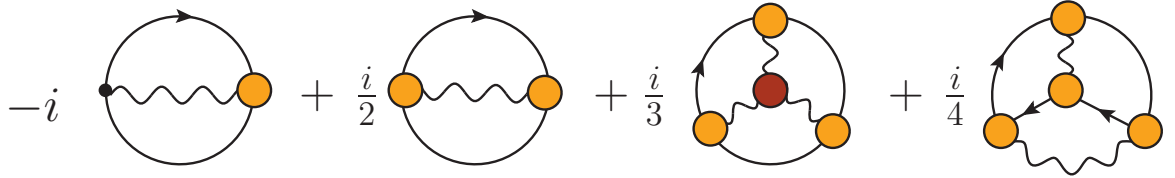


Figure 2.11: Non-trivial terms of the 3PI effective action, Eq. (2.76) for the quark-gluon vertex SDE [43, 75].

and we attain

$$\begin{aligned} \frac{\delta\Gamma[D, V_3, V_4]}{\delta V_q} \Big|_0 &= \frac{\delta\Phi[D, V_3, V_4]}{\delta V_q} \Big|_0 = 0, \\ \Rightarrow -ig^2 V_q^{(0)} + ig^2 V_q + ig^4 \Delta S^2 V_q^3 + ig^4 \Delta^2 S V_q^2 V_{3g} &= 0. \end{aligned} \quad (2.79)$$

Therefore,

$$V_q = V_q^{(0)} - g^2 \Delta S^2 V_q^3 - g^2 \Delta^2 S V_q^2 V_{3g}. \quad (2.80)$$

Expressing in our standard notation, we identify the following quantities as

$$\begin{aligned} S &\rightarrow S(p^2), & V_q^{(0)} &\rightarrow igt^a \Gamma_\mu^{(0)}(q, p_2, -p_1), & V_{3g} &\rightarrow f^{abc} \Pi_{\alpha\mu\nu}(r, p, q), \\ \Delta &\rightarrow \delta^{ab} \Delta_{\mu\nu}(q), & V_q &\rightarrow igt^a \Gamma_\mu(q, p_2, -p_1). \end{aligned} \quad (2.81)$$

Finally, by representing Eq. (2.80) in momentum space and in our notation, we arrive

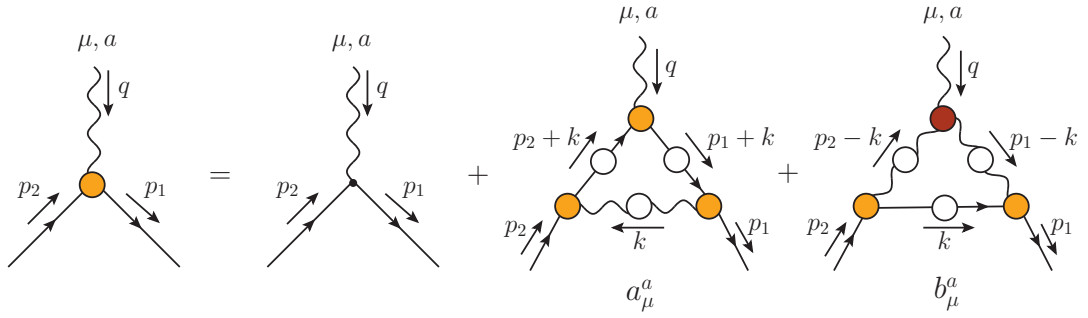


Figure 2.12: Diagrammatic representation of the SDE for quark-gluon vertex in the 3PI formalism.

in Fig. 2.12, where we show the diagrammatic representation of the SDE for the quark-gluon vertex in the 3PI formalism, whose expression is given by

$$\mathbb{\Gamma}_\mu(q, p_2, -p_1) = \Gamma_\mu^{(0)} + a_\mu(q, p_2, -p_1) + b_\mu(q, p_2, -p_1), \quad (2.82)$$

where  $a_\mu(q, p_2, -p_1)$  and  $b_\mu(q, p_2, -p_1)$  are the contributions expressed as,

$$\begin{aligned} a_\mu(q, p_2, -p_1) &= \kappa_a \int_k \Delta_{\rho\nu}(k) \mathbb{\Gamma}^\nu(-k, k_1, -p_1) S(k_1) \mathbb{\Gamma}_\mu(q, k_2, -k_1) S(k_2) \mathbb{\Gamma}^\rho(k, p_2, -k_2), \\ b_\mu(q, p_2, -p_1) &= \kappa_b \int_k \Delta_{\alpha\nu}(\ell_1) \Delta_{\beta\rho}(\ell_2) \mathbb{\Gamma}_{\mu\alpha\beta}(q, \ell_1, -\ell_2) \mathbb{\Gamma}^\nu(-\ell_1, k, -p_1) S(k) \mathbb{\Gamma}^\rho(\ell_2, p_2, -k), \end{aligned} \quad (2.83)$$

whose momentum configuration is given according to Fig. 2.12 and for compactness, we define color theoretical factors as

$$\kappa_a = -ig^2 \left( C_F - \frac{C_A}{2} \right), \quad \kappa_b = ig^2 \frac{C_A}{2}. \quad (2.84)$$

where we employ the following relations

$$\left( C_F - \frac{C_A}{2} \right) t^a = t^b t^a t^b, \quad it^a \frac{C_A}{2} = t^b f^{bca} t^c. \quad (2.85)$$

Notice that  $C_F$  and  $C_A$  denote the eigenvalues of the Casimir operator in the fundamental and adjoint representations, respectively [ $C_F = (N^2 - 1)/2N$  and  $C_A = N$  for  $SU(N)$ ].

Additionally, we introduce the notation for the momenta

$$\begin{aligned} k_1 &= p_1 + k, & \ell_1 &= k - p_1, \\ k_2 &= p_2 + k, & \ell_2 &= k - p_2. \end{aligned} \quad (2.86)$$

Note that this equation is not renormalized yet; so far, we have only dealt with unrenormalized quantities. The renormalization process will be carried out in the next chapter, where we will further analyze Eq. (2.82). We can anticipate that the equation in the 3PI formalism will bring us advantages in renormalization procedure, since within the

---

integrals there are only dressed quantities which will combine creating renormalization group invariant (RGI) products, therefore only the bare vertex,  $\Gamma_\mu^{(0)}$ , will be multiplied by a renormalization constant.

---

# Chapter 3

## The quark-gluon vertex

In the previous chapter, we introduced the functional method employed to study the nonperturbative regime of QCD: the SDEs in the 3PI formalism. We derived the quark SDE as an application of master equation and we outlined its connection with dynamical mass generation, in which the quark-gluon vertex is engaging in this process. Then, we presented the SDE for the quark-gluon vertex derived from the 3PI formalism, which we will explore further in this chapter. Therefore, this chapter will focus on the central objective of the work: *the nonperturbative structure of the transversely projected quark-gluon vertex*.

The chapter is structured as follows. We begin by defining the general notations and main elements that will be used throughout this work. Next, we present the transversely projected quark-gluon vertex, focusing on its tensor structure. We then elaborate on a few features of its most general tensorial structure in general kinematics. Finally, we examine its SDE truncated in the 3PI formalism, establishing its connection with the tensor decomposition. In this process, we derive a set of projectors which we will allow us to express the form factors of this vertex as a coupled system of integrals equation. We conclude the chapter discuss in details the renormalization procedure of this system of equations, setting the stage for the numerical treatment in the next chapter.

### 3.1 The transversely projected quark-gluon vertex

The full quark-gluon vertex, represented diagrammatically in Fig. 3.1, is a three-point Green's function comprising quark, antiquark, and gluon fields.

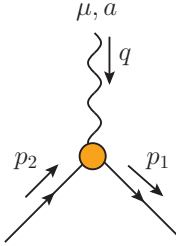
$$\mathbb{\Gamma}_\mu^a(q, p_2, -p_1) =$$


Figure 3.1: Diagrammatic representation of the full quark-gluon vertex,  $\mathbb{\Gamma}_\mu^a(q, p_2, -p_1)$ , defined in Eq. (3.1). This momenta convention will be used throughout the article.

The quark-gluon vertex possesses two indices: one for its color structure and another for its Lorentz (or tensor) structure. The latter can be decomposed in Minkowski space as a function of the the two independent momenta associated with its legs. By factoring out the color structure  $t^a$ , we can separate the Minkowski space from the color space,

$$\mathbb{\Gamma}_\mu^a(q, p_2, -p_1) = ig t^a \mathbb{\Gamma}_\mu(q, p_2, -p_1), \quad (3.1)$$

we also take the opportunity to factor out an  $i$  and the coupling constant  $g$ , allowing us to focus solely on the tensor structure without additional complications.

Note that in Fig. 3.1, and in Eq. (3.1) a specific convention is adopted with respect to the order of the arguments of this function: the gluon momentum  $q$  is listed first, followed by the quark momentum  $p_2$ , and lastly the antiquark momentum  $-p_1$ . Momentum conservation imposes  $q + p_2 - p_1 = 0$ , which means that we have two independent momenta, whereas the third one can be expressed in term of the other two.

Regarding the color structure,  $t^a$  (with  $a = 1, 2, \dots, N^2 - 1$ ) are matrices that denote the generators of the group  $SU(N)$  in the fundamental representation. These matrices are Hermitian and traceless, and they are responsible for generating the closed algebra, *i.e.*,

$$[t^a, t^b] = i f^{abc} t^c. \quad (3.2)$$

In the case of  $SU(3)$ , the group generators  $t^a$  are the Gell-Mann matrices  $\lambda^a$ , with  $t^a = \lambda^a/2$ , as mentioned in Chapter 1.

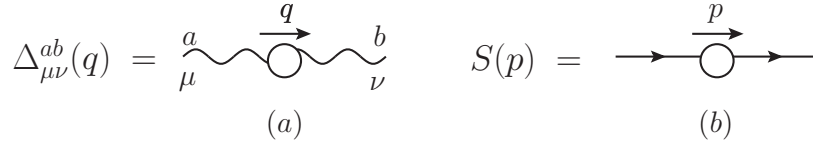


Figure 3.2: Diagrammatic representations of: (a) the fully dressed gluon propagator,  $\Delta_{\mu\nu}^{ab}(q)$ ; (b) the complete quark propagator,  $S(p)$ .

At tree-level, the quark-gluon vertex simplifies to a Dirac matrix.

$$\Gamma_{\mu}^{(0)}(q, p_2, -p_1) = \gamma_{\mu}. \quad (3.3)$$

The central goal of this work is the transversely projected quark-gluon vertex, which is defined as the contraction of the transverse projector, carrying the gluon momentum, with the vertex, *i.e.*,

$$\bar{\Pi}_{\mu}(q, p_2, -p_1) = P_{\mu\nu}(q)\Pi^{\nu}(q, p_2, -p_1), \quad (3.4)$$

where the transverse projection  $P_{\mu\nu}(q)$  is

$$P_{\mu\nu}(q) = g_{\mu\nu} - \frac{q_{\mu}q_{\nu}}{q^2}. \quad (3.5)$$

The tree-level transversely projected vertex, denoted by  $\bar{\Gamma}_{\mu}^{(0)}(q, p_2, -p_1)$ , is obtained from Eq. (3.4) through the substitution  $\Pi_{\mu}(q, p_2, -p_1) \rightarrow \Gamma_{\mu}^{(0)}(q, p_2, -p_1)$ .

Moreover, our analysis will involve other elements such as the gluon and quark propagators and the three-gluon vertex.

In the *Landau gauge* that we employ, the gluon propagator,  $\Delta_{\mu\nu}^{ab}(q) = -i\delta^{ab}\Delta_{\mu\nu}(q)$ , is fully transverse, *i.e.*,

$$\Delta_{\mu\nu}(q) = P_{\mu\nu}(q)\Delta(q^2), \quad \Delta(q^2) = \mathcal{Z}(q^2)/q^2, \quad (3.6)$$

where  $\Delta(q^2)$  denotes the scalar component of the gluon propagator and  $\mathcal{Z}(q^2)$  the corresponding dressing function. The diagrammatic representation of  $\Delta_{\mu\nu}(q)$  is given in panel (a) of Fig. 3.2,

In addition, we denote by  $S(p)$  the quark propagator [see panel (b) of Fig. 3.2], whose standard decomposition in terms of the functions  $A(p^2)$  and  $B(p^2)$ , or equivalently, in terms of the dynamical quark mass function  $\mathcal{M}(p^2)$ , is given by Eq. (2.41)

$$S^{-1}(p) = A(p^2)\not{p} - B(p^2) = A(p^2) [\not{p} - \mathcal{M}(p^2)]. \quad (3.7)$$

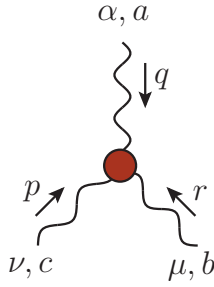
$$\Gamma_{\alpha\mu\nu}^{abc}(q, r, p) =$$


Figure 3.3: Diagrammatic representation of the full three-gluon vertex,  $\Gamma_{\alpha\mu\nu}^{abc}(q, r, p)$ .

At tree-level,

$$S_{(0)}^{-1}(p) = \not{p} - m, \quad (3.8)$$

such that  $A^{(0)} = 1$  and  $B^{(0)} = m$ , where  $m$  is the current quark mass.

Finally, we introduce the three-gluon vertex,  $\Gamma_{\alpha\mu\nu}^{abc}(q, r, p) = gf^{abc}\mathbb{\Gamma}_{\alpha\mu\nu}(q, r, p)$ , depicted in Fig. 3.3. At tree-level,  $\mathbb{\Gamma}_{\alpha\mu\nu}(q, r, p)$  reduces itself to the standard expression

$$\Gamma_{\alpha\mu\nu}^{(0)}(q, r, p) = g_{\mu\nu}(r - p)_\alpha + g_{\alpha\nu}(p - q)_\mu + g_{\alpha\mu}(q - r)_\nu. \quad (3.9)$$

In our analysis, the three-gluon vertex is naturally contracted by three transverse projectors, namely

$$\bar{\mathbb{\Gamma}}_{\alpha\mu\nu}(q, r, p) = P_\alpha^{\alpha'}(q)P_\mu^{\mu'}(r)P_\nu^{\nu'}(p)\mathbb{\Gamma}_{\alpha'\mu'\nu'}(q, r, p). \quad (3.10)$$

### 3.1.1 General tensorial structure

The quark-gluon vertex exhibits a complex tensor structure. As mentioned above, this Green's function depends on the two independent momenta associated with its legs, and at tree-level, it simplifies to the Dirac matrix, as given by Eq. (3.3). By Lorentz invariance, it is possible to construct a basis consisting of twelve independent Lorentz tensors, allowing the quark-gluon vertex to be expressed as [47, 95],

$$\mathbb{\Gamma}^\mu(q, p_2, -p_1) = \sum_{i=1}^{12} f_i(q, p_2, -p_1)t_i^\mu, \quad (3.11)$$

each tensor  $t_i^\mu$  is associated with a scalar function  $f_i(q, p_2, -p_1)$ , known as the *form-factor*, which depends on the three momenta that parameterize the vertex.

We can construct a naive basis, the simplest basis, for the quark-gluon vertex through

combinations involving  $\gamma^\mu$ ,  $p_2^\mu$ ,  $q^\mu$  with the matrices  $\mathbb{I}$ ,  $\not{p}_2$ ,  $\not{q}$  and  $\not{p}_2\not{q}$ . Following this, the basic tensor structures can be expressed as follows [47, 95],

$$\begin{aligned} t_1^\nu &= \gamma^\nu, & t_4^\nu &= \gamma^\nu \not{p}_2, & t_7^\nu &= \gamma^\nu \not{q}, & t_{10}^\nu &= \gamma^\nu \not{p}_2 \not{q}, \\ t_2^\nu &= p_2^\nu, & t_5^\nu &= p_2^\nu \not{p}_2, & t_8^\nu &= p_2^\nu \not{q}, & t_{11}^\nu &= p_2^\nu \not{p}_2 \not{q}, \\ t_3^\nu &= q^\nu, & t_6^\nu &= q^\nu \not{p}_2, & t_9^\nu &= q^\nu \not{q}, & t_{12}^\nu &= q^\nu \not{p}_2 \not{q}. \end{aligned} \quad (3.12)$$

The advantage of this basis system lies in the simplicity of its elements. However, the trade-off for these straightforward structures is that the basis tensors are not free from kinematic singularities. A more sophisticated basis, which are free from such singularities, can be obtained from combinations of these twelve elements considering desired features.

The tensor structure we will employ is divided into longitudinal  $\Pi_\mu^L$  and transverse  $\Pi_\mu^T$  parts [47, 95, 96],

$$\Pi_\mu(q, p_2, -p_1) = \Pi_\mu^L(q, p_2, -p_1) + \Pi_\mu^T(q, p_2, -p_1), \quad (3.13)$$

the longitudinal basis consists of four structures, whereas the transverse part comprises eight.

In the literature, the most widely adopted basis for studying the quark-gluon vertex is the generalized Ball-Chiu basis [33, 57, 59, 96–98], initially developed for QED. This basis is well-suited for exploring the longitudinal structure using the Slavnov-Taylor identity (STI) [33, 59, 97–99]. However, the part that is of particular interest to us—the transverse part—remains undetermined by this method. To access the transverse part, we will employ the basis proposed in [60, 64, 78].

This basis, denoted by  $\tau_i^\mu$ , comprises eight independent tensor structures, which are given by

$$\begin{aligned} \tau_1^\nu(p_2, -p_1) &= \gamma^\nu, & \tau_2^\nu(p_2, -p_1) &= (p_1 + p_2)^\nu, \\ \tau_3^\nu(p_2, -p_1) &= (\not{p}_1 + \not{p}_2)\gamma^\nu, & \tau_4^\nu(p_2, -p_1) &= (\not{p}_1 - \not{p}_2)\gamma^\nu, \\ \tau_5^\nu(p_2, -p_1) &= (\not{p}_1 - \not{p}_2)(p_1 + p_2)^\nu, & \tau_6^\nu(p_2, -p_1) &= (\not{p}_1 + \not{p}_2)(p_1 + p_2)^\nu, \\ \tau_7^\nu(p_2, -p_1) &= -\frac{1}{2}[\not{p}_1, \not{p}_2]\gamma^\nu, & \tau_8^\nu(p_2, -p_1) &= -\frac{1}{2}[\not{p}_1, \not{p}_2](p_1 + p_2)^\nu. \end{aligned} \quad (3.14)$$

The set of twelve basis elements is given by the transverse and longitudinal projections of the elements of Eq. (3.14), where the longitudinal projector is defined as  $P_{\mu\nu}^L(q) = g_{\mu\nu} - P_{\mu\nu}(q)$ ,

$$\{P_{\mu\nu}(q)\tau_i^\nu, P_{\mu\nu}^L(q)\tau_{\{1,2,6,8\}}^\nu\}, \quad (3.15)$$

and in this case, the transversal part coincides with the vertex transversely projected,  $\mathbb{\Pi}_\mu^T \equiv \overline{\mathbb{\Pi}}_\mu$ . Then  $\overline{\mathbb{\Pi}}_\mu(q, p_2, -p_1)$  can be decomposed in terms of eight independent tensors which in Minkowski space are written as

$$\overline{\mathbb{\Pi}}_\mu(q, p_2, -p_1) = \sum_{i=1}^8 \lambda_i(q, p_2, -p_1) P_{\mu\nu}(q) \tau_i^\nu(p_2, -p_1), \quad (3.16)$$

where  $\lambda_i(q, p_2, -p_1)$  denotes the scalar form factors, which depend on three Lorentz scalars. Specifically, in Euclidean space, the scalars are two square momenta and an angle, and  $\tau_i^\nu(p_2, -p_1)$  are the tensors given by Eq. (3.14).

One property that  $\overline{\mathbb{\Pi}}_\mu(q, p_2, -p_1)$  must obey is charge conjugation, the same transformation property as the tree-level vertex [47, 95].

$$C \overline{\mathbb{\Pi}}_\mu(q, p_2, -p_1) C^{-1} = -\overline{\mathbb{\Pi}}_\mu^T(q, -p_1, p_2), \quad (3.17)$$

Under the charge conjugation condition, Eq. (3.17), interchanging the momenta  $p_1 \leftrightarrow -p_2$  in the basis defined in Eq. (3.14) and using the fact that

$$C \gamma_\mu C^{-1} = -\gamma_\mu^T, \quad C[\gamma_\mu, \gamma_\nu] C^{-1} = [\gamma_\nu^T, \gamma_\mu^T], \quad (3.18)$$

we find that

$$\begin{aligned} C \tau_i^\nu(p_2, -p_1) C^{-1} &= -[\tau_i^\nu(-p_1, p_2)]^T, \quad i = 1, 2, 4, 6, 8, \\ C \tau_3^\nu(p_2, -p_1) C^{-1} &= [\tau_3^\nu(-p_1, p_2)]^T - 2[\tau_2^\nu(-p_1, p_2)]^T, \\ C \tau_5^\nu(p_2, -p_1) C^{-1} &= [\tau_5^\nu(-p_1, p_2)]^T, \\ C \tau_7^\nu(p_2, -p_1) C^{-1} &= -[\tau_7^\nu(-p_1, p_2)]^T - [\tau_5^\nu(-p_1, p_2)]^T, \end{aligned} \quad (3.19)$$

where we have already canceled all terms proportional to  $q^\nu$ , which will vanish when contracted with  $P_{\mu\nu}(q)$ . Therefore to satisfy Eq. (3.17), we find that

$$\begin{aligned} \lambda_i(q, p_2, -p_1) &= \lambda_i(q, -p_1, p_2), \quad i = 1, 4, 6, 7, 8, \\ \lambda_2(q, p_2, -p_1) + 2\lambda_3(q, p_2, -p_1) &= \lambda_2(q, -p_1, p_2), \\ \lambda_3(q, p_2, -p_1) &= -\lambda_3(q, -p_1, p_2), \\ \lambda_5(q, p_2, -p_1) - \lambda_7(q, p_2, -p_1) &= -\lambda_5(q, -p_1, p_2). \end{aligned} \quad (3.20)$$

To conclude this section, it is useful to classify the tensor basis into two subsets based on their properties with respect to chiral symmetry. In the Sec. 1.1.1, we have discussed the concept of chiral symmetry and stated that the necessary condition for preserving this symmetry is given by Eq. (1.22)

$$\{\gamma_5, \overline{\mathbb{\Pi}}^\mu\} = 0. \quad (3.21)$$

When this condition is violated, chiral symmetry is broken. Therefore, it follows that for tensor structures with an odd number of  $\gamma$  matrices, the above condition is satisfied, and they form the chiral symmetry (CS) subset  $\tau_{cs}$ . Conversely, tensors with an even number of  $\gamma$  matrices break chiral symmetry and thus belong to the chiral symmetry breaking (CSB) subset  $\tau_{csb}$  [57, 63]. Consequently, we have

$$\tau_{cs} = \{\tau_1^\nu, \tau_5^\nu, \tau_6^\nu, \tau_7^\nu\}, \quad \tau_{csb} = \{\tau_2^\nu, \tau_3^\nu, \tau_4^\nu, \tau_8^\nu\}. \quad (3.22)$$

More specifically, one finds that the quark functions  $A(p^2)$  and  $B(p^2)$  from Eq. (3.23) will be given by

$$\begin{aligned} A(p^2) &= 1 - \frac{C_F g^2}{4p^2} \int_k \frac{\Delta(q^2)}{k^2 A^2(k^2) - B^2(k^2)} \left\{ A(k^2) \left[ f_1^A \lambda_1(q, k, -p) + f_5^A \lambda_5(q, k, -p) + \right. \right. \\ &\quad \left. \left. f_6^A \lambda_6(q, k, -p) + f_7^A \lambda_7(q, k, -p) \right] + B(k^2) \left[ f_2^A \lambda_2(q, k, -p) + f_3^A \lambda_3(q, k, -p) + \right. \right. \\ &\quad \left. \left. f_4^A \lambda_4(q, k, -p) + f_8^A \lambda_8(q, k, -p) \right] \right\}, \\ B(p^2) &= m + \frac{C_F g^2}{4} \int_k \frac{\Delta(q^2)}{k^2 A^2(k^2) - B^2(k^2)} \left\{ A(k^2) \left[ f_2^B \lambda_2(q, k, -p) + f_3^B \lambda_3(q, k, -p) + \right. \right. \\ &\quad \left. \left. f_4^B \lambda_4(q, k, -p) + f_8^B \lambda_8(q, k, -p) \right] + B(k^2) \left[ f_1^B \lambda_1(q, k, -p) + f_5^B \lambda_5(q, k, -p) + \right. \right. \\ &\quad \left. \left. f_6^B \lambda_6(q, k, -p) + f_7^B \lambda_7(q, k, -p) \right] \right\}, \end{aligned} \quad (3.23)$$

where  $f_i^{A(B)}$  are kinematic functions that depends on the momenta  $p$  and  $k$ , and can be found at the github [100]. It is evident, from Eq. (3.23), that the form factors naturally separate into their respective subsets—either chiral symmetry-preserving (CS) or chiral symmetry breaking (CSB)—within the expressions for the quark functions  $A(p^2)$  and  $B(p^2)$ .

## 3.2 The SDE for the quark-gluon vertex

As discussed in the previous chapter, solving SDEs is generally feasible only after implementing some form of truncation. In this work, we employ the SDE formulation for the quark-gluon vertex, derived within the framework of the 3PI effective action [94, 101] truncated at three-loop level [43, 57, 75–77, 102].

In the  $n$ PI formalism, the SDE for a given Green's function is obtained through the functional differentiation with respect to this  $n$ -point function in question, as it was shown in the section 2.4.1. For the particular case of the 3PI effective action, the relevant SDEs are derived from the set of diagrams shown in Fig. 2.11 [43, 75]. At this level of

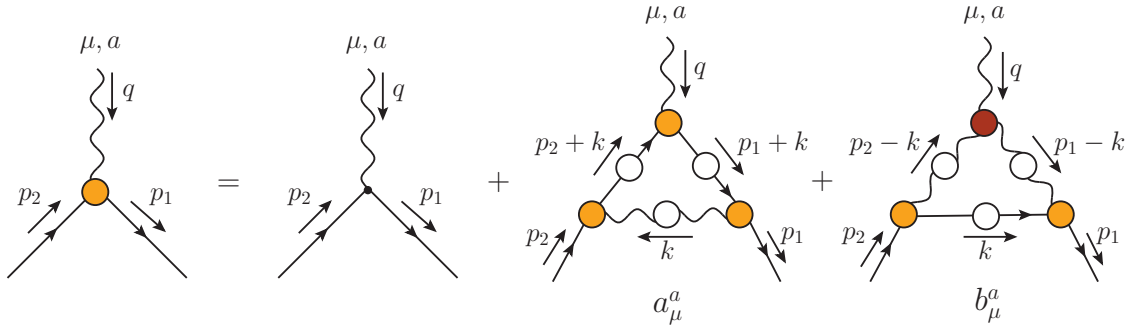


Figure 3.4: Diagrammatic representation of the SDE for the full quark-gluon vertex,  $\Gamma_\mu^a(q, p_2, -p_1)$ , derived from the 3PI effective action at the three-loop level. White circles denote full gluon and quark propagators, the orange (red) circles denote the fully dressed quark-gluon (three-gluon)-vertices.

approximation, all propagators (gluon, ghost, and quark) comprising this action are fully dressed, as well as the quark-gluon and three-gluon vertices (the tree-point function); instead, the four-gluon vertex (four point function) is kept at its tree-level.

Focusing on the quark-gluon vertex, the corresponding SDE is diagrammatically depicted in Fig. 3.4. The diagram  $a_\mu^a$  has the same structure observed in Abelian theories like QED, while the diagram  $b_\mu^a$  is restricted to non-Abelian theories, due to the self-interaction of the gauge boson, which in our case takes the form of the three-gluon vertex. Consequently, these contributions are referred to as Abelian and non-Abelian diagrams, respectively. In particular, the transversely projected quark-gluon vertex, defined in Eq. (3.4), can be expressed in terms of these contributions as

$$\bar{\Gamma}_\mu(q, p_2, -p_1) = \bar{\Gamma}_\mu^{(0)}(q, p_2, -p_1) + \bar{a}_\mu(q, p_2, -p_1) + \bar{b}_\mu(q, p_2, -p_1), \quad (3.24)$$

where the transverse projections of  $a_\mu$  and  $b_\mu$  diagrams are defined as

$$\bar{a}_\mu(q, p_2, -p_1) = P_{\mu\nu}(q)a^\nu(q, p_2, -p_1), \quad \bar{b}_\mu(q, p_2, -p_1) = P_{\mu\nu}(q)b^\nu(q, p_2, -p_1). \quad (3.25)$$

After performing the color algebra and Lorentz contractions, the corresponding contributions in Minkowski space are given by

$$\begin{aligned} \bar{a}_\mu(q, p_2, -p_1) &= \kappa_a \int_k \Delta(k^2) \bar{\Gamma}^\alpha(-k, k_1, -p_1) S(k_1) \bar{\Gamma}_\mu(q, k_2, -k_1) S(k_2) \bar{\Gamma}_\alpha(k, p_2, -k_2), \\ \bar{b}_\mu(q, p_2, -p_1) &= \kappa_b \int_k \Delta(\ell_1^2) \Delta(\ell_2^2) \bar{\Gamma}_{\mu\alpha\beta}(q, \ell_1, -\ell_2) \bar{\Gamma}^\alpha(-\ell_1, k, -p_1) S(k) \bar{\Gamma}^\beta(\ell_2, p_2, -k), \end{aligned} \quad (3.26)$$

where we have already defined the momenta combinations  $k_1$ ,  $k_2$ ,  $\ell_1$ , and  $\ell_2$  in Eq. (2.86). In addition, we have also introduced the group-theoretic factors  $\kappa_a$  and  $\kappa_b$  in Eq. (2.84),

and the integration measure in Eq. (2.40).

### 3.2.1 Form factors from the SDE

In what follows, we will establish the connection between Eqs. (3.16) and (3.24), which allow us to derive the dynamical equations governing the form factors  $\lambda_i(q, p_2, -p_1)$  in general kinematics.

The approach is to construct a set of projectors  $\mathcal{P}_i^\mu(q, p_2, -p_1)$  that, when applied to the Eqs. (3.16), isolate each form factor [65]. To do that, first observe that with respect to the basis of Eq. (3.14), these projectors must satisfy the basic property

$$\text{Tr} [\mathcal{P}_i^\mu(q, p_2, -p_1) P_{\mu\nu}(q) \tau_j^\nu(p_2, -p_1)] = \delta_{ij}, \quad (3.27)$$

such that the trace of the contraction with the vertex of Eqs. (3.16) yields the form factors

$$\lambda_i(q, p_2, -p_1) = \text{Tr} [\mathcal{P}_{i\mu}(q, p_2, -p_1) \bar{\Gamma}^\mu(q, p_2, -p_1)]. \quad (3.28)$$

The construction of the projectors  $\mathcal{P}_i^\mu$  can be achieved by expressing them in the form

$$\mathcal{P}_i^\mu(q, p_2, -p_1) = \sum_{j=1}^8 C_{ij}(p_2, -p_1) \tau_j^\mu(p_2, -p_1), \quad (3.29)$$

where the coefficients  $C_{ij}$  are obtained imposing Eq. (3.27) and solving the resulting system. This yields

$$\begin{aligned} \mathcal{P}_1^\mu &= c_1 [4h\tau_1^\mu + r^2\tau_5^\mu - q^2\tau_6^\mu], & \mathcal{P}_5^\mu &= c_2 [4h(r^2\tau_1^\mu - 2\tau_7^\mu) + (3r^4 + 4h)\tau_5^\mu - 3r^2q^2\tau_6^\mu], \\ \mathcal{P}_2^\mu &= c_1 [q^2(\tau_2^\mu + \tau_3^\mu) - r^2\tau_4^\mu], & \mathcal{P}_6^\mu &= -c_2 [4hq^2\tau_1^\mu + 3q^2(r^2\tau_5^\mu - q^2\tau_6^\mu)], \\ \mathcal{P}_3^\mu &= c_1 [q^2(\tau_2^\mu - \tau_3^\mu) + r^2\tau_4^\mu], & \mathcal{P}_7^\mu &= -2c_1 [\tau_5^\mu + 2\tau_7^\mu], \\ \mathcal{P}_4^\mu &= c_1 [r^2(\tau_3^\mu - \tau_2^\mu) - (p_1 + p_2)^2\tau_4^\mu - 2\tau_8^\mu], & \mathcal{P}_8^\mu &= -4c_2 [2h\tau_4^\mu + 3q^2\tau_8^\mu], \end{aligned} \quad (3.30)$$

to keep a compact notation, the arguments of the  $\mathcal{P}_i^\mu$  and  $\tau_i^\mu$  are omitted, and we introduced the definitions

$$r^2 = p_1^2 - p_2^2, \quad h = p_1^2 p_2^2 - (p_1 \cdot p_2)^2, \quad c_1 = 1/32h, \quad c_2 = 1/128h^2. \quad (3.31)$$

Contracting the above projectors,  $\mathcal{P}_i^\mu$  with the SDE of Eq. (3.24), one can derive the individual dynamical equations for the eight form factors  $\lambda_i(q, p_2, -p_1)$ . To that end, it is convenient to denote by  $\mathbb{A}_i$  and  $\mathbb{B}_i$  the contributions arising from the contraction of the projectors  $\mathcal{P}_i^\mu$ , with the diagrams  $a_\mu$  and  $b_\mu$ , shown in Fig. (3.4), respectively. More

specifically, one has

$$\begin{aligned}\delta_{i1} &= \text{Tr} \left[ \mathcal{P}_i^\mu(q, p_2, -p_1) P_{\mu\nu}(q) \gamma_\mu \right], \\ \mathbb{A}_i(q, p_2, -p_1) &= \text{Tr} \left[ \mathcal{P}_{i\mu}(q, p_2, -p_1) \bar{a}^\mu(q, p_2, -p_1) \right], \\ \mathbb{B}_i(q, p_2, -p_1) &= \text{Tr} \left[ \mathcal{P}_{i\mu}(q, p_2, -p_1) \bar{b}^\mu(q, p_2, -p_1) \right].\end{aligned}\quad (3.32)$$

Then, using Eqs. (3.27), (3.24), and (3.32) it is straightforward to arrive in the following coupled system of eight integral equations

$$\lambda_i(q, p_2, -p_1) = \delta_{i1} + \mathbb{A}_i(q, p_2, -p_1) + \mathbb{B}_i(q, p_2, -p_1), \quad i = 1, \dots, 8. \quad (3.33)$$

### 3.2.2 Renormalized form factors

Now, we proceed to the renormalization of the SDE for the quark-gluon vertex. Up to this point, all quantities discussed so far are unrenormalized. All Green's functions appearing in Eq. (3.24) are all bare. To convert to their renormalized counterparts, we employ the standard relations,

$$\begin{aligned}\Delta_R(q^2) &= Z_A^{-1} \Delta(q^2), \quad S_R(p) = Z_F^{-1} S(p), \quad g_R = Z_g^{-1} g, \\ \mathbb{\Pi}_R^{\alpha\mu\nu}(q, r, p) &= Z_3 \mathbb{\Pi}^{\alpha\mu\nu}(q, r, p), \quad \mathbb{\Pi}_R^\mu(q, p_2, -p_1) = Z_1 \mathbb{\Pi}^\mu(q, p_2, -p_1),\end{aligned}\quad (3.34)$$

where the subscript “ $R$ ” denotes renormalized quantities, and  $Z_A$ ,  $Z_F$ ,  $Z_1$ ,  $Z_3$ , and  $Z_g$  are the corresponding renormalization constants, which are related to each other through the STIs, which impose that

$$Z_g^{-1} = Z_1^{-1} Z_A^{1/2} Z_F = Z_3^{-1} Z_A^{3/2}. \quad (3.35)$$

By substituting all quantities in Eq. (3.24) with their renormalized counterparts from Eq. (3.34), and applying Eq. (3.35), we obtain the renormalized version of the SDE Eq. (3.24), expressed as

$$\bar{\mathbb{\Pi}}_R^\mu(q, p_2, -p_1) = Z_1 \bar{\mathbb{\Gamma}}_{(0)}^\mu(q, p_2, -p_1) + \bar{a}_R^\mu(q, p_2, -p_1) + \bar{b}_R^\mu(q, p_2, -p_1). \quad (3.36)$$

Then renormalized equation for the form factors, akin to Eq. (3.33), can be readily derived, namely

$$\lambda_{i,R}(q, p_2, -p_1) = Z_1 \delta_{i1} + \mathbb{A}_{i,R}(q, p_2, -p_1) + \mathbb{B}_{i,R}(q, p_2, -p_1), \quad i = 1, \dots, 8. \quad (3.37)$$

Since all vertices in the diagrams  $\bar{a}^\mu$  and  $\bar{b}^\mu$  are fully dressed, no renormalization constants appear multiplying them in Eq. (3.36). The only renormalization constant that remains in Eq. (3.36) is  $Z_1$ , which multiplies the tree-level contribution. This converts

the renormalization process from a multiplicative to a subtractive one, a key advantage of the 3PI formulation [43, 77, 102], resulting in significant operational simplification.

To determine  $Z_1$ , we use the  $\widetilde{\text{MOM}}$  scheme [103], a variant of the momentum subtraction (MOM) scheme. Specifically, the prescription for the classical form factor  $\lambda_1$  requires it to be evaluated in the soft-gluon limit, where the gluon momentum approaches zero ( $q \rightarrow 0$ ). In this limit, we denote  $\lambda_1^{sg}(p^2) = \lambda_1(0, p, -p)$ . This particular scheme is defined by the following prescriptions

$$\Delta_R^{-1}(\mu^2) = \mu^2, \quad A_R(\mu^2) = 1, \quad \lambda_{1,R}^{sg}(\mu^2) = 1. \quad (3.38)$$

To implement this condition in Eq. (3.37), we consider the case  $i = 1$  and take the limit  $q \rightarrow 0$ . Using the notation  $f(0, p, -p) = f(p^2)$ , we obtain

$$\lambda_{1,R}^{sg}(p^2) = Z_1 + \mathbb{A}_{1,R}^{sg}(p^2) + \mathbb{B}_{1,R}^{sg}(p^2), \quad (3.39)$$

Then, by imposing the renormalization condition of Eq. (3.38), we find

$$Z_1 = 1 - \mathbb{A}_{1,R}^{sg}(\mu^2) - \mathbb{B}_{1,R}^{sg}(\mu^2). \quad (3.40)$$

Thus, substituting Eq. (3.40) into Eq. (3.37), we arrive at the renormalized version of Eq. (3.37), namely

$$\lambda_{i,R}(q, p_2, -p_1) = [1 - \mathbb{A}_{i,R}^{sg}(\mu^2) - \mathbb{B}_{i,R}^{sg}(\mu^2)]\delta_{i1} + \mathbb{A}_{i,R}(q, p_2, -p_1) + \mathbb{B}_{i,R}(q, p_2, -p_1). \quad (3.41)$$

From now on, the index ‘‘R’’ will be suppressed to reduce notational clutter.

The SDEs in Eq. (3.41) constitute the main equation of this work and will be solved under certain simplifying assumptions, which we discuss in detail in the next chapter.

---

# Chapter 4

## Numerical analysis of the quark-gluon vertex

As presented in the previous chapter, our approach to studying the nonperturbative behavior of the quark-gluon vertex involves decomposing it into a basis where each element is associated with a form factor. These form factors can then be determined by acting a set of projectors on the SDE, resulting in a coupled system of eight integral equations formulated in Minkowski space [see Eq. (3.41)]. This chapter is dedicated to numerically solving these equations.

To achieve this, the chapter is organized as follows: first, we introduce some approximations in Eq. (3.41) for the transversely projected three-gluon and quark-gluon vertices that appear internally in the loop diagrams, significantly reducing the complexity of our problem. Next, we convert our final equation from Minkowski to Euclidean space to facilitate numerical treatment. This conversion transforms the four-dimensional integral into a more manageable form in hyperspherical coordinates. Then, we provide our numerical inputs, which basically consist of fits for the quark and gluon lattice propagators, as well as the three-gluon form factor lattice data.

Finally, we present all our results for the quark-gluon form factors. We start with the results obtained from solving the integral equation for the classical (tree-level) form factor,  $\lambda_1$ , followed by the seven non-classical form factors in general kinematics. Additionally, we provide a thorough analysis of the angular dependence of all form factors and compare our results with the lattice data available in the literature.

## 4.1 Quark-gluon vertex SDE in Euclidean space

Before converting the form factors into Euclidean space, some simplifications must be stated. We observe that Eq. (3.33) provides a system of eight coupled integral equations, where  $\bar{\Pi}_\mu$  appears on both sides. To reduce the algebraic complexity of this system, we approximate all transversely projected quark-gluon vertices appearing on the right hand side by retaining only their classical tensorial structures. Specifically, we set

$$\bar{\Pi}_\mu(q, p_2, -p_1) \rightarrow \lambda_1(q, p_2, -p_1) P_{\mu\nu}(q) \gamma^\nu. \quad (4.1)$$

Notice that implementing this approximation leads to two major simplifications:

1. The dynamical equation for the classical form factor,  $\lambda_1(q, p_2, -p_1)$ , decouples from the seven remaining form factors;
2. The equation for the remaining form factors,  $\lambda_i(q, p_2, -p_1)$  for  $i \neq 1$ , are expressed in terms of only  $\lambda_1$ .

Therefore,  $\lambda_1(q, p_2, -p_1)$  is described by an integral equation, whereas the remaining  $\lambda_i(q, p_2, -p_1)$  are expressed as ordinary integrals that requires the form factor  $\lambda_1$  as input.

Regarding the three-gluon vertex, we retain only its tree-level tensor structure and employ the recent planar degeneracy approximation for the associated form factor, which has been validated by a series of studies [66, 69–71]. Specifically, the planar degeneracy ensures that  $\bar{\Pi}^{\alpha\mu\nu}(q, \ell_1, \ell_2)$  can be accurately approximated by the compact form

$$\bar{\Pi}^{\mu\alpha\beta}(q, \ell_1, \ell_2) = L_{sg}(s^2) \bar{\Gamma}_{(0)}^{\mu\alpha\beta}(q, \ell_1, \ell_2), \quad s^2 = \frac{1}{2}(q^2 + \ell_1^2 + \ell_2^2), \quad (4.2)$$

where  $\bar{\Gamma}_{(0)}^{\mu\alpha\beta}(q, \ell_1, \ell_2) = P_{\mu'}^\mu(q) P_{\alpha'}^\alpha(\ell_1) P_{\beta'}^\beta(\ell_2) \Gamma_{(0)}^{\mu'\alpha'\beta'}(q, \ell_1, \ell_2)$ , with  $\Gamma_{(0)}^{\mu\alpha\beta}$  denoting the three-gluon vertex at tree-level given by Eq. (3.9). The function  $L_{sg}(s^2)$  is the three-gluon form factor in the the soft-gluon limit *i.e.*, ( $q = 0, \ell_1 = -\ell_2$ ), which has been determined in various lattice simulations [69, 104–109].

The transition from Minkowski to Euclidean space is achieved through Wick rotation, where the time component of four-vectors takes on imaginary values, *i.e.*,

$$q = (q_0, \mathbf{q}) \rightarrow q_E = (iq_0, \mathbf{q}), \quad (4.3)$$

where  $q_0$  denotes the time and  $\mathbf{q}$  the spatial components of the four-vector. The index “E” indicates that this quantity is represented in Euclidean space. Simultaneously, the metric

reduces to the Kronecker delta in 4D,  $g_{\mu\nu} \rightarrow \delta_{\mu\nu}$ , which implies that,

$$q^2 \rightarrow -q_E^2 \quad \text{and} \quad (k \cdot q) \rightarrow -(k_E \cdot q_E). \quad (4.4)$$

The integration measure defined by Eq. (2.40) changes correspondingly,

$$\int_k \rightarrow i \int_{k_E}. \quad (4.5)$$

The integral measure in hyperspherical coordinates is given by

$$i \int_{k_E} \rightarrow \frac{i}{16\pi^3} \int = \frac{i}{16\pi^3} \int_0^\infty dz z \int_0^\pi d\phi_1 s_{\phi_1}^2 \int_0^\pi d\phi_2 s_{\phi_2}, \quad (4.6)$$

where  $s_{\phi_i} := \sin \phi_i$ .

The structure of the Clifford algebra should be preserved; therefore, the Dirac matrices  $\gamma^\mu$  transform slightly differently from the four-vectors,

$$\gamma^0 \rightarrow \gamma_E^4 \quad \text{and} \quad \gamma^j \rightarrow i\gamma_E^j. \quad (4.7)$$

Contractions between four-vectors and Dirac matrices acquire a factor of  $i$ , *i.e.*,

$$\not{q} \rightarrow i\not{q}_E. \quad (4.8)$$

We must state, additionally, the conversion for scalar functions to Euclidean space, such as propagators functions and the form factor of the three-gluon vertex,

$$\Delta_E(q_E^2) = -\Delta(-q_E^2), \quad A_E(q_E^2) = A(-q_E^2), \quad B_E(q_E^2) = B(-q_E^2), \quad L_{sg}^E(q_E^2) = L_{sg}(-q_E^2). \quad (4.9)$$

In hyperspherical coordinates, it is convenient to express all relevant form factors as functions of the squared momenta,  $p_1^2$  and  $p_2^2$ , and the angle  $\theta^1$ . Therefore, in what follows, we will adopt the following notation

$$\lambda_i(q, p_2, -p_1) \rightarrow \lambda_i(p_1^2, p_2^2, \theta). \quad (4.10)$$

After applying the aforementioned simplifications to Eq. (3.41), we convert it to Euclidean space and obtain

$$\begin{aligned} \lambda_i(x, y, \theta) = & Z_1 \delta_{i1} - \frac{\alpha_s}{24\pi^2} \int \mathcal{K}_A^i \Delta(z) \lambda_1(x, u, \theta_1) \lambda_1(v, y, \theta_2) \lambda_1(u, v, \theta_{12}) \\ & + \frac{3\alpha_s}{8\pi^2} \int \mathcal{K}_B^i L_{sg}(r) \Delta(w) \Delta(t) \lambda_1(z, y, \pi - \phi) \lambda_1(x, z, \pi - \phi_1), \end{aligned} \quad (4.11)$$

where  $\mathcal{K}_A^i$  and  $\mathcal{K}_B^i$  are the kernels originating from the diagrams (a) and (b) respectively of Fig. (3.4), and associated with the index  $i$  of the form factor  $\lambda_i$ , and  $\alpha_s(\mu^2) \equiv g^2/4\pi$ . The explicit form of these kernels for each  $\lambda_i$  can be found on GitHub [100]. From this point forward, we will omit the subscript ‘‘E’’ that denotes quantities in Euclidean space.

---

<sup>1</sup>The angle  $\theta$  is defined as the angle between the quark  $p_2$  and the antiquark  $-p_1$ .

Since we will not return to Minkowski space, this will not lead to any ambiguity.

In the above equation, we introduced the auxiliary variables

$$\begin{aligned} x &= p_1^2, & y &= p_2^2, & z &= k^2, & u &= k_1^2, & v &= k_2^2, & w &= \ell_1^2, & t &= \ell_2^2, \\ r &= s^2, & p_1 \cdot p_2 &= \sqrt{xy}c_\theta, & p_1 \cdot k &= \sqrt{xz}c_{\phi_1}, & p_2 \cdot k &= \sqrt{yz}c_\phi, \end{aligned} \quad (4.12)$$

and  $c_\phi = c_\theta c_{\phi_1} + s_\theta s_{\phi_1} c_{\phi_2}$ , where  $c_\theta := \cos \theta$  and  $s_\theta := \sin \theta$ , and  $\theta_1, \theta_2$ , and  $\theta_{12}$  the angles

$$c_{\theta_1} = -\frac{\sqrt{x} + \sqrt{z}c_{\phi_1}}{\sqrt{u}}, \quad c_{\theta_2} = -\frac{\sqrt{y} + \sqrt{z}c_{\phi_1}}{\sqrt{v}}, \quad c_{\theta_{12}} = -\frac{\sqrt{xy}c_\theta + \sqrt{zy}c_\phi + \sqrt{zx}c_{\phi_1} + z}{\sqrt{uv}}. \quad (4.13)$$

Moreover, the renormalization constant,  $Z_1$ , is obtained from Eq. (3.40), through the exact limit of Eq. (4.11) when  $i = 1$  setting  $q = 0$ , or  $|p_1| = |p_2| = p$ , and  $\theta = 0$ , for each diagram. More specifically, from Eq. (3.39), which we repeat here for convenience, one finds

$$\lambda_1^{sg}(x) = Z_1 + \mathbb{A}_1^{sg}(x) + \mathbb{B}_1^{sg}(x), \quad (4.14)$$

with

$$\begin{aligned} \mathbb{A}_1^{sg}(x) &= -\frac{\alpha_s}{24\pi^2} \int \mathcal{K}_{1\mathbb{A}}^{sg} \Delta(z) \lambda_1^2(x, u, \theta_1) \lambda_1(u, u, \pi), \\ \mathbb{B}_1^{sg}(x) &= \frac{3\alpha_s}{8\pi^2} \int \mathcal{K}_{1\mathbb{B}}^{sg} L_{sg}(w) \Delta^2(w) \lambda_1^2(x, z, \pi - \phi_1), \end{aligned} \quad (4.15)$$

where the kernels  $\mathcal{K}_{1\mathbb{A}}^{sg}$  and  $\mathcal{K}_{1\mathbb{B}}^{sg}$  can be found on GitHub [100].

Then, it follows that  $Z_1$  can be expressed as

$$Z_1 = 1 - \mathbb{A}_1^{sg}(\mu^2) - \mathbb{B}_1^{sg}(\mu^2). \quad (4.16)$$

Thus, the system of equations for the  $\lambda_i$  formed by Eqs. (4.11) and (4.16) are solved treating  $\Delta(q^2)$ ,  $A(p^2)$ ,  $B(p^2)$ , and  $L_{sg}(r^2)$  as external inputs.

## 4.2 Numerical inputs

To numerically solve Eq. (4.11), the first step is to provide the necessary inputs for the integrands. Specifically,  $\Delta(q^2)$ ,  $A(p^2)$ ,  $\mathcal{M}(p^2)$ , and  $L_{sg}(r^2)$  are functions determined by the lattice simulations.

For the form factor  $\lambda_1$ , in general kinematics, we will solve its integral equation iteratively. Once this is accomplished, we can use the result to compute the remaining form factors as ordinary integrals.

In the following, we present the functional forms used to fit the lattice QCD data for

the gluon and quark propagators, as well as the form factor of the three-gluon vertex. These fitting functions utilize common elements, but differ in the specific values assigned to certain parameters. In particular, the adjustment parameters  $\delta$ ,  $\kappa^2$ ,  $\eta_i^2$ , and  $b_i$  will appear across various fits, each with distinct numerical values. The sets of numerical values applied are detailed in Table 4.1. In addition to the parameters, each functional form includes the following definitions in its construction.

$$U(p^2) = 1 + \frac{\ln[(p^2 + \eta^2(p^2))/(\mu^2 + \eta^2(p^2))]}{\ln(\mu^2/\Lambda^2)}, \quad (4.17)$$

where

$$\eta^2(p^2) = \frac{\eta_1^2}{1 + p^2/\eta_2^2}, \quad (4.18)$$

and

$$R(p^2) = \frac{b_0 + p^2/b_1^2}{1 + p^2/b_2^2 + (p^2/b_3^2)^2} - \frac{b_0 + \mu^2/b_1^2}{1 + \mu^2/b_2^2 + (p^2/b_3^2)^2}. \quad (4.19)$$

In our study we will consider lattice QCD data in the unquenched scenario, where quark effects are considered in the simulations.

For the gluon propagator,  $\Delta(p^2)$ , with  $N_f = 2$ , *i.e.*, two degenerate light quarks, we employ a set of lattice data from [110, 111] calculated with a current mass varying between 20 – 50 MeV. In the Fig. 4.1, we show the lattice data for  $\Delta(p^2)$  (left panel) and its dressing function  $\mathcal{Z}(p^2)$  (right panel) together with the functional form that accurately fits this set of data [112] which is given by

$$\Delta^{-1}(p^2) = p^2 \left[ \frac{\delta}{1 + (p^2/\kappa^2)} \ln\left(\frac{p^2}{\mu^2}\right) + U^{d_A}(p^2) \right] + \nu^2 R(p^2), \quad d_A = \frac{39 - 4N_f}{6\beta_0}, \quad (4.20)$$

where  $\beta_0 = 11 - 2N_f/3$  and  $\nu = 1$  GeV is a dimensional parameter that only serves to make  $R(p^2)$  consistent with the dimension of  $\Delta^{-1}(p^2)$ .

Notice that the IR saturation of  $\Delta^{-1}(p^2)$  to a finite, non-zero value can be interpreted as a dynamically generated gluon mass [13, 26].

For the quark propagator expressed in terms of the quark wave function  $A(p^2)$ , and the corresponding dynamical mass  $\mathcal{M}(p^2) = B(p^2)/A(p^2)$ , we employ the setup denominated ‘‘L08’’ which are obtained in the lattice simulation of [55, 113]. This simulation was performed for small current quark mass,  $m_q = 6.2$  MeV, and pion mass,  $m_\pi = 280$  MeV. The functional forms of the fits for  $A(p^2)$  and  $\mathcal{M}(p^2)$  are given by [112]

$$A(p^2) = \frac{T(p^2)}{T(\mu^2)}, \quad T(p^2) = \frac{b_0 + p^2/b_1 + (p^2/\kappa^2)^2}{1 + p^2/b_2 + (p^2/b_3)^2}, \quad (4.21)$$

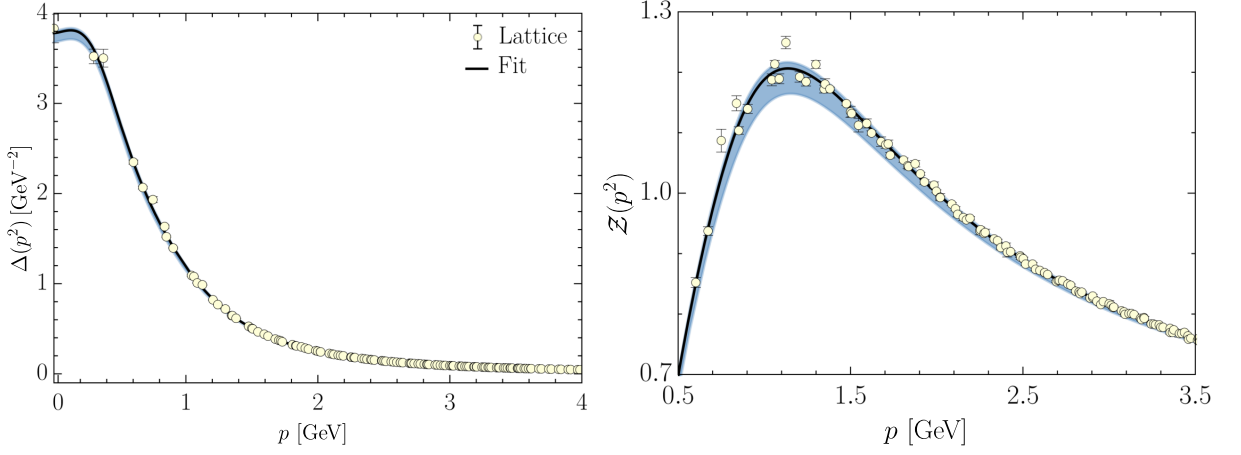


Figure 4.1: Lattice data of [110, 111], with  $N_f = 2$  (points) for the gluon propagator,  $\Delta(p^2)$  and its fit (black solid line) given by Eq. (4.20) [112] (left panel). The gluon dressing function,  $\mathcal{Z}(p^2) = p^2\Delta(p^2)$  (right panel).

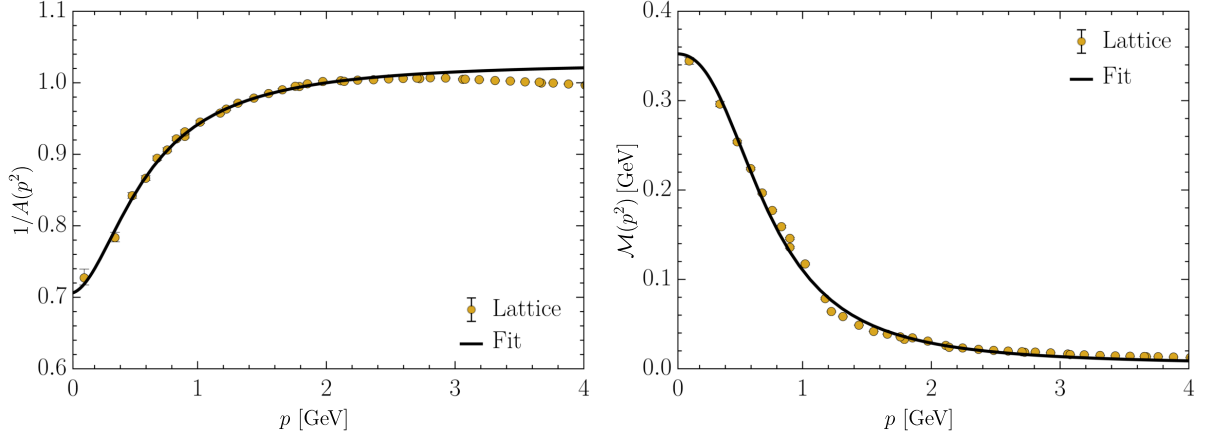


Figure 4.2: Lattice data of [55, 113] corresponding to the L08 step up for the quark wave function,  $1/A(p^2)$ , (left) and running mass,  $\mathcal{M}(p^2)$  (right) and the fits given by Eqs. (4.21) and (4.22) [112].

$$\mathcal{M}(p^2) = \frac{m_0}{1 + (p^2/\kappa^2)^{1+\delta}} + m_q \left[ \frac{1}{2} \ln \left( \frac{p^2 + \eta^2(p^2)}{\Lambda^2 + \eta^2(p^2)} \right) \right]^{-d_{\mathcal{M}}}, \quad d_{\mathcal{M}} = \frac{4}{\beta_0}. \quad (4.22)$$

Note that these functional forms were constructed to eliminate visible artifacts in the UV region of the lattice data and to reproduce the corresponding one-loop resummed perturbative behavior [112]. Both the lattice data and the corresponding fits for  $A(p^2)$  and  $\mathcal{M}(p^2)$  are displayed in Fig. 4.2.

Finally, for the form factor of the three-gluon vertex in soft-gluon limit,  $L_{sg}(p^2)$ , we fit the lattice data obtained from simulations with  $N_f = 2 + 1$ , *i.e.*, two light quark with current mass of 1.3 MeV, and a heavier one with a current mass of 63 MeV [107], since currently there is no available data for  $N_f = 2$  in the literature. However, it is natural

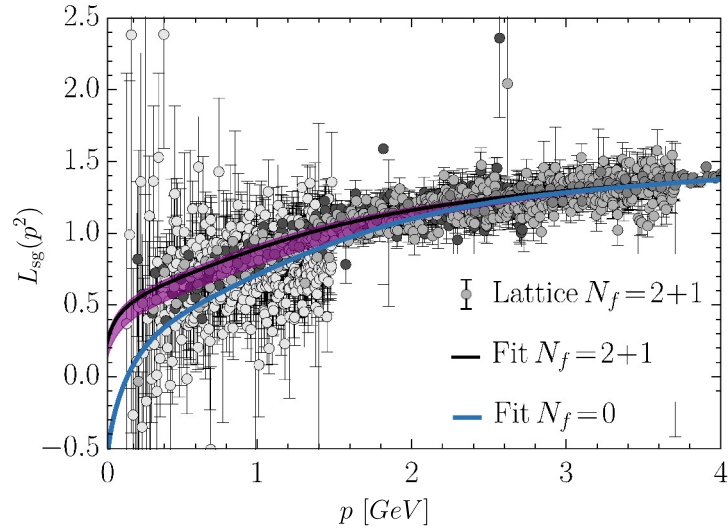


Figure 4.3: Lattice data of for  $L_{sg}(p^2)$  for  $N_f = 2 + 1$  (point) [107] together its fit given by Eq. (4.23) [112] (purple continuous). For the sake of comparison, we show the fit for  $L_{sg}(p^2)$  with  $N_f = 0$  (blue curve) given by Eq. (4.24) [114].

to expect the result of the  $L_{sg}(p^2)$  for  $N_f = 2$  lies between  $N_f = 2 + 1$  and  $N_f = 0$ . The functional form employed to fit the unquenched lattice data [112] is given by

$$L_{sg}(p^2) = 1.16 \left\{ \frac{\delta}{1 + (p^2/\kappa^2)} \ln \left( \frac{p^2}{\mu^2} \right) + U^{d_{3g}}(p^2) + R(p^2) \right\}, \quad d_{3g} = \frac{51 - 8N_f}{12\beta_0}, \quad (4.23)$$

where  $U(p^2)$  and  $R(p^2)$  are given in (4.17) and (4.19). In the Fig. 4.3 we show the lattice data for  $L_{sg}(p^2)$  for  $N_f = 2 + 1$  of [107], and its fit (purple curve) given by Eq. (4.23) [112]. For the sake of comparison, we also show a fit for the quenched,  $N_f = 0$ ,  $L_{sg}(r^2)$  (blue curve) given by [114].

$$L_{sg}(p^2) = \frac{\delta}{1 + (p^2/\kappa^2)} \ln \left( \frac{p^2}{\mu^2} \right) + U^{d_{3g}}(p^2) + R(p^2), \quad d_{3g} = \frac{51 - 8N_f}{12\beta_0}. \quad (4.24)$$

We emphasize that in our analysis, we will explore how modifications on the functional form of  $L_{sg}(p^2)$ , indicated by the purple band, may affect the results of the quark-gluon form factors. Therefore, the modifications that we will implement in the functional form used for the  $L_{sg}(p^2)$  can also be seen as an approximate version of the  $N_f = 2$  case.

It is important to mention that all these inputs are renormalized in the  $\widetilde{\text{MOM}}$  scheme defined by Eq. (3.38), at the renormalization point  $\mu = 2$  GeV. For this particular  $\mu$  we use  $\alpha_s(\mu^2) \equiv g^2/4\pi = 0.55$ ; the estimate of this value was performed [112], by relating the values of the couplings in the Taylor and  $\widetilde{\text{MOM}}$  schemes at one-loop.

	$\delta$	$\kappa^2[\text{GeV}^2]$	$\eta_1^2[\text{GeV}^2]$	$\eta_2^2[\text{GeV}^2]$	$b_0$	$b_1[\text{GeV}^2]$	$b_2[\text{GeV}^2]$	$b_3[\text{GeV}^2]$
$\Delta(q^2)$	0.112	71.8	10.1	0.895	-0.0998	-1.67	0.684	0.321
$A(p^2)$ [L08]	-	0.930	-	-	0.360	0.642	0.175	0.462
$\mathcal{M}(p^2)$ [L08]	0.294	0.520	1.31	13.0	-	-	-	-
$L_{sg}(p^2)$ [Unq]	0.0629	12.3	1.00	1.48	0.102	25.9	1.70	19.0
$L_{sg}(p^2)$ [Que]	0.11	18.2	0.20	6.36	0.241	-0.646	0.310	1.28

Table 4.1: Fitting parameters used for Eqs. (4.20), (4.21), (4.22), and (4.23). For  $\mathcal{M}(p^2)$  we use a current mass of  $m_q = 6.2$  MeV and  $m_0 = 345$  MeV, and we employ  $\Lambda = 610$  MeV.

### 4.3 General results

With all numerical ingredients defined in Section 4.2, now we can proceed to the solution of Eq. (4.11) and present in this section our numerical results for the quark-gluon vertex form factors  $\lambda_i(p_1^2, p_2^2, \theta)$ .

For integrations, we employ a Fortran code and implement a double precision adaptive routine based on Gauss-Kronrod integration rule [115]. The external momenta squared grid range from  $[10^{-3}, 10^3]$   $\text{GeV}^2$  with 30 points. Since our focus is on the IR region, we distribute the grid points logarithmically to ensure a high density of points at low momenta. The external angle grid is distributed across 10 points, ranging from  $\theta = [0, \pi]$ .

In order to obtain  $\lambda_1$  in general kinematics, first, we solve Eq. (4.11) for  $i = 1$  iteratively. Once the results for  $\lambda_1$  are available, they are used as inputs into Eq. (4.11) for  $i = 2, \dots, 8$ , which furnishes all remaining  $\lambda_i$  through a single integration.

For the three-dimensional interpolations of our outputs, we employed a multidimensional B-splines interpolation method [116, 117]. Specifically, we implemented cubic B-splines in our procedure.

#### 4.3.1 Tree-level form factor

In this section, we present the numerical results, obtained from the iterative solution of Eq. (4.11), for the form factor associated with the tree-level structure, the  $\lambda_1(p_1^2, p_2^2, \theta)$ . The results are shown in Fig. 4.4, which is divided into four panels, each representing a 3D surface at a different angle  $\theta$ . Along the diagonals of the surfaces, defined by  $p_1 = p_2$ , special kinematic configurations are identified and summarized below:

1. *The soft-gluon limit:* when the gluon momentum  $q = 0$ . In this configuration  $p_1$

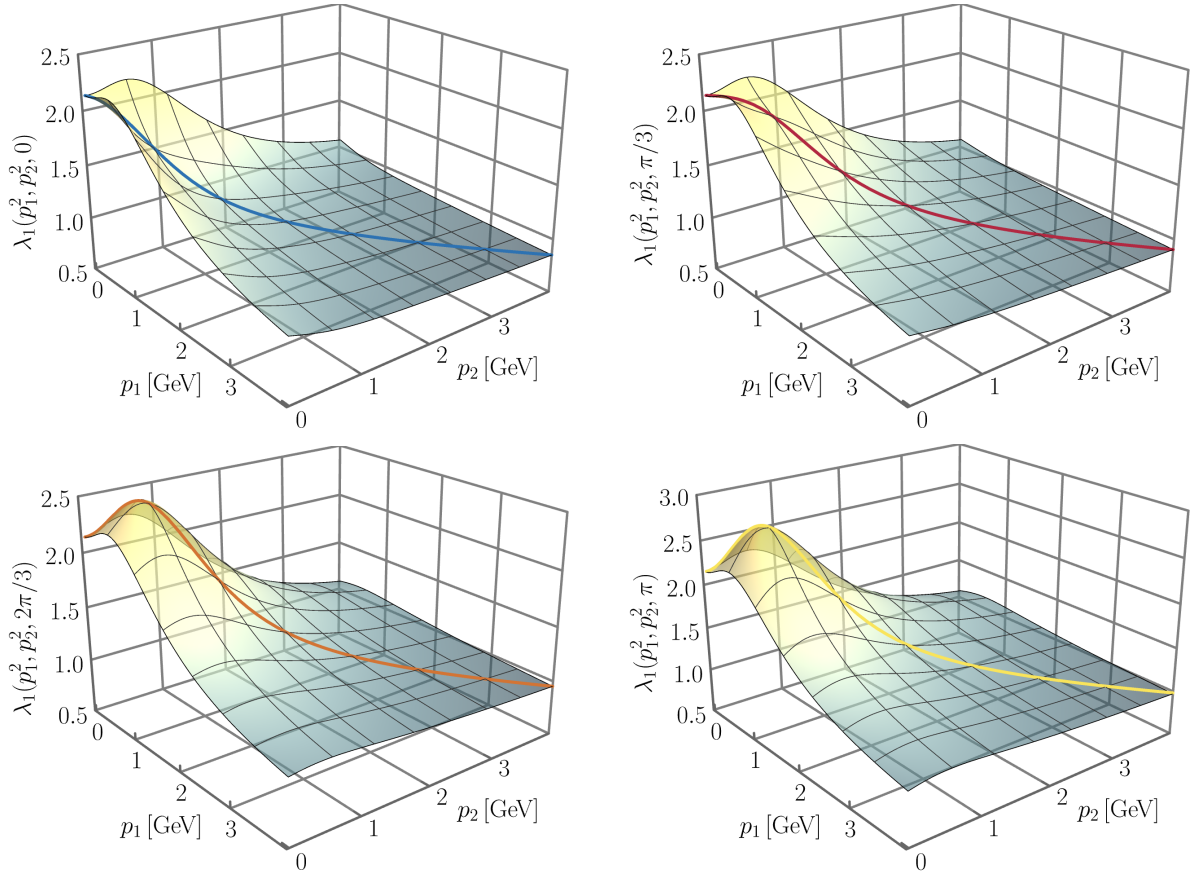


Figure 4.4: The form factor  $\lambda_1(p_1^2, p_2^2, \theta)$  plotted as a function of the antiquark,  $p_1$ , and quark,  $p_2$ , momenta, for fixed angles  $\theta = 0$  (upper left),  $\theta = \pi/3$  (upper right),  $\theta = 2\pi/3$  (lower left), and  $\theta = \pi$  (lower right). Four kinematic limits are highlighted in the diagonals of each of the 3D surfaces: soft-gluon (blue), totally symmetric (red), quark-symmetric (brown), and asymmetric (yellow) configurations.

and  $p_2$  have the same magnitude,  $|p_1| = |p_2| = p$ , and are parallel vectors, *i.e.*, the angle between them is  $\theta = 0$ . We represent this configuration by the blue curve in the upper left panel of Fig. 4.4;

2. *The totally symmetric limit:* when all momenta square are equal  $q^2 = p_1^2 = p_2^2 = p^2$ . In this case, the angle between  $p_1$  and  $p_2$  is  $\theta = \pi/3$ <sup>2</sup>. This limit is shown by the red curve in the upper right panel of Fig. 4.4;
3. *The quark-symmetric limit:* when the momenta square of the quark and antiquark are equal  $p_1^2 = p_2^2$  and  $\theta = 2\pi/3$ . This configuration is depicted by the brown curve in the lower left panel of Fig. 4.4;
4. *The asymmetric limit:* when  $p_1$  and  $p_2$  have the same magnitude,  $|p_1| = |p_2| = p$ ,

<sup>2</sup>Note that the angle is not  $2\pi/3$  since in our convention the anti-quark momentum is outgoing.

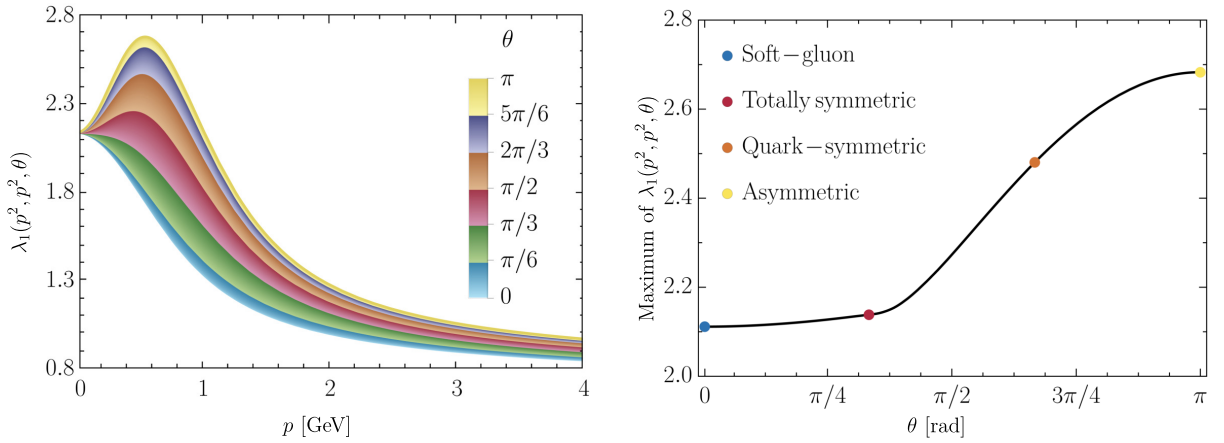


Figure 4.5: *Left panel:* The angular dependence of  $\lambda_1(p_1^2, p_2^2, \theta)$  on  $\theta$ , when we set  $p_1^2 = p_2^2 = p^2$ . *Right panel:* The maximum value  $\lambda_1(p^2, p^2, \theta)$  as function of the angle  $\theta$ .

and are anti-parallel vectors, *i.e.*,  $\theta = \pi$ . This configuration is represented by the yellow curve in the lower right panel of Fig. 4.4.

Note that all configurations exhibit a similar qualitative pattern: in each case, the peak is located in the same momentum region, specifically between 0 and 550 MeV, with moderate differences in their heights. As predicted in [47], the tail of the form factors decreases logarithmically in the UV, eventually recovering its perturbative (tree-level) behavior, when  $\lambda_1 \rightarrow 1$ .

In Fig. 4.5, we explore the angular dependence of  $\lambda_1$ , with the angle varying within the interval  $[0, \pi]$ , for the case when  $p_1^2 = p_2^2 = p^2$ . The figure is divided into two panels: in the left panel, we plot a sequence of diagonal curves,  $\lambda_1(p^2, p^2, \theta)$ , for different values of the angles  $\theta$ . The curves highlighted on the surfaces in Fig. 4.4 are representative examples of this sequence. In the right panel, we plot the corresponding maximum values of  $\lambda_1(p^2, p^2, \theta)$  as a function of the angle  $\theta$ .

With this result, we see that as the angle  $\theta$  increases, the peak of the form factor becomes more pronounced, as shown in the right panel of the figure. For  $\theta = 0$  (lowest curve - blue), we recover the soft-gluon configuration, while for  $\theta = \pi$  (highest curve - yellow), we reach the asymmetric limit, which displays the highest peak. Notably, there is a 27% increase between the maxima of the soft-gluon and asymmetric configurations.

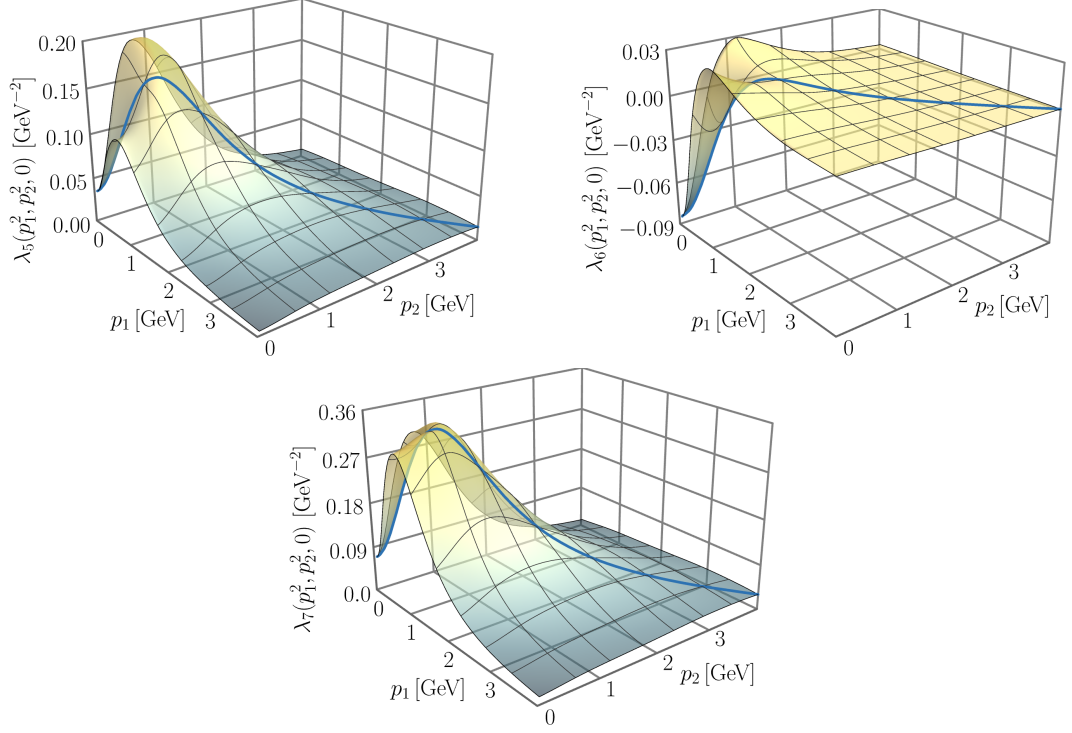


Figure 4.6: The chirally symmetric quark-gluon form factors  $\lambda_i(p_1^2, p_2^2, \theta)$ , with  $i = 5, 6$  (upper row) and  $i = 7$  (lower row) plotted as functions of the magnitudes of the momenta  $p_1$  and  $p_2$ , for a fixed value of the angle,  $\theta = 0$ . The blue curves along the diagonals represent the corresponding soft-gluon limits of each form factor.

### 4.3.2 Remaining form factors

After determining the solution for  $\lambda_1(p_1^2, p_2^2, \theta)$  in general kinematics, the remaining form factors are obtained by solving an ordinary integral given by Eq. (4.11) using the result of  $\lambda_1(p_1^2, p_2^2, \theta)$  as an additional input. We categorize the results for the form factors into chirally symmetric and chirally symmetric breaking form factors, following the division of the basis outlined in Eq. (3.22). The chirally symmetric form factors, shown in Fig. 4.6, include  $\lambda_5$ ,  $\lambda_6$ , and  $\lambda_7$ . The chirally symmetric breaking form factors,  $\lambda_2$ ,  $\lambda_3$ ,  $\lambda_4$ , and  $\lambda_8$ , are displayed in Fig. 4.7. In both figures, each form factor is plotted in terms of the antiquark momentum  $p_1$  and quark momentum  $p_2$ , for a representative angle  $\theta = 0$ .

Initially, note that all the results shown in Figs. 4.6 and 4.7 satisfy the relations derived from charge symmetry outlined in Eq.(3.20). The form factors  $\lambda_4$ ,  $\lambda_6$ ,  $\lambda_7$ , and  $\lambda_8$  are symmetric with respect to the diagonal, which we represent with blue or purple curves. This symmetry becomes apparent in the 3D surfaces only when the form factor  $\lambda_i(p_1^2, p_2^2, \theta)$  is plotted as a function of the momenta  $p_1$  and  $p_2$ . For  $\lambda_2$ , the symmetry with respect to the diagonal is approximately satisfied since  $\lambda_3$  is very small, as shown in

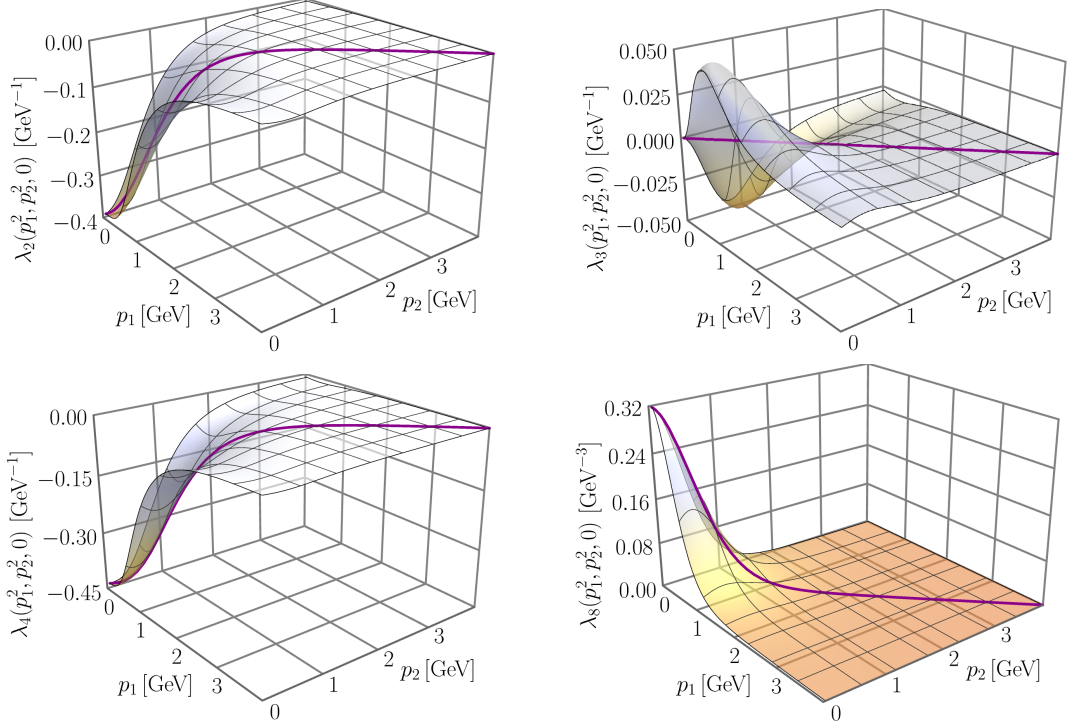


Figure 4.7: The chirally broken quark-gluon form factors  $\lambda_i(p_1^2, p_2^2, \theta)$ , with  $i = 2, 3$  (upper row) and  $i = 4, 8$  (lower row) plotted as functions of the magnitudes of the momenta  $p_1$  and  $p_2$ , for a fixed value of the angle,  $\theta = 0$ . The purple curves along the diagonals represent the corresponding soft-gluon limit of each form factor.

Fig. 4.7. The relation for  $\lambda_5$  is also numerically satisfied.

The continuous curves along the diagonals in these 3D surfaces, depicted in blue or purple, represent the corresponding soft-gluon limit for each form factor, where  $p_1 = p_2$ , or equivalently  $q = 0$ , with the angle fixed at  $\theta = 0$  in all panels. As a general observation, we note that the form factors remain finite in the IR and deviate significantly from their vanishing tree-level values, while gradually aligning with their expected perturbative behavior in the deep UV.

In Fig. 4.8, we plot the angular dependence for all form factors except  $\lambda_3$ , which, though nonvanishing, is heavily suppressed. In each panel, the variation of the angle  $\theta$  forms a band defined by the soft-gluon limit ( $\theta = 0$ ) and the asymmetric limit ( $\theta = \pi$ ), similar to Fig. 4.5 for  $\lambda_1$ . The weakest angular dependence are observed in  $\lambda_2$  and  $\lambda_8$ . The form factors  $\lambda_4$  and  $\lambda_6$  exhibits a slightly stronger dependence on  $\theta$  primarily in the momentum region where  $p \leq 2$  GeV. Finally,  $\lambda_5$  and  $\lambda_7$  show a noticeably stronger dependence across almost the entire momentum range, although still less pronounced than the angular dependence of  $\lambda_1$  shown in Fig. 4.5.

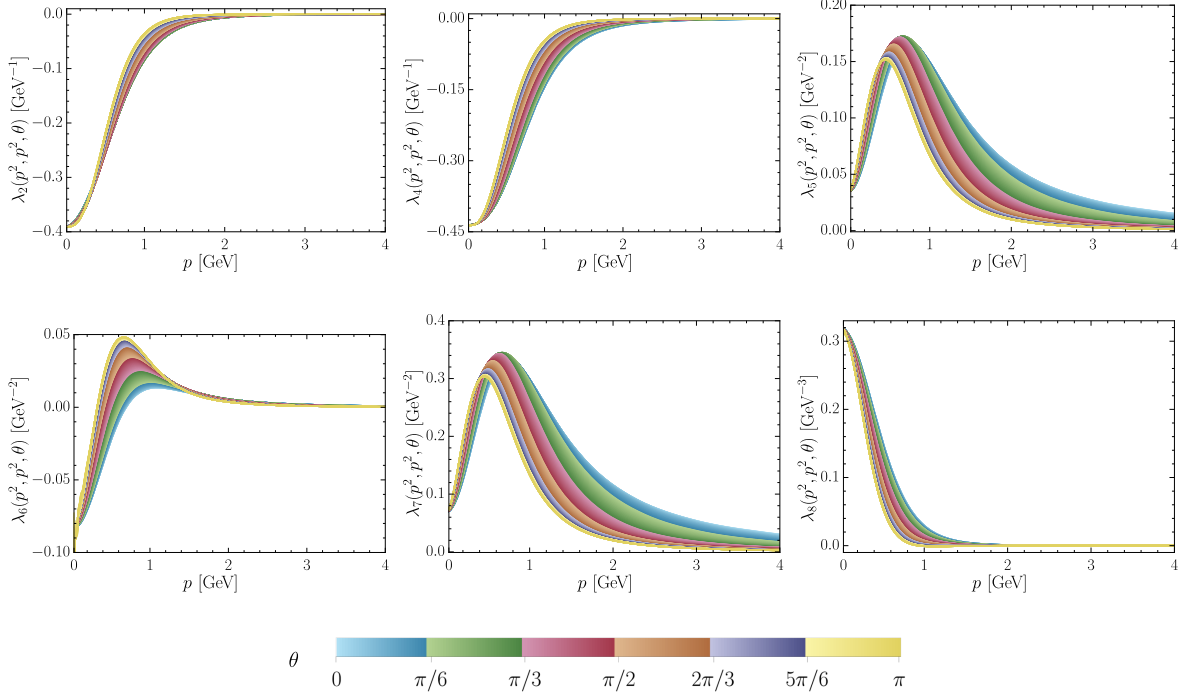


Figure 4.8: The angular dependence of  $\lambda_i(p_1^2, p_2^2, \theta)$  on  $\theta$  for  $i = 2, 4, 5, 6, 7, 8$ , when we set  $p_1^2 = p_2^2$ .

### 4.3.3 Hierarchy of form factors

The form factors  $\lambda_i$ , whose results were presented in the previous sections, have different dimensionalities, making direct comparisons meaningless. To facilitate a relative comparison of their magnitudes and establish a hierarchical classification, we introduce dimensionless renormalization-group invariant (RGI) combinations that generalize the effective coupling. In particular, we focus on special kinematic configurations (in this particular case: the soft-gluon limit), where the  $\lambda_i^{sg}(p^2)$  depend on a single momentum  $p$ , and construct a family of dimensionless effective couplings,  $\widehat{g}_i^{sg}(p^2)$ , we define [60, 64, 104, 107, 118]

$$\widehat{g}_i^{sg}(p^2) = g(\mu^2) [p^{n_i} \lambda_i^{sg}(p^2)] A^{-1}(p^2) \mathcal{Z}^{1/2}(p^2), \quad \text{with } n_1 = 0, \quad n_{2,3,4} = 1, \\ n_{5,6,7} = 2, \quad n_8 = 3. \quad (4.25)$$

where  $\mathcal{Z}(p^2)$  and  $A(p^2)$  are defined in Eqs. (3.6) and (3.7), respectively. Notice that we have introduced the compact notation  $\lambda_i^{sg}(p^2) = \lambda_i(0, p, -p)$ .

In Fig. 4.9, we present the results for  $\widehat{g}_i^{sg}(p^2)$  divided into two subsets: the effective couplings for the chirally symmetric form factors (left panel), and those for the chirally broken form factors (right panel). Since these quantities are dimensionless, they provide

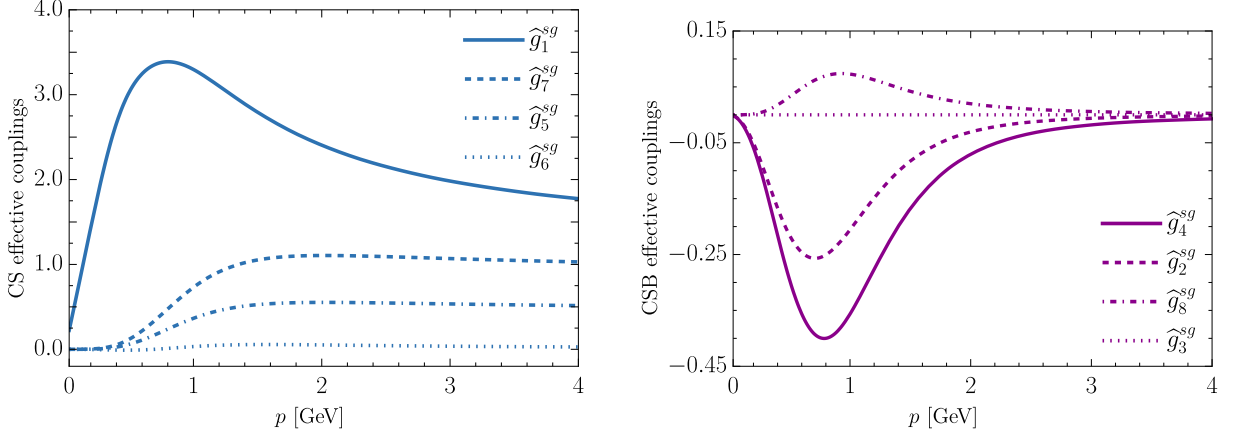


Figure 4.9: The quark-gluon effective coupling,  $\widehat{g}_i^{sg}(p^2)$ , for the chirally-symmetric tensor structures  $\tau_{1,5,6,7}$  (left panel); and for the chirally-broken tensors  $\tau_{2,3,4,8}$  (right panel). The effective couplings were determined using Eq. (4.25) when the quark-gluon vertex form factors are in the soft-gluon kinematics.

a clear indication of the physical relevance of the corresponding form factors  $\lambda_i$ .

Through Fig. 4.9, we can observe that the hierarchy of the effective coupling is as follows:

$$\widehat{g}_1^{sg}(p^2) > \widehat{g}_7^{sg}(p^2) > \widehat{g}_5^{sg}(p^2), \quad |\widehat{g}_4^{sg}(p^2)| > |\widehat{g}_2^{sg}(p^2)| > g_8^{sg}(p^2). \quad (4.26)$$

Note that  $\widehat{g}_3^{sg}$  vanishes identically, and  $\widehat{g}_7^{sg}(p^2) = 2\widehat{g}_5^{sg}(p^2)$ , reflecting the charge conjugation symmetry of the vertex as expressed in Eq. (3.20). We have confirmed that the hierarchies given in Eq. (4.26) are consistent across the totally symmetric, quark-symmetric, and soft-gluon limits. Additionally, our results are in qualitative agreement with those presented in [64], where the effective couplings were computed in the totally symmetric configuration.

#### 4.3.4 Comparisons with lattice

In this subsection we compare our results for the quark-gluon vertex in the soft-gluon configuration with those obtained in unquenched lattice simulation of [55].

We recall that in the soft-gluon limit ( $q \rightarrow 0$ ), the transversely projected quark-gluon vertex given by Eq. (3.16) reduces to

$$\overline{\Gamma}_\mu(0, p, -p) = \gamma_\mu \lambda_1^{sg}(p^2) + 2p_\mu \lambda_2^{sg}(p^2) + 4\not{p} p_\mu \lambda_6^{sg}(p^2), \quad (4.27)$$

Note that, although the tensor  $\tau_3'(p, -p)$ , defined in Eq. (3.14), is non-zero in this kinematic limit, the associated form factor  $\lambda_3^{sg}(p^2)$  vanishes due to charge conjugation.

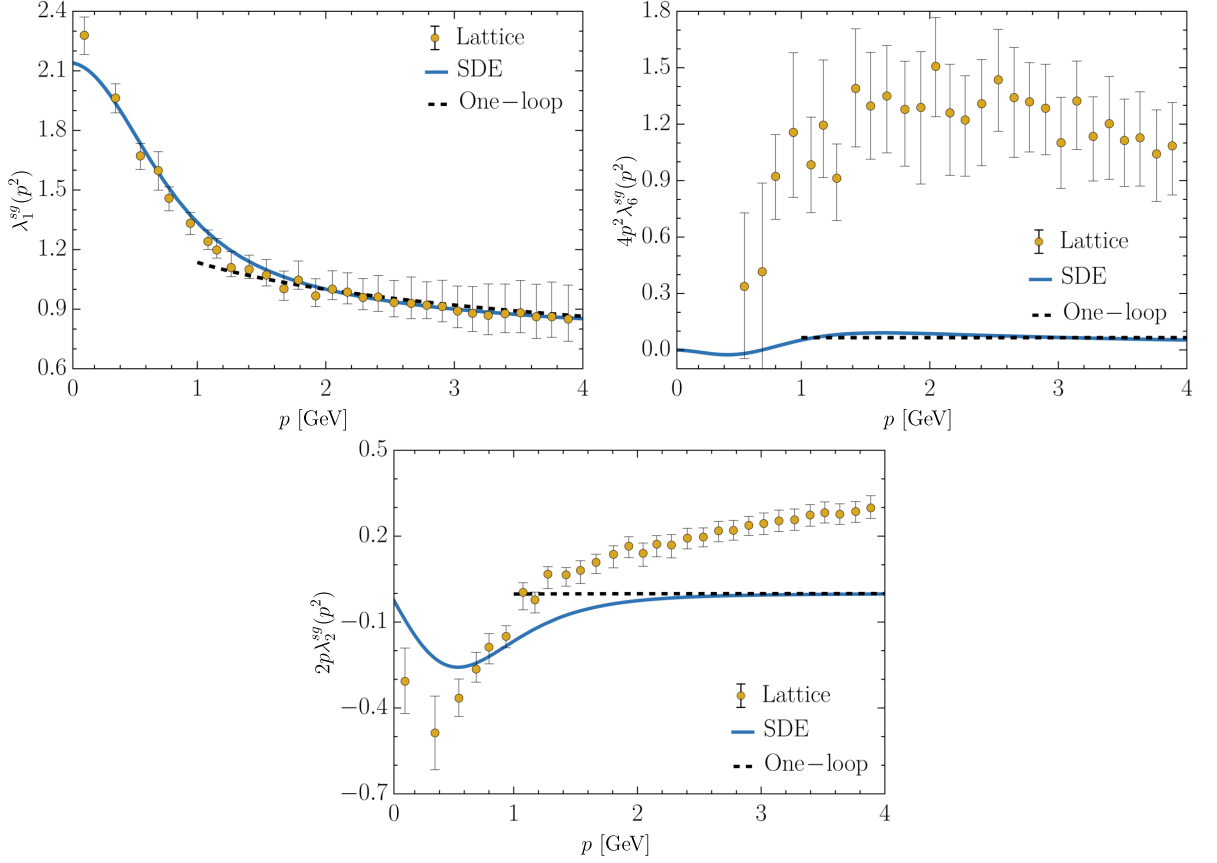


Figure 4.10: Comparison of the dimensionless soft-gluon form factors  $\lambda_1^{sg}(p^2)$  (upper left),  $4p^2\lambda_6^{sg}(p^2)$  (upper right), and  $2p\lambda_2^{sg}(p^2)$  (lower) with lattice data of [55]. We also plot the corresponding one-loop expressions.

In order to make a direct contact with the lattice data of [55], we first need to convert Eq. (4.27) to Euclidean space. Following the discussion presented in the Appendix A, it is straightforward to construct the Euclidean version of Eq. (4.27), which is given by Eq. (A.9). In addition, a relabelling of the corresponding form factors is necessary: our form factors  $\lambda_i^{sg}(p^2)$ , with  $i = 1, 2, 6$ , and the lattice form factors  $\lambda_i^L(p^2)$ , with  $i = 1, 2, 3$  from [55] are related by (Euclidean space)

$$\lambda_1^{sg}(p^2) = \lambda_1^L(p^2), \quad \lambda_6^{sg}(p^2) = \lambda_2^L(p^2), \quad \lambda_2^{sg}(p^2) = \lambda_3^L(p^2). \quad (4.28)$$

In Fig. 4.10, we compare our results for the dimensionless form factors  $\lambda_1^{sg}(p^2)$ ,  $4p^2\lambda_6^{sg}(p^2)$ , and  $2p\lambda_2^{sg}(p^2)$  (blue continuous curves) with the “L08” lattice data obtained in [55] (circles). In addition, on the same plots, we show the perturbative one-loop behavior (black dashed curve). Specifically, the one-loop curves corresponds to the perturbative analytic expressions for the  $\lambda_i^{sg}(p^2)$  given in Eq. (32)-(34) of [55]; they are renormalized in the  $\widetilde{\text{MOM}}$  scheme, for  $\alpha_s(\mu^2) = 0.55$  at  $\mu = 2$  GeV.

We can clearly see that our result for  $\lambda_1^{sg}(p^2)$  have an excellent agreement with the general pattern found by the  $N_f = 2$  lattice simulation of [55]. In particular, both curves nearly coincide over most of the momentum range, showing a minor deviation only in the deep IR, where the corresponding saturation points differ by approximately 7%. As we will see in the next subsection, this discrepancy may be reduced by making minor modifications to the three-gluon form factor,  $L_{sg}(s^2)$ , and the gluon propagator,  $\Delta(q^2)$ , used as inputs for the SDE. Moreover, we observe that for  $p \leq 1.4$  GeV,  $\lambda_1^{sg}(p^2)$  begins to show a significant deviation from its tree-level value, whereas, for larger values of  $p$ , we recover the expected one-loop behavior as given by Eq. (32) of [55]. Notably, the numerical solution for  $\lambda_1^{sg}(p^2)$  that minimizes the  $\chi^2$  relative to the lattice data, yielding  $\chi^2 = 0.036$ , is obtained when we set  $\alpha_s(\mu^2) = 0.55$ , which is very close to the value estimated in [112]. Quite interestingly, this value happens to be very close to the critical value of the coupling,  $\alpha_s^c(\mu^2) = 0.597$ , for which the Eq. (4.11), for  $i = 1$ , ceases to converge.

The  $\chi^2$  is defined as,

$$\chi^2 = \sum_{i=1}^k \frac{(x_i - y_i)^2}{y_i}, \quad (4.29)$$

where  $x_i$  represents the numerical values obtained from our computations, and  $y_i$  corresponds to the lattice data.

On the other hand, as can be clearly seen from the upper right and lower panels of Fig. 4.10, our results for  $4p^2\lambda_6^{sg}(p^2)$  and  $2p\lambda_2^{sg}(p^2)$  are vastly different from the curves found on the lattice. Note that, for large momenta, both SDE-derived curves match accurately the respective one-loop results.

It is important to mention that, although the present SDE analysis was carried out for  $N_f = 2$ , our result for  $4p^2\lambda_6^{sg}(p^2)$  are in qualitative agreement with the general pattern found by all previous analytic quenched determinations [43, 56, 59, 61, 119]. In particular, all quenched curves share the characteristic feature of vanishing at the origin and tending to a constant value in the UV, showing moderate increase in the intermediate region.

On the other hand, our result for  $2p\lambda_2^{sg}(p^2)$  displays a minimum whose depth is much smaller than that observed in the previous analytic quenched studies [43, 56, 59, 61, 119], being the latter, more compatible with the unquenched lattice data of [55].

	$\epsilon^+$	$\epsilon^-$	$\kappa[\text{GeV}^2]$
$L_{sg}^\pm$	0.030	0.120	5.000
$\Delta^\pm$	0.025	0.100	0.900

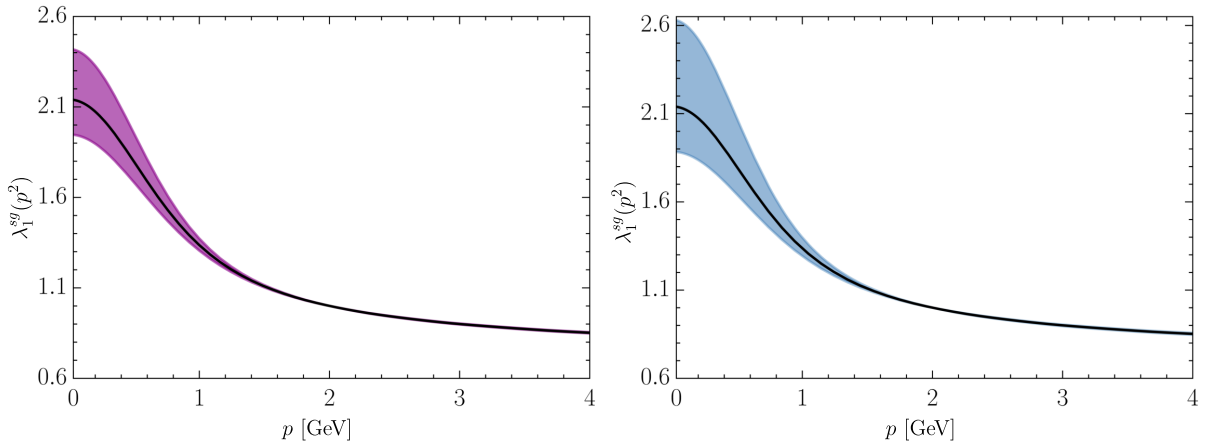
Table 4.2: Parameters used in Eq. (4.30) to obtain the bands on the left panel of Fig. 4.11.

### 4.3.5 Varying the inputs

As noted previously by [63], the result for the form factor  $\lambda_1^{sg}(p^2)$  is highly sensitive to variations in the gauge sector inputs. To investigate this feature, we construct a band around the curves obtained from the lattice fits for the dressing of the three-gluon vertex,  $L_{sg}$ , and the gluon propagator,  $\Delta$ . This band is generated by adding or subtracting a function depending on the parameters  $\epsilon^\pm$  and  $\kappa^2$ , as follows

$$L_{sg}^\pm(p^2) = L_{sg}(p^2) \pm \epsilon^\pm/[1 + (p^2/\kappa^2)^2], \quad \Delta^\pm(p^2) = \Delta(p^2) \pm \epsilon^\pm/[1 + (p^2/\kappa^2)^2]. \quad (4.30)$$

In Fig. 4.11, we illustrate how the changes in these two quantities significantly impact the form factor, for values of  $\epsilon^\pm$  and  $\kappa$  specified for each ingredient in Table 4.2. Note that the values of  $\epsilon^+$  are much lower than the values of  $\epsilon^-$ , for both ingredients, even though the effect on the form factor  $\lambda_1^{sg}(p^2)$  is similar. Specifically, increasing these components leads to a dramatic increase in the form factor.

Figure 4.11: The effect on the form factor  $\lambda_1^{sg}(p^2)$  from the corresponding bands highlighted in these plots are shown on the right panel.

Moreover, bigger values for the  $\epsilon^+$  presented in Table 4.2 causes the equation to reach its convergence limit. Also, setting the three-gluon vertex to its tree-level form prevents the equation from converging. This result shows the importance of the suppression of the three-gluon vertex in order to the convergence of the quark-gluon SDE for a value of  $\alpha_s(\mu^2)$  that fits best the lattice data.

Note that although a narrower band in the gluon propagator produces approximately the same effect on  $\lambda_1^{sg}(p^2)$ , the dependence of this form factor on the gluon propagator is quadratic, whereas it is linearly dependent on  $L_{sg}$ . This is because the largest contribution to  $\lambda_1^{sg}(p^2)$  comes from the non-Abelian (b) diagram. Changes in the quark propagator do not change  $\lambda_1^{sg}(p^2)$  so dramatically as in the gauge inputs.

## 4.4 Checking multiplicative renormalizability

As previously mentioned, one of the main advantages of the 3PI formalism is that, because all vertices appearing in the SDE are fully dressed, there are no renormalization constants multiplying the Abelian and non-Abelian diagrams. Therefore, a self-consistent treatment of the vertices ensures that all divergences can be absorbed into these renormalization constants in a manner that preserves the multiplicative renormalizability of the theory.

To verify explicitly this property of our Eqs. (4.11) and (4.16), we repeat the calculation of  $\lambda_1$  with Eq. (4.11) renormalized in the same scheme,  $\widetilde{\text{MOM}}$ , but at a different renormalization point,  $\nu = 4.3$  GeV, *i.e.*, imposing

$$\Delta_R^{-1}(\nu^2) = \nu^2, \quad A_R(\nu^2) = 1, \quad \lambda_{1,R}^{sg}(\nu^2) = 1. \quad (4.31)$$

As such,  $Z_1$  continues to be determined by Eq. (4.16), but with  $\mu \rightarrow \nu$ .

Then, we will check whether our numerical solutions for  $\lambda_1$  renormalized at  $\mu = 2$  GeV and at  $\nu = 4.3$  GeV, respect multiplicative renormalizability, *i.e.*, if they satisfy the following relation

$$\lambda_1^{sg}(q^2, \mu^2) = \frac{\lambda_1^{sg}(q^2, \nu^2)}{\lambda_1^{sg}(\mu^2, \nu^2)}, \quad (4.32)$$

which we derive below.

In order to do that, we need to have at our disposal the inputs for  $\Delta(q^2)$ ,  $L_{sg}(s^2)$ , and  $A(p^2)$  shown in Figs. 4.1, 4.2 and 4.3, respectively, at different renormalization points<sup>3</sup>. To that end, we exploit the property of multiplicative renormalizability, which allows one to connect a Green's function renormalized at  $\mu$  with the corresponding one renormalized at  $\nu$ .

Specifically, it follows from Eq. (3.34) and the fact that the unrenormalized Green's

---

<sup>3</sup>Notice that the quark dynamical mass,  $\mathcal{M}(p^2)$ , is a  $\mu$ -independent quantity, and therefore does not need to be rescaled.

functions do not depend on  $\mu$ , that

$$\begin{aligned}\Delta(q^2, \mu^2) &= \Delta(q^2, \nu^2) \frac{Z_A(\nu^2)}{Z_A(\mu^2)}, & A(p^2, \mu^2) &= A(p^2, \nu^2) \frac{Z_F(\mu^2)}{Z_F(\nu^2)}, \\ \lambda_1^{sg}(q^2, \mu^2) &= \lambda_1^{sg}(q^2, \nu^2) \frac{Z_1(\mu^2)}{Z_1(\nu^2)}, & L_{sg}(s^2, \mu^2) &= L_{sg}(s^2, \nu^2) \frac{Z_3(\mu^2)}{Z_3(\nu^2)}.\end{aligned}\quad (4.33)$$

Now, the values  $\Delta(\mu^2, \mu^2)$ ,  $A(\mu^2, \mu^2)$ , and  $\lambda_1^{sg}(\mu^2, \mu^2)$ , are fixed by the renormalization prescription of Eq. (3.38). Hence, evaluating Eq. (4.33) at  $q^2 = p^2 = \mu^2$  entails

$$\frac{Z_A(\nu^2)}{Z_A(\mu^2)} = \frac{1}{\mu^2 \Delta(\mu^2, \nu^2)}, \quad \frac{Z_F(\mu^2)}{Z_F(\nu^2)} = \frac{1}{A(\mu^2, \nu^2)}, \quad \frac{Z_1(\mu^2)}{Z_1(\nu^2)} = \frac{1}{\lambda_1^{sg}(\mu^2, \nu^2)}. \quad (4.34)$$

Then, substituting the above into Eq. (4.33) furnishes Eq. (4.32), together with

$$\Delta(q^2, \mu^2) = \frac{\Delta(q^2, \nu^2)}{\mu^2 \Delta(\mu^2, \nu^2)}, \quad A(p^2, \mu^2) = \frac{A(p^2, \nu^2)}{A(\mu^2, \nu^2)}. \quad (4.35)$$

On the other hand, the renormalization conditions of Eq. (3.38) do not specify the value of  $L_{sg}(\mu^2, \mu^2)$ . Instead, to determine  $Z_1(\mu^2)/Z_1(\nu^2)$ , we employ the STI  $Z_3 = Z_1 Z_A / Z_F$ , together with the previously obtained Eq. (4.34), to find

$$\frac{Z_3(\mu^2)}{Z_3(\nu^2)} = \frac{\mu^2 \Delta(\mu^2, \nu^2) A(\mu^2, \nu^2)}{\lambda_1^{sg}(\mu^2, \nu^2)}, \quad (4.36)$$

which implies

$$L_{sg}(s^2, \mu^2) = \frac{L_{sg}(s^2, \nu^2) \mu^2 \Delta(\mu^2, \nu^2) A(\mu^2, \nu^2)}{\lambda_1^{sg}(\mu^2, \nu^2)}. \quad (4.37)$$

The next step is to relate the values of  $\alpha_s(\nu^2)$  and  $\alpha_s(\mu^2)$ , which we achieve by invoking the effective coupling  $\widehat{g}_1^{sg}(p^2)$  of Eq. (4.25). Since  $\widehat{g}_1^{sg}(p^2)$  is RGI, its value is the same when computed with ingredients renormalized at either  $\mu$  or  $\nu$ , *i.e.*,

$$\widehat{g}_1^{sg}(p^2) = \frac{g(\mu^2) \lambda_1^{sg}(p^2, \mu^2) \mathcal{Z}^{1/2}(p^2, \mu^2)}{A(p^2, \mu^2)} = \frac{g(\nu^2) \lambda_1^{sg}(p^2, \nu^2) \mathcal{Z}^{1/2}(p^2, \nu^2)}{A(p^2, \nu^2)}. \quad (4.38)$$

Therefore, setting  $p = \nu$  in the above, using the renormalization prescription of Eq. (4.31), and  $g^2 = 4\pi\alpha_s$ , leads to

$$\alpha_s(\nu^2) = \alpha_s(\mu^2) [\lambda_1^{sg}(\nu^2, \mu^2)]^2 A^{-2}(\nu^2, \mu^2) \nu^2 \Delta(\nu^2, \mu^2). \quad (4.39)$$

Then, using the previously obtained curve for  $\lambda_1^{sg}(q^2, \mu^2)$ , shown in Fig. 4.10, together with the external inputs renormalized at  $\mu = 2$  GeV, discussed in Sec. 4.2, we obtain all the necessary inputs renormalized at  $\nu = 4.3$  GeV through Eqs. (4.35), (4.37) and (4.39). In particular, we find  $\alpha_s(\nu^2) = 0.28$ .

With all the necessary inputs in hand, we solve Eqs. (4.11) and (4.16) again to obtain  $\lambda_1^{sg}(q^2, \nu^2)$  at  $\nu = 4.3$  GeV. The result is then rescaled to  $\mu = 2$  GeV using Eq. (4.32), and compared to the  $\lambda_1^{sg}(q^2, \mu^2)$  obtained by solving the SDE directly at  $\mu$ . The comparison is shown in Fig. 4.12, where the blue continuous curve shows the result of the SDE renormal-

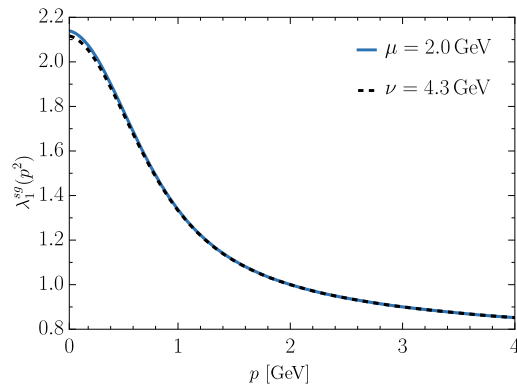


Figure 4.12: Verification that our solution for  $\lambda_1^{sg_1(p^2)}$  satisfies the multiplicative renormalizability property given by Eq. (4.32).

ized at  $\mu$ , whereas the black dashed corresponds to the result of the SDE renormalized at  $\nu$ , after rescaling to  $\mu$  through Eq. (4.32). The agreement between the two curves confirms that indeed multiplicative renormalizability is satisfied in our truncation.

---

# Chapter 5

## Conclusions

In this thesis, we have determined the nonperturbative behavior of the transversely projected quark-gluon vertex, one of the fundamental Green's function composing quark sector of QCD. In this nonperturbative study, we considered the SDE for the quark-gluon vertex derived in the 3PI formalism.

In Section 2.4, we introduced the  $n$ PI formalism, from which we derive the version of the SDE for the quark-gluon vertex used in this work. Specifically, we use the 3PI formalism, which offers advantages over the traditional method, particularly in terms of renormalization and truncation. In this approach, all propagators and vertices in the SDE are fully dressed, simplifying the renormalization process, as the only contribution requiring a renormalization constant is the tree-level term [see Eqs. (3.36) and (3.37)]. Additionally, because the truncation is performed at the level of the effective action, in 3-loop order, the 3PI method inherently provides a truncated equation without the need for external approximations to break the tower of SDEs.

In Chapter 3, we focused on the transversely projected quark-gluon vertex, discussing its key aspects. This vertex is decomposed into eight Lorentz structures,  $\tau_i^\mu(p_2, -p_1)$ , which form the basis given in Eq. (3.14). In this decomposition, each basis element is associated with a form factor,  $\lambda_i(q, p_2, -p_1)$ , which we fully determine in Euclidean space for general kinematics. In our analysis, we relate each form factor to the SDE of the quark-gluon vertex by applying a set of basis projectors [see Eq. (3.30)] onto the SDE, thereby converting the form factors into integral equations.

Next, after defining our main equations for the form factors, we stated two fundamen-

tal simplifications in Section 4.1 to reduce considerably the numerical complexity of our problem. First, we considered only the tree-level structure for the quark-gluon vertex [see Eq.(4.1)] that appears in the SDE. This implies that only the form factor  $\lambda_1$  is treated as an integral equation solved iteratively, while all other form factors decouple from each other, relying on  $\lambda_1$  as an input and are determined by solving simple integrals. The second simplification involves the three-gluon vertex, where, based on several studies[66, 69–71], we assume the so-called planar degeneracy. Here, the vertex is approximated by its tree-level structure multiplied by a scalar function  $L_{sg}(s^2)$ , which is computed in the soft-gluon limit and is well-determined by lattice QCD simulations [69, 104–109].

We then proceed to express the form factors in Euclidean space, where the variables are the two momenta and the angle between them, leading to  $\lambda_i(p_1^2, p_2^2, \theta)$  [see Eq.(4.11)]. The components necessary for calculating the form factors were presented in Section 4.2, where we provided the fits used for the corresponding lattice data.

In Section 4.3, we presented our results in general kinematics (3D surfaces in terms of the momentum  $p_1$  and  $p_2$  with the angle fixed), starting with the form factor related to the tree-level,  $\lambda_1$  [see Fig. 4.4]. Using the results for  $\lambda_1$ , we determine the remaining form factors,  $\lambda_i$  [see Figs. 4.6 and 4.7]. All form factors are finite in the IR region, and we observe significant deviations from their tree-level behavior in this region. The perturbative behavior (tree-level) is recovered in the UV limit, where  $\lambda_1 \rightarrow 1$  while  $\lambda_i \rightarrow 0$  for  $i \neq 1$ . When plotted in terms of  $p_1$  and  $p_2$ , all form factors exhibit the respective basis charge symmetry as described in Eq. (3.20).

We also study the angular dependence of each form factor. We plot a slice of the 3D-surfaces in  $p_1 = p_2$ , and the angular variation from  $\theta = 0$  to  $\theta = \pi$  forms a band [see 4.5 and 4.8]. First, for the form factor  $\lambda_1$  we observe that the maximum peak of the curve increases as the angle increases with a difference of 27% between the soft-gluon ( $\theta = 0$ ) and asymmetric ( $\theta = \pi$ ). For the remaining form factors we find that  $\lambda_2$  and  $\lambda_8$  are weakly dependent on angular variation, followed by  $\lambda_4$  and  $\lambda_6$  which have a slightly stronger angular dependence in low momentum region. Finally the  $\lambda_5$  and  $\lambda_7$  shows the strongest dependence among those form factors, with exception of  $\lambda_1$ . The form factor  $\lambda_3$  is the more suppress form factor and identically 0, when  $p_1 = p_2$ .

To compare the relative magnitudes of the form factors, we calculated the dimensionless quark-gluon effective couplings using combinations of renormalization group invariants

[see Fig. 4.9]. The results reveal a hierarchy [see Eq. (4.25)], where, as expected,  $\lambda_1$  is the dominant form factor, followed by  $\lambda_7$  and  $\lambda_4$ . For phenomenological applications, these three form factors are expected to have the most significant impact.

Furthermore, we compare our results with the more recent data of lattice for the quark-gluon vertex [55]. The lattice calculate the quark-gluon in the soft-gluon limit, where the tensorial structure of the quark-gluon reduces only to three non trivial form factors [see Eq. (4.27)], namely,  $\lambda_1^{sg}(p^2)$ ,  $\lambda_2^{sg}(p^2)$ , and  $\lambda_3^{sg}(p^2)$ . The result shows a excellent agreement for  $\lambda_1^{sg}(p^2)$  between SDE and lattice, the opposite occurs with the other two form factors. Whereas,  $\lambda_3^{sg}(p^2)$ , although it has the same pattern, the results differ considerably. The  $\lambda_2^{sg}(p^2)$  is completely different. Both  $\lambda_2^{sg}(p^2)$ , and  $\lambda_3^{sg}(p^2)$  calculated by the lattice fail to capture the perturbative behavior in the UV [see Fig. 4.10]. Finally, we conclude by verifying the multiplicative renormalizability property of our form factors.

We have seen that the quark-gluon vertex couples to the SDE of the quark propagator [see Eq. (2.39)], which serves as a key tool in the phenomenological study of chiral symmetry breaking and the resulting dynamical mass generation for quarks. Since, it is well know that this vertex plays a crucial role in chiral symmetry breaking and dynamical mass generation for quarks, it is natural to explore future applications of our results to analyze the phenomenological impact that the nonperturbative structure of this vertex has on this process.

# Bibliography

- <sup>1</sup>W. J. Marciano and H. Pagels, “Quantum chromodynamics: a review”, *Phys. Rept.* **36**, 137 (1978).
- <sup>2</sup>N. Brambilla et al., “QCD and Strongly Coupled Gauge Theories: Challenges and Perspectives”, *Eur. Phys. J. C* **74**, 2981 (2014).
- <sup>3</sup>D. J. Gross and F. Wilczek, “Ultraviolet Behavior of Nonabelian Gauge Theories”, *Phys. Rev. Lett.* **30**, 1343–1346 (1973).
- <sup>4</sup>H. D. Politzer, “Reliable Perturbative Results for Strong Interactions?”, *Phys. Rev. Lett.* **30**, 1346–1349 (1973).
- <sup>5</sup>C. D. Roberts and A. G. Williams, “Dyson-Schwinger equations and their application to hadronic physics”, *Prog. Part. Nucl. Phys.* **33**, 477–575 (1994).
- <sup>6</sup>P. Maris and C. D. Roberts, “Dyson-Schwinger equations: A Tool for hadron physics”, *Int. J. Mod. Phys.* **E12**, 297–365 (2003).
- <sup>7</sup>M. R. Pennington, “Swimming with quarks”, *J. Phys. Conf. Ser.* **18**, 1–73 (2005).
- <sup>8</sup>R. Alkofer and L. von Smekal, “The Infrared behavior of QCD Green’s functions: Confinement dynamical symmetry breaking, and hadrons as relativistic bound states”, *Phys. Rept.* **353**, 281 (2001).
- <sup>9</sup>C. S. Fischer, “Infrared properties of QCD from Dyson-Schwinger equations”, *J. Phys. G* **32**, R253–R291 (2006).
- <sup>10</sup>C. D. Roberts, “Three Lectures on Hadron Physics”, *J. Phys. Conf. Ser.* **706**, 022003 (2016).

- <sup>11</sup>D. Binosi and J. Papavassiliou, “Pinch Technique: Theory and Applications”, [Phys. Rept. \*\*479\*\*, 1–152 \(2009\)](#).
- <sup>12</sup>A. C. Aguilar, D. Binosi, and J. Papavassiliou, “The Gluon Mass Generation Mechanism: A Concise Primer”, [Front. Phys.\(Beijing\) \*\*11\*\*, 111203 \(2016\)](#).
- <sup>13</sup>J. M. Cornwall, “Dynamical Mass Generation in Continuum QCD”, [Phys. Rev. D \*\*26\*\*, 1453 \(1982\)](#).
- <sup>14</sup>K. G. Wilson, “Confinement of Quarks”, [Phys. Rev. D \*\*10\*\*, 2445–2459 \(1974\)](#).
- <sup>15</sup>M. Creutz, “Monte Carlo Study of Quantized SU(2) Gauge Theory”, [Phys. Rev. D \*\*21\*\*, 2308–2315 \(1980\)](#).
- <sup>16</sup>F. J. Dyson, “The S matrix in quantum electrodynamics”, [Phys. Rev. \*\*75\*\*, 1736–1755 \(1949\)](#).
- <sup>17</sup>J. S. Schwinger, “On the Green’s functions of quantized fields. 1.”, [Proc. Nat. Acad. Sci. \*\*37\*\*, 452–455 \(1951\)](#).
- <sup>18</sup>F. J. Yndurain, *The theory of quark and gluon interactions* (Springer, 2006).
- <sup>19</sup>R. Gupta, “Introduction to lattice QCD: Course”, [arXiv:hep-lat/9807028 \(1997\)](#).
- <sup>20</sup>M. Luscher, “Advanced lattice QCD”, [arXiv:hep-lat/9802029 \(1998\)](#).
- <sup>21</sup>C. Itzykson and J. B. Zuber, *Quantum field theory*, International Series in Pure and Applied Physics (New York, USA: Mcgraw-Hill (1980) 705 p., 1980).
- <sup>22</sup>E. S. Swanson, “A Primer on Functional Methods and the Schwinger-Dyson Equations”, [AIP Conf. Proc. \*\*1296\*\*, 75–121 \(2010\)](#).
- <sup>23</sup>M. Q. Huber, “Nonperturbative properties of Yang-Mills theories”, [Phys. Rept. \*\*879\*\*, 1–92 \(2020\)](#).
- <sup>24</sup>A. C. Aguilar and A. A. Natale, “A Dynamical gluon mass solution in a coupled system of the Schwinger-Dyson equations”, [J. High Energy Phys. \*\*08\*\*, 057 \(2004\)](#).
- <sup>25</sup>P. Boucaud, J. Leroy, L. Y. A., J. Micheli, O. Pène, and J. Rodríguez-Quintero, “On the IR behaviour of the Landau-gauge ghost propagator”, [J. High Energy Phys. \*\*06\*\*, 099 \(2008\)](#).
- <sup>26</sup>A. C. Aguilar, D. Binosi, and J. Papavassiliou, “Gluon and ghost propagators in the Landau gauge: Deriving lattice results from Schwinger-Dyson equations”, [Phys. Rev. \*\*D78\*\*, 025010 \(2008\)](#).

- <sup>27</sup>J. Rodríguez-Quintero, “On the massive gluon propagator, the PT-BFM scheme and the low-momentum behaviour of decoupling and scaling DSE solutions”, *J. High Energy Phys.* **01**, 105 (2011).
- <sup>28</sup>D. Binosi and J. Papavassiliou, “Gauge-invariant truncation scheme for the Schwinger-Dyson equations of QCD”, *Phys. Rev.* **D77**, 061702 (2008).
- <sup>29</sup>D. Binosi and J. Papavassiliou, “New Schwinger-Dyson equations for non-Abelian gauge theories”, *J. High Energy Phys.* **11**, 063 (2008).
- <sup>30</sup>Y. Nambu and G. Jona-Lasinio, “Dynamical model of elementary particles based on an analogy with superconductivity. I”, *Phys. Rev.* **122**, 345–358 (1961).
- <sup>31</sup>Y. Nambu and G. Jona-Lasinio, “Dynamical model of elementary particles based on an analogy with superconductivity. II”, *Phys. Rev.* **124**, 246–254 (1961).
- <sup>32</sup>C. S. Fischer and R. Alkofer, “Nonperturbative propagators, running coupling and dynamical quark mass of Landau gauge QCD”, *Phys. Rev.* **D67**, 094020 (2003).
- <sup>33</sup>A. C. Aguilar and J. Papavassiliou, “Chiral symmetry breaking with lattice propagators”, *Phys. Rev.* **D83**, 014013 (2011).
- <sup>34</sup>I. C. Cloet and C. D. Roberts, “Explanation and Prediction of Observables using Continuum Strong QCD”, *Prog. Part. Nucl. Phys.* **77**, 1–69 (2014).
- <sup>35</sup>M. Hopper, A. Windisch, and R. Alkofer, “The Quark-Gluon Vertex in Landau gauge QCD”, *PoS ConfinementX*, 073 (2012).
- <sup>36</sup>A. Bender, C. D. Roberts, and L. Von Smekal, “Goldstone theorem and diquark confinement beyond rainbow ladder approximation”, *Phys. Lett.* **B380**, 7–12 (1996).
- <sup>37</sup>P. Maris and P. C. Tandy, “Bethe-Salpeter study of vector meson masses and decay constants”, *Phys. Rev.* **C60**, 055214 (1999).
- <sup>38</sup>A. Bender, W. Detmold, C. Roberts, and A. W. Thomas, “Bethe-Salpeter equation and a nonperturbative quark gluon vertex”, *Phys. Rev.* **C65**, 065203 (2002).
- <sup>39</sup>M. Bhagwat, A. Holl, A. Krassnigg, C. Roberts, and P. Tandy, “Aspects and consequences of a dressed quark gluon vertex”, *Phys. Rev.* **C70**, 035205 (2004).
- <sup>40</sup>A. Holl, A. Krassnigg, and C. D. Roberts, “Confinement, DCSB, bound states, and the quark-gluon vertex”, *Nucl. Phys. Proc. Suppl.* **141**, 47–52 (2005).

- <sup>41</sup>L. Chang and C. D. Roberts, “Sketching the Bethe-Salpeter kernel”, *Phys. Rev. Lett.* **103**, 081601 (2009).
- <sup>42</sup>R. Williams, “The quark-gluon vertex in Landau gauge bound-state studies”, *Eur. Phys. J.* **A51**, 57 (2015).
- <sup>43</sup>R. Williams, C. S. Fischer, and W. Heupel, “Light mesons in QCD and unquenching effects from the 3PI effective action”, *Phys. Rev.* **D93**, 034026 (2016).
- <sup>44</sup>G. Eichmann, H. Sanchis-Alepuz, R. Williams, R. Alkofer, and C. S. Fischer, “Baryons as relativistic three-quark bound states”, *Prog. Part. Nucl. Phys.* **91**, 1–100 (2016).
- <sup>45</sup>H. Sanchis-Alepuz and R. Williams, “Probing the quark–gluon interaction with hadrons”, *Phys. Lett.* **B749**, 592–596 (2015).
- <sup>46</sup>L. F. Abbott, P. Sikivie, and M. B. Wise, “Constraints on Charged Higgs Couplings”, *Phys. Rev. D* **21**, 1393 (1980).
- <sup>47</sup>A. I. Davydychev, P. Osland, and L. Saks, “Quark gluon vertex in arbitrary gauge and dimension”, *Phys. Rev.* **D63**, 014022 (2001).
- <sup>48</sup>J. A. Gracey, “Two loop QCD vertices at the symmetric point”, *Phys. Rev.* **D84**, 085011 (2011).
- <sup>49</sup>J. Gracey, “Off-shell two-loop QCD vertices”, *Phys. Rev. D* **90**, 025014 (2014).
- <sup>50</sup>R. Bermudez, L. Albino, L. X. Gutiérrez-Guerrero, M. E. Tejada-Yeomans, and A. Bashir, “Quark-gluon Vertex: A Perturbation Theory Primer and Beyond”, *Phys. Rev.* **D95**, 034041 (2017).
- <sup>51</sup>J. I. Skullerud, P. O. Bowman, A. Kizilersu, D. B. Leinweber, and A. G. Williams, “Nonperturbative structure of the quark gluon vertex”, *J. High Energy Phys.* **04**, 047 (2003).
- <sup>52</sup>H.-W. Lin, “Quark-gluon vertex with an off-shell  $O(a)$ -improved chiral fermion action”, *Phys. Rev.* **D73**, 094511 (2006).
- <sup>53</sup>A. Kizilersu, D. B. Leinweber, J.-I. Skullerud, and A. G. Williams, “Quark-gluon vertex in general kinematics”, *Eur. Phys. J.* **C50**, 871–875 (2007).
- <sup>54</sup>A. Sternbeck, P.-H. Balduf, A. Kizilersu, O. Oliveira, P. J. Silva, J.-I. Skullerud, and A. G. Williams, “Triple-gluon and quark-gluon vertex from lattice QCD in Landau gauge”, *PoS LATTICE2016*, 349 (2017).

- <sup>55</sup>A. Kızılersü, O. Oliveira, P. J. Silva, J.-I. Skullerud, and A. Sternbeck, “Quark-gluon vertex from  $N_f=2$  lattice QCD”, *Phys. Rev. D* **103**, 114515 (2021).
- <sup>56</sup>M. Bhagwat and P. Tandy, “Quark-gluon vertex model and lattice-QCD data”, *Phys. Rev. D* **70**, 094039 (2004).
- <sup>57</sup>R. Alkofer, C. S. Fischer, F. J. Llanes-Estrada, and K. Schwenzer, “The Quark-gluon vertex in Landau gauge QCD: Its role in dynamical chiral symmetry breaking and quark confinement”, *Annals Phys.* **324**, 106–172 (2009).
- <sup>58</sup>A. Windisch, M. Hopfer, and R. Alkofer, “Towards a self-consistent solution of the Landau gauge quark-gluon vertex Dyson-Schwinger equation”, *Acta Phys. Polon. Supp.* **6**, 347–352 (2013).
- <sup>59</sup>A. C. Aguilar, D. Binosi, D. Ibañez, and J. Papavassiliou, “New method for determining the quark-gluon vertex”, *Phys. Rev. D* **90**, 065027 (2014).
- <sup>60</sup>M. Mitter, J. M. Pawłowski, and N. Strodthoff, “Chiral symmetry breaking in continuum QCD”, *Phys. Rev. D* **91**, 054035 (2015).
- <sup>61</sup>A. C. Aguilar, J. C. Cardona, M. N. Ferreira, and J. Papavassiliou, “Non-Abelian Ball-Chiu vertex for arbitrary Euclidean momenta”, *Phys. Rev. D* **96**, 014029 (2017).
- <sup>62</sup>A. L. Blum, R. Alkofer, M. Q. Huber, and A. Windisch, “Three-point vertex functions in Yang-Mills Theory and QCD in Landau gauge”, *EPJ Web Conf.* **137**, 03001 (2017).
- <sup>63</sup>A. L. Blum, “Three-gluon vertex and quark-gluon vertex functions in the Landau gauge”, *Graz U.* (2017).
- <sup>64</sup>F. Gao, J. Papavassiliou, and J. M. Pawłowski, “Fully coupled functional equations for the quark sector of QCD”, *Phys. Rev. D* **103**, 094013 (2021).
- <sup>65</sup>A. C. Aguilar, M. N. Ferreira, G. T. Linhares, B. M. Oliveira, and J. Papavassiliou, “Infrared properties of the quark-gluon vertex in general kinematics”, [arXiv:2408.15370](https://arxiv.org/abs/2408.15370) (2024).
- <sup>66</sup>G. Eichmann, R. Williams, R. Alkofer, and M. Vujanovic, “The three-gluon vertex in Landau gauge”, *Phys. Rev. D* **89**, 105014 (2014).
- <sup>67</sup>A. Blum, M. Q. Huber, M. Mitter, and L. von Smekal, “Gluonic three-point correlations in pure Landau gauge QCD”, *Phys. Rev. D* **89**, 061703 (2014).

- <sup>68</sup>M. Q. Huber, “Correlation functions of three-dimensional Yang-Mills theory from Dyson-Schwinger equations”, [Phys. Rev. D \*\*93\*\*, 085033 \(2016\)](#).
- <sup>69</sup>F. Pinto-Gómez, F. De Soto, M. N. Ferreira, J. Papavassiliou, and J. Rodríguez-Quintero, “Lattice three-gluon vertex in extended kinematics: Planar degeneracy”, [Phys. Lett. B \*\*838\*\*, 137737 \(2023\)](#).
- <sup>70</sup>M. N. Ferreira and J. Papavassiliou, “Gauge Sector Dynamics in QCD”, [Particles \*\*6\*\*, 312–363 \(2023\)](#).
- <sup>71</sup>A. C. Aguilar, M. N. Ferreira, J. Papavassiliou, and L. R. Santos, “Planar degeneracy of the three-gluon vertex”, [Eur. Phys. J. C \*\*83\*\*, 549 \(2023\)](#).
- <sup>72</sup>F. Pinto-Gómez, F. De Soto, and J. Rodríguez-Quintero, “Complete analysis of the Landau-gauge three-gluon vertex from lattice QCD”, [Phys. Rev. D \*\*110\*\*, 014005 \(2024\)](#).
- <sup>73</sup>A. C. Aguilar, M. N. Ferreira, J. Papavassiliou, and L. R. Santos, “Four-gluon vertex in collinear kinematics”, [Eur. Phys. J. C \*\*84\*\*, 676 \(2024\)](#).
- <sup>74</sup>A. C. Aguilar, F. De Soto, M. N. Ferreira, J. Papavassiliou, F. Pinto-Gómez, J. Rodríguez-Quintero, and L. R. Santos, “Nonperturbative four-gluon vertex in soft kinematics”, [arXiv:2408.06135 \(2024\)](#).
- <sup>75</sup>J. Berges, “N-particle irreducible effective action techniques for gauge theories”, [Phys. Rev. D \*\*70\*\*, 105010 \(2004\)](#).
- <sup>76</sup>M. C. A. York, G. D. Moore, and M. Tassler, “3-loop 3PI effective action for 3D SU(3) QCD”, [JHEP \*\*06\*\*, 077 \(2012\)](#).
- <sup>77</sup>M. Carrington and Y. Guo, “Techniques for n-Particle Irreducible Effective Theories”, [Phys. Rev. D \*\*83\*\*, 016006 \(2011\)](#).
- <sup>78</sup>A. K. Cyrol, M. Mitter, J. M. Pawłowski, and N. Strodthoff, “Nonperturbative quark, gluon, and meson correlators of unquenched QCD”, [Phys. Rev. \*\*D97\*\*, 054006 \(2018\)](#).
- <sup>79</sup>M. Gell-Mann, “The Eightfold Way: A Theory of strong interaction symmetry”, [OSTI Information Bridge Server, 10.2172/4008239 \(1961\)](#).
- <sup>80</sup>G. Zweig, “An SU(3) model for strong interaction symmetry and its breaking. Version 1”, [10.17181/CERN-TH-401 \(1964\)](#).
- <sup>81</sup>T. Muta, *Foundations of quantum chromodynamics: An Introduction to perturbative methods in gauge theories*, Vol. 5 (World Sci. Lect. Notes Phys., 1987), pp. 1–409.

- <sup>82</sup>C.-N. Yang and R. L. Mills, “Conservation of Isotopic Spin and Isotopic Gauge Invariance”, *Phys. Rev.* **96**, 191–195 (1954).
- <sup>83</sup>L. D. Faddeev and V. N. Popov, “Feynman Diagrams for the Yang-Mills Field”, *Phys. Lett. B* **25**, 29–30 (1967).
- <sup>84</sup>M. Gell-Mann, “Symmetries of baryons and mesons”, *Phys. Rev.* **125**, 1067–1084 (1962).
- <sup>85</sup>M. E. Peskin and D. V. Schroeder, *An introduction to quantum field theory*, Advanced book program, Autre tirage : 1997 (Westview Press Reading (Mass.), Boulder (CO.), 1995).
- <sup>86</sup>P. Zyla et al. (Particle Data Group), “Review of Particle Physics”, *PTEP* **2020**, 083C01 (2020).
- <sup>87</sup>R. P. Feynman, “Space-time approach to nonrelativistic quantum mechanics”, *Rev. Mod. Phys.* **20**, 367–387 (1948).
- <sup>88</sup>R. P. Feynman, “Relativistic cutoff for quantum electrodynamics”, *Phys. Rev.* **74**, 1430–1438 (1948).
- <sup>89</sup>R. J. Rivers, *Path integral methods in quantum field theory*, Cambridge Monographs on Mathematical Physics (Cambridge University Press, Oct. 1988).
- <sup>90</sup>A. X. Arrizabalaga, “Quantum field dynamics and the 2PI effective action”, *Amsterdam U.* (2004).
- <sup>91</sup>R. Alkofer, M. Q. Huber, and K. Schwenzer, “Algorithmic derivation of Dyson-Schwinger Equations”, *Comput. Phys. Commun.* **180**, 965–976 (2009).
- <sup>92</sup>J. D. Bjorken and S. D. Drell, *Relativistic Quantum Field Theory. (German Translation)* (1979).
- <sup>93</sup>J. Berges, “Introduction to nonequilibrium quantum field theory”, *AIP Conf. Proc.* **739**, 3–62 (2004).
- <sup>94</sup>J. M. Cornwall, R. Jackiw, and E. Tomboulis, “Effective Action for Composite Operators”, *Phys. Rev. D* **10**, 2428–2445 (1974).
- <sup>95</sup>A. Kizilersu, M. Reenders, and M. Pennington, “One loop QED vertex in any covariant gauge: Its complete analytic form”, *Phys. Rev.* **D52**, 1242–1259 (1995).
- <sup>96</sup>J. S. Ball and T.-W. Chiu, “Analytic Properties of the Vertex Function in Gauge Theories. 1.”, *Phys. Rev.* **D22**, 2542 (1980).

- <sup>97</sup>E. Rojas, J. de Melo, B. El-Bennich, O. Oliveira, and T. Frederico, “On the Quark-Gluon Vertex and Quark-Ghost Kernel: combining Lattice Simulations with Dyson-Schwinger equations”, *J. High Energy Phys.* **10**, 193 (2013).
- <sup>98</sup>A. C. Aguilar, J. C. Cardona, M. N. Ferreira, and J. Papavassiliou, “Quark gap equation with non-abelian Ball-Chiu vertex”, *Phys. Rev.* **D98**, 014002 (2018).
- <sup>99</sup>J. R. Lessa, F. E. Serna, B. El-Bennich, A. Bashir, and O. Oliveira, “Gauge dependence of the quark gap equation: An exploratory study”, *Phys. Rev. D* **107**, 074017 (2023).
- <sup>100</sup>G. L. Teixeira, “Numerical Kernels and Kinematic Functions in Wolfram Mathematica”, [GLTeixeira/tese \(2024\)](#).
- <sup>101</sup>J. Cornwall and R. Norton, “Spontaneous Symmetry Breaking Without Scalar Mesons”, *Phys. Rev. D* **8**, 3338–3346 (1973).
- <sup>102</sup>M. E. Carrington, W. Fu, T. Fugleberg, D. Pickering, and I. Russell, “Bethe-Salpeter Equations from the 4PI effective action”, *Phys. Rev. D* **88**, 085024 (2013).
- <sup>103</sup>J. Skullerud and A. Kizilersu, “Quark gluon vertex from lattice QCD”, *J. High Energy Phys.* **09**, 013 (2002).
- <sup>104</sup>A. Athenodorou, D. Binosi, P. Boucaud, F. De Soto, J. Papavassiliou, J. Rodríguez-Quintero, and S. Zafeiropoulos, “On the zero crossing of the three-gluon vertex”, *Phys. Lett.* **B761**, 444–449 (2016).
- <sup>105</sup>A. G. Duarte, O. Oliveira, and P. J. Silva, “Further Evidence For Zero Crossing On The Three Gluon Vertex”, *Phys. Rev.* **D94**, 074502 (2016).
- <sup>106</sup>P. Boucaud, F. De Soto, J. Rodríguez-Quintero, and S. Zafeiropoulos, “Refining the detection of the zero crossing for the three-gluon vertex in symmetric and asymmetric momentum subtraction schemes”, *Phys. Rev.* **D95**, 114503 (2017).
- <sup>107</sup>A. C. Aguilar, F. De Soto, M. N. Ferreira, J. Papavassiliou, J. Rodríguez-Quintero, and S. Zafeiropoulos, “Gluon propagator and three-gluon vertex with dynamical quarks”, *Eur. Phys. J.* **C80**, 154 (2020).
- <sup>108</sup>A. C. Aguilar, F. De Soto, M. N. Ferreira, J. Papavassiliou, and J. Rodríguez-Quintero, “Infrared facets of the three-gluon vertex”, *Phys. Lett. B* **818**, 136352 (2021).

- <sup>109</sup>A. C. Aguilar, C. O. Ambrósio, F. De Soto, M. N. Ferreira, B. M. Oliveira, J. Papavasiliou, and J. Rodríguez-Quintero, “Ghost dynamics in the soft gluon limit”, *Phys. Rev. D* **104**, 054028 (2021).
- <sup>110</sup>A. Ayala, A. Bashir, D. Binosi, M. Cristoforetti, and J. Rodríguez-Quintero, “Quark flavour effects on gluon and ghost propagators”, *Phys. Rev.* **D86**, 074512 (2012).
- <sup>111</sup>D. Binosi, C. D. Roberts, and J. Rodríguez-Quintero, “Scale-setting, flavor dependence, and chiral symmetry restoration”, *Phys. Rev. D* **95**, 114009 (2017).
- <sup>112</sup>A. C. Aguilar, M. . N. Ferreira, D. Ibañez, and J. Papavassiliou, “Schwinger displacement of the quark–gluon vertex”, *Eur. Phys. J. C* **83**, 967 (2023).
- <sup>113</sup>O. Oliveira, P. J. Silva, J.-I. Skullerud, and A. Sternbeck, “Quark propagator with two flavors of O(a)-improved Wilson fermions”, *Phys. Rev. D* **99**, 094506 (2019).
- <sup>114</sup>A. C. Aguilar, M. N. Ferreira, and J. Papavassiliou, “Exploring smoking-gun signals of the schwinger mechanism in qcd”, *Phys. Rev. D* **105**, 014030 (2022).
- <sup>115</sup>J. Berntsen, T. O. Espelid, and A. Genz, “Algorithm 698: dcuhre: an adaptive multidimensional integration routine for a vector of integrals”, *ACM Trans. Math. Softw.* **17**, 452–456 (1991).
- <sup>116</sup>C. de Boor, *A practical guide to splines*, Applied Mathematical Sciences (Springer New York, 2001).
- <sup>117</sup>J. Williams, “Multidimensional b-spline interpolation of data on a regular grid”, [github-  
bspline-fortran](#) (2019).
- <sup>118</sup>W.-j. Fu, J. M. Pawłowski, and F. Rennecke, “QCD phase structure at finite temperature and density”, *Phys. Rev. D* **101**, 054032 (2020).
- <sup>119</sup>F. J. Llanes-Estrada, C. S. Fischer, and R. Alkofer, “Semiperturbative construction for the quark-gluon vertex”, *Nucl. Phys. B Proc. Suppl.* **152**, 43–46 (2006).

# Appendix A

## Transformation from Minkowski to Euclidean space

In this Appendix, we explain how to compare our results with those in the literature, which frequently calculates the form factors of the quark-gluon vertex directly in Euclidean space. The choice of basis specified in Eq. (3.14) was made to ensure a clear correspondence between our form factors and those in [60]. In that reference, the vertex is defined in Euclidean space as

$$\overline{\Pi}_\mu^{\text{E}}(q^{\text{E}}, p_2^{\text{E}}, -p_1^{\text{E}}) = \sum_{i=1}^8 \lambda_i^{\text{E}}(q^{\text{E}}, p_2^{\text{E}}, -p_1^{\text{E}}) P_{\mu\nu}(q^{\text{E}}) \tau_i^\nu(p_2^{\text{E}}, -p_1^{\text{E}}), \quad (\text{A.1})$$

with

$$\begin{aligned} \tau_1^\nu(p_2^{\text{E}}, -p_1^{\text{E}}) &= \gamma_{\text{E}}^\nu, & \tau_2^\nu(p_2^{\text{E}}, -p_1^{\text{E}}) &= i(p_1^{\text{E}} + p_2^{\text{E}})^\nu, \\ \tau_3^\nu(p_2^{\text{E}}, -p_1^{\text{E}}) &= i(\not{p}_1^{\text{E}} + \not{p}_2^{\text{E}})\gamma_{\text{E}}^\nu, & \tau_4^\nu(p_2^{\text{E}}, -p_1^{\text{E}}) &= i(\not{p}_2^{\text{E}} - \not{p}_1^{\text{E}})\gamma_{\text{E}}^\nu, \\ \tau_5^\nu(p_2^{\text{E}}, -p_1^{\text{E}}) &= (\not{p}_1^{\text{E}} - \not{p}_2^{\text{E}})(p_1^{\text{E}} + p_2^{\text{E}})^\nu, & \tau_6^\nu(p_2^{\text{E}}, -p_1^{\text{E}}) &= -(\not{p}_1^{\text{E}} + \not{p}_2^{\text{E}})(p_1^{\text{E}} + p_2^{\text{E}})^\nu, \\ \tau_7^\nu(p_2^{\text{E}}, -p_1^{\text{E}}) &= -\frac{1}{2}[\not{p}_1^{\text{E}}, \not{p}_2^{\text{E}}]\gamma_{\text{E}}^\nu, & \tau_8^\nu(p_2^{\text{E}}, -p_1^{\text{E}}) &= -\frac{i}{2}[\not{p}_1^{\text{E}}, \not{p}_2^{\text{E}}](p_1^{\text{E}} + p_2^{\text{E}})^\nu. \end{aligned} \quad (\text{A.2})$$

The definition above is the Euclidean space equivalent of the vertex defined in Eqs. (3.16) and (3.14).

This can be demonstrated by following the procedure outlined in [103], which involves computing the contraction of the Dirac matrix  $\gamma^\mu$  with the quark-gluon vertex  $\overline{\Pi}_\mu$ , and verifying that the Wick-rotated Minkowski result matches the result obtained from direct calculations in Euclidean space. In our notation, this is expressed as

$$[\overline{\Pi}_\mu(q, p_2, -p_1)\gamma^\mu]^{\text{WR}} = \overline{\Pi}_\mu^{\text{E}}(q, p_2, -p_1)\gamma_{\text{E}}^\mu. \quad (\text{A.3})$$

Next, we exemplify this procedure showing only the contributions from the form factors  $\lambda_1$  and  $\lambda_3$ . Contracting the quark-gluon vertex given in Eq. (3.16) from the right with  $\gamma^\mu$  one obtains

$$\overline{\Pi}_\mu(q, p_2, -p_1)\gamma^\mu = (d-1) \left[ \lambda_1(q, p_2, -p_1) + \lambda_3(q, p_2, -p_1)(\not{p}_1 + \not{p}_2) \right] + \dots, \quad (\text{A.4})$$

where  $d$  is the dimension of the space. Using the standard rules to convert the above result to Euclidean space, and assuming that the form factors do not change the sign in this process, that is,

$$\not{p} \rightarrow i\not{p}_E, \quad p^2 \rightarrow -p_E^2, \quad \lambda_i(q, p_2, -p_1) \rightarrow \lambda_i^E(q^E, p_2^E, -p_1^E), \quad (\text{A.5})$$

one gets that

$$\left[ \overline{\Pi}_\mu(q, p_2, -p_1)\gamma^\mu \right]^{\text{WR}} = (d-1) \left[ \lambda_1^E(q^E, p_2^E, -p_1^E) - i\lambda_3^E(q^E, p_2^E, -p_1^E)(\not{p}_1^E + \not{p}_2^E) \right] + \dots. \quad (\text{A.6})$$

Now, an additional step is required depending on the definition of the quark propagator. If it is defined such that its inverse at tree-level is  $i\not{p} + m$ , and not  $i\not{p} - m$ , to compensate the relative sign in the definition in Eq. (3.7), an additional transformation  $p_E \rightarrow -p_E$  is necessary [5]. This is the case of [60], and therefore we make this extra transformation to obtain that

$$\left[ \overline{\Pi}_\mu(q, p_2, -p_1)\gamma^\mu \right]^{\text{WR}} = (d-1) \left[ \lambda_1^E(q^E, p_2^E, -p_1^E) + i\lambda_3^E(q^E, p_2^E, -p_1^E)(\not{p}_1^E + \not{p}_2^E) \right] + \dots. \quad (\text{A.7})$$

The result above is exactly what we obtain when contracting the vertex in Eq. (A.1) with  $\gamma_E^\mu$  from the right. From this calculation one can note that there is a difference between contracting the vertex with the Dirac matrix from the right or from the left. In particular for this basis, contracting it from the left makes the term proportional to  $\lambda_7$  to vanish.

The same procedure can be applied to the vertex in the soft-gluon limit, given in Eq. (4.27). In this case contracting the vertex with the Dirac matrix from right or left will give the same result, and the additional change  $p_E \rightarrow -p_E$  is necessary to compare with the results in [55]. In this situation, the Wick rotated contraction is

$$\left[ \gamma^\mu \overline{\Pi}_\mu(0, p_E, -p_E) \right]^{\text{WR}} = d\lambda_{1E}^{sg}(p_E^2) - 2i\not{p}_E \lambda_{2E}^{sg}(p_E^2) - 4p_E^2 \lambda_{6E}^{sg}(p_E^2), \quad (\text{A.8})$$

where again we consider that the form factors do not change sign from one space to the other, *i.e.*,  $\lambda_{iE}^{sg}(p_E^2) = \lambda_i^{sg}(-p_E^2)$ .

From Eq. (A.8) we conclude that using the definition in Eq. (4.27) is analogous to the

definition of the vertex in Euclidean space as

$$\overline{\Pi}_{\mu}^{\text{E}}(0, p_{\text{E}}, -p_{\text{E}}) = \gamma_{\mu}^{\text{E}} \lambda_{1\text{E}}^{\text{sg}}(p_{\text{E}}^2) - 2ip_{\mu}^{\text{E}} \lambda_{2\text{E}}^{\text{sg}}(p_{\text{E}}^2) - 4p_{\mu}^{\text{E}} p_{\mu}^{\text{E}} \lambda_{6\text{E}}^{\text{sg}}(p_{\text{E}}^2). \quad (\text{A.9})$$

Therefore, the comparison between the results in this work for  $\lambda_i^{\text{sg}}(p_{\text{E}}^2)$  for  $i = 1, 2, 6$ , and the lattice results  $\lambda_i^{\text{L}}(p_{\text{E}}^2)$  for  $i = 1, 2, 3$  from [55] is direct as given in Eq. (4.28).